Synthesis, Structural characterization and molecular docking analysis of novel β-ketiminate palladium(II) complexes with anticancer properties

Deeb Taher,[a]* Belal Khalil,[a] Sara AlNaimat,[a] Morad Mustafa,[b,c] Zakariyya Ishtaiwi,[d] Wissam Helal,[a] Marcus Korb,[e] Tuqa Abu Thiab,[f] Amer Imraish,[f] Tareq Alhindi,[f] Ahmad Makahleh,[a] Mohammad W. Amer, [a] Duha H. Abdelrahman, [a]

a Chemistry Department, The University of Jordan, Amman, 11942, Jordan.

b Department of Pharmacy, College of Pharmacy, Al-Zaytoonah University, P.O. Box:130, Amman 11733, Jordan.

c Chemistry Program, Science Division, New York University Abu Dhabi, P.O. Box: 129188, Abu Dhabi, United Arab Emirates.

d Department of Chemistry, Faculty of Science, Al-Balqa Applied University, Al Salt 19117, Jordan.

e School of Molecular Sciences, The University of Western Australia, 35 Stirling Highway, Crawley, Perth, Western Australia 6009, Australia.

f Department of Biological Sciences, The University of Jordan, Amman, 11942, Jordan.

Table of Contents

1. Experimental

1.1. Materials and Methods

Generally, all reactions were carried out under aerobic conditions. The respective substituted-anilines, palladium (II) chloride, potassium *tert*-butoxide, *p*-toluenesulfonic acid and solvents used within the studies were purchased from commercial suppliers and were used as received. $[PdCl_2(NCCH_3)_2]$ and β-ketiminate ((methyl-substituted anilino)pent-3-en-2-one) ligands (**3a–j**) (**Scheme 1**), were synthesized according to literature procedures [1–8]. Compounds **4a**–**c** were prepared according to modified literature procedures. [9,10]

1.2. Instruments

Infrared spectra were collected using a Thermo Nicolet NEXUS 670 FT-IR spectrometer. NMR spectra were recorded using a BrukerAvance III 500 FT-NMR spectrometer (^{1}H at 500.303 MHz, ^{13}C at 125.813 MHz) at ambient temperature. Chemical shifts (δ) are reported in parts per million (ppm) relative to tetramethylsilane using the solvent as internal reference ($CDCl_3$: ^{1}H NMR δ = 7.26 ppm; $^{13}C\{^1H\}$ NMR δ = 77.16 ppm). Coupling constants (*J*) are reported in Hertz (Hz) and integrations are reported in number of protons. The following abbreviations are used to describe peak patterns: s = single, d = doublet, dd = doublet of doublets, t = triplet, m = multiplet. The melting points were determined using an AELAB UK melting point ap*para*tus. Microanalysis was performed using a Thermo FLASHEA 1112 Series instrument. High resolution mass spectra were recorded with a BrukermicrOTOF QII with an Apollo II ESI source. Thermogravimetric analyses were performed on a NETZSCH STA 409 PG/PC. UV-Vis absorption bands were measured by using UV-Vis double beam spectrophotometer model UV 1900i (SHIMAZDU). HPLC analyses were carried out utilizing a Dionex Summit HPLC system composed from P680 gradient pump, ASI-100 autosampler, TCC-100 column oven and ultimate 3000 VWD-3400RS detector that provided by Thermo Fisher Scientific. The results obtained using licensed chromeleon software version 6.8.

1.3. Computational Method

All calculations were performed using ORCA code version 4.2.0. [11] Full geometry optimizations of the ligands **3a–i** and complexes **4a–i** were carried out using the hybrid GGA functional PBE0, [12] and the Ahlrichs triple-zeta def2-TZVP basis set. [13] The impact of the

chloroform solvent was taken into account in all geometry optimizations and excited state calculations for both ligands and complexes using the conductor-like polarizable continuum model (CPCM). [14,15] The lowest 20 singlet-singlet vertical electronic excitations based on PBE0 optimized geometries were computed using the Time-Dependent Density Functional Theory (TD-DFT) [16] formalism in chloroform solvent applying the CPCM solvation model using the hybrid Coulomb-Attenuating Method B3LYP (CAM-B3LYP) functional [17] and the def2-TZVP basis set. Gabedit program [18] was used to compute and draw the isosurface densities of the molecular orbitals.

1.4. Crystallography

Single crystals suitable for X-ray structure determination of compound **4c** were obtained by slow evaporation of a chloroform solution containing **4c** at ambient temperature. Crystallographic data for **4c** are summarized in **Table S5**. Data for compound **4c** were collected with graphite-monochromated Cu Kα radiation (λ = 1.54184 Å) at 100 K with an Oxford Rigaku diffractometer. Data were acquired and processed to give hkl files using CrysAlisPro software. The molecular structures were solved by direct methods using SHELXS-18/3 [19] and refined by full-matrix least-squares procedures on F^2 using SHELXL-18/3 [20–22]. All non-hydrogen atoms were refined anisotropically and a riding model was employed in the treatment of the hydrogen atom positions.

1.5. Hirshfeld Surfaces

Hirshfeld surfaces of compound **4c** and their associated 2D fingerprint plots were generated using CrystalExplorer17.5 program [23,24] and were analyzed to identify the most relevant intermolecular interactions. The Hirshfeld surfaces were mapped over the normalized contact distance (d_{norm}), which is defined in terms of d_e, d_i, and the vdW radii of the atoms, where d_e and d_i are the distances from a point on the surface to the nearest atom outside and inside, respectively. The Hirshfeld surface colors are used to visualize the inter-atomic contacts as: longer than vdW contacts (blue), equal to vdW (white), and shorter than vdW (red). The colors of the points on the 2-D fingerprint plots correspond to the frequency of the d_e and d_i combinations on the Hirshfeld surface, where red represents larger fraction or contribution and green to blue represent moderate to small contributions, respectively. [25]

1.6. Cytotoxicity assay

Cancer cell lines were obtained from the ATCC (Manassas, VA), MCF7 human breast cancer cell line (ATCC® HTB-22™, USA), HCT-116 colon cancer cell line (ATCC CCL-247 ™, USA and human skin fibroblast (ATCC® PCS-201-012™). The cells were cultivated in DMEM-F12 supplemented with glutamine, 1% penicillin-streptomycin and 10% (V/V) fetal bovine serum. To achieve 80–90% confluency the cells were cultivated as a monolayer in a T-75 flask at 37°C 5% CO_2 and high humidity. Trypsin-EDTA solution (0. 25%) was used to subculture the cells. In order to find the IC_{50} of the synthesized compounds on cancer cell lines, the anti-proliferative activity of the compounds was assessed using the Tetrazolium colorimetric assay (MTT). After being plated into 96-well plates cancer cells were given overnight incubation period. Different concentrations of compounds were added to the cells and incubated for 72 hours. After replacing the medium with 100 µL of fresh medium, 100 µL of freshly filtered MTT (3-(4,5-dimethylthiazol-2-yl)-2,5-diphenyltetrazolium bromide) was added at a concentration of 0.5 mg/ml. Following that, the mixture was incubated for four hours. After adding DMSO to dissolve the insoluble purple formazan product, the optical density (OD) was measured using a spectrophotometer at 750 nm. Subsequently cell viability was calculated using equation 1:

$$Cell\ Viability = \frac{optical\ density\ of\ sample\ -\ optical\ density\ of\ blank}{optical\ density\ of\ control\ -\ optical\ density\ of\ blank} \times 100\% \quad (1)$$

1.7. Stability Monitored by UV–Visible Spectroscopy

The stability of the stock solution of **4i** was evaluated in DMSO and aqueous media using UV–visible spectroscopy over a wavelength range of 260–800 nm with a 1 cm path length cuvette. The initial sample was divided into two equal portions for the stability study; one portion was exposed to diffuse light and monitored over time. The samples were prepared by diluting a 5 mM stock solution of the respective complex in DMSO with the medium to obtain a final concentration of 10^{-6} M. The UV–Vis spectra of the resulting solutions were recorded periodically for up to 72 h.

1.8. HPLC Methods and Sample Preparation

Ligand and complex **4i** solutions were freshly prepared as described in the previous work in Quiroga et al [26,27] for UV–Vis stability assay. Prior to injection into the column, 20 µL of the

sample was withdrawn at different time points (t = 0 and 72 h) and diluted with 180 μL of HPLC-grade acetonitrile. Subsequently, 20 μL of the diluted solution was injected into a Zorbax Eclipse XDB-C18 column (4.6 × 150 mm, 5 μm). The chromatographic conditions were as follows: flow rate of 1 mL/min, UV detection at 350 nm, and a mobile phase consisting of acetonitrile/water (95:5, v/v). The analysis was monitored for a total run time of 12 min.

1.9. Molecular Docking

The structure of the Pd(II) complexes were obtained from our computational method study. Because the anticancer activities of the novel Pd(II) complexes were evaluated against MCF-7 (breast cancer) and HCT-116 (colon cancer) cell lines, the top 20 genes in both breast and colon cancers were investigated using the Catalogue Of Somatic Mutations In Cancer (COSMIC). [28] In the MCF-7 cell line, only two genes from the top 20 genes in breast cancer have somatic mutations and representative crystal structures: the PIK3CA protein harbors the E545K mutation and the ERBB4 protein contains the Y1242C mutation. In contrast, in HCT-116 cell line, only three genes from the top 20 genes in colon cancer have a somatic mutation and representative crystal structures; that is, the KRAS protein exhibits the G13D mutation, the PIK3CA protein harbors the H1047R mutation, and the ATM protein contains the A112V mutation. Consequently, five proteins were used in molecular docking studies; that is, PIK3CA-E545K with PDB entry (8GUD), [29] ERBB4-Y1242C with PDB entry (2R4B), [30] KRAS-G13D with PDB entry (8UN5), [31] PIK3CA-H1047R with PDB entry (8TGD), [32] and ATM-A112V with PDB entry (7NI5). [33]

To predict potential binding sites on the target proteins, P2Rank (version 2.5), [34,35] a tool designed to analyze protein structure and sequence for the identification of likely binding regions, was employed. The molecular docking of the Pd(II) complexes was performed using AutoDock Vina (version 1.2.7) [36,37], a widely utilized docking tool. Open babel [38] was used to assign partial atomic charges before using AutoDock Vina. The palladium ion was assigned Universal Force Field (UFF) parameters. [39] Partial charges were assigned to the protein atoms using the Gasteiger-Marsili sigma method, while the palladium complexes were assigned partial charges using the Electronegativity Equalization Method (EEM). The docking process was carried out with a grid box size of 25 × 25 × 25 $Å^3$ surrounding the protein binding site. To enhance the accuracy and thoroughness of the docking process, the exhaustiveness parameter was set to 24, and the number of modes to 100. The grid box center for each protein in *x*, *y*, and *z* directions, respectively were

as following: PIK3CA-E545K (124.4906, 137.8921, 153.6301 Å), ERBB4-Y1242C (–13.5465, 17.0451, –2.7001 Å), KRAS-G13D (10.4143, –8.3606, –6.705 Å), PIK3CA-H1047R (34.8644, –21.8444, 81.0607 Å), and ATM-A112V (112.9832, 155.4942, 215.1651 Å).

Limitations and ligand speciation: Docking was performed using the intact, neutral Pd(II) complexes as model ligands. This choice represents a simplification: Pd(II) centers are known to be kinetically labile and may undergo aquation or ligand exchange under physiological conditions, potentially yielding distinct species with different protein affinities. The present docking therefore models the intact complexes as a structural hypothesis and does not account for possible hydrolysed or exchanged forms. Future work will be required to address speciation experimentally.

Following docking, the interactions between the compounds and the target protein were analyzed using LigPlot+ (version 2.2). [40,41] This tool was used to create 2D diagrams of the ligand-protein interactions, which facilitated the examination of the binding modes and interaction patterns of the docked compounds. ChimeraX [42–44] was used for visualizing biomolecular structures, generating publication-quality images, studying protein-ligand interactions, examining molecular surfaces, assessing electrostatic potentials, and analyzing trajectories.

1.10. General procedure for preparation of 3j

A catalytic amount of *p*-toluenesulfonic acid was added in a single portion to a solution of 4-Chloro-2-methylaniline (**2j)** (20.00 mmol) and 2, 4-pentanedione (**1**) (20.00 mmol) in 100 mL of toluene. The reaction solution was refluxed for 24 h with water removed using a Dean–Stark trap. The reaction mixture was evaporated to dryness under reduced pressure and the obtained residue was dissolved in diethyl ether (10 mL). The reaction mixture was extracted with water (10 mL). The combined organic phases were dried over $MgSO_4$. All the volatiles were removed in *vacuo* and the residue was recrystallized from ethanol at −18 °C temperature to afford **3j** as a white solid.

1.10.1. [4-(4-chloro-2-methylphenyl)amino-3-penten-2-one] (3j)

Yield: 4.823 g (14.5 mmol, 72% based on **1**). M. p.: 71 °C. IR (KBr, cm^{-1}): *v* 3414 (s), 3049 (m), 1611 (s), 1559 (s), 1507 (s), 1477 (s), 1433 (m), 1382 (s), 1274 (s), 1174 (s), 1122 (s), 1021 (m), 993 (m), 922 (m), 868 (m), 846 (m), 825 (m), 757 (m), 624. ^{1}H NMR (500 MHz, $CDCl_3$): δ = 12.25 (s, 1H, NH), 7.21 (s, 1H, Ph), 7.14 (d, J_{HH}= 8.4 Hz, 1H, Ph), 6.99 (d, J_{HH}= 8.3 Hz, 1H, Ph), 5.20 (s, 1H, CH NAcAc backbone), 2.24 (s, 3H, CH_3), 2.09 (s, 3H, CH_3), 1.84 (s, 3H, CH_3) ppm. ^{13}C{^{1}H} NMR (125 MHz, $CDCl_3$): δ = 196.5 (CO), 160.8 (N-C=), 136.2 (*ipso*-CPh), 135.6 (*ipso*-CPh), 131.7 (*ipso*-CPh), 130.7 (CH, Ph), 127.4 (CH, Ph), 126.5 (CH, Ph), 97.6 (CH NAcAc backbone), 29.2 (CH_3 NAcAc backbone), 19.7 (CH_3 NAcAc backbone) ppm, 18.1 (CH_3-Ph). $UV_{\lambda max}$ ($CHCl_3$) = 309 nm, ε = 17314 $Lmol^{-1}cm^{-1}$. HR-ESI-MS (positive ion mode) m/z: Calcd. For $C_{12}H_{15}ClNO$ (M+H) 224.08367 found 224.08352.

1.11. General procedure for the preparation of 4a–j

KO^{t}Bu (173 mg, 1.54 mmol) was added in a single portion to a solution of the respective enaminone ligands **3a–j** (1.54 mmol) in 35 mL of methanol. The formed reaction mixture was stirred at ambient temperature for 1 h and then [$PdCl_2(NCCH_3)_2$] (200 mg, 0.77 mmol) was added in one portion at ambient temperature. The resulting reaction mixture was stirred at ambient temperature for 3 days. The solids formed of **4a**–**j** were filtered through a filter paper and washed with methanol (4 × 25 mL). The obtained yellow solids were dried under high vacuum.

1.11.1. Bis(4-((2-methylphenyl)amino)pent-3-en-2- one)palladium(II) complex (4a) [9,10]

Yield: 0.306 g (0.634 mmol, 82% based on **2a**). M. p.: 192 °C. IR (KBr, cm^{-1}): *v* 2918 (m), 1616 (m), 1578 (s), 1544 (s), 1510 (s), 1484 (s), 1403 (s), 1273 (m), 1244 (m), 1188 (m), 1113 (m), 1022

(m), 947 (m), 875 (m), 766 (m), 620 (m) and 453 (m). ^{1}H NMR (500 MHz, $CDCl_3$): δ = 7.12 (t, J_{HH} = 7.5, 2H, Ph), 7.06 (d, J_{HH} = 7.1, 1H, Ph), 6.91 (t, J_{HH} = 7.5 Hz, 1H, Ph), 4.85 (s, 1H, CH nacac backbone), 2.26 (s, 3H, CH_3), 1.59 (s, 3H, CH_3), 1.37 (s, 3H, CH_3) ppm. ^{13}C{^{1}H} NMR (125 MHz, $CDCl_3$): δ = 176.4 (C=O), 162.6 (N-C=), 147.6 (*ipso*-Cph-N), 133.3 (*ipso*-Cph), 129.5 (CH, Ph), 125.8 (CH, Ph), 125.7 (CH, Ph), 124.9 (CH, Ph), 97.7 (CH NAcAc backbone), 23.5 (CH_3), 23.4 (CH_3), 18.7 (CH_3) ppm. $UV_{\lambda max}$ ($CHCl_3$) = 339 nm, ε = 10265 $Lmol^{-1}cm^{-1}$, 400 nm, ε = 1905 $Lmol^{-1}cm^{-1}$. HR-ESI-MS (positive ion mode) m/z: Calcd. For $C_{24}H_{29}N_2O_2Pd$ (M+H) 483.12584 found 483.12391.

1.11.2. Bis(4-((3-methylphenyl)amino)pent-3-en-2- one)palladium(II) complex (4b) [9,10]

Yield: 0.336 g (0.696 mmol, 90% based on **2b**). M. p.: 174 °C. IR (KBr, cm^{-1}): ν 2917 (m), 1585 (s), 1508 (s), 1405 (s), 1271 (m), 1210 (m), 1161 (m), 1024 (m), 944 (m), 878 (w), 760 (m), 620 (m) and 476 (m). ^{1}H NMR (500 MHz, $CDCl_3$): δ = 7.13 (t, J_{HH} = 7.6 Hz, 1H, Ph), 6.94 (d, J_{HH} = 7.6 Hz, 1H, Ph), 6.79 (s, 1H, Ph), 6.76 (d, J_{HH} = 7.8 Hz, 1H, Ph), 4.83 (s, 1H, CH NAcAc backbone), 2.33 (s, 3H, CH_3), 1.66 (s, 3H, CH_3), 1.39 (s, 3H, CH_3) ppm. ^{13}C{^{1}H} NMR (125 MHz, $CDCl_3$): δ = 176.1 (C=O), 162.8 (N-C=), 148.6 (*ipso* -Cph-N), 137.5 (*ipso* -Cph), 127.7 (CH, Ph), 126.8 (CH, Ph), 125.4 (CH, Ph), 123.1 (CH, Ph), 97.9 (CH NAcAc backbone), 23.9 (CH_3), 23.7 (CH_3), 21.4 (CH_3) ppm. $UV_{\lambda max}$ ($CHCl_3$) = 341 nm, ε = 12263 $Lmol^{-1}cm^{-1}$, 420 nm, ε = 1087 $Lmol^{-1}cm^{-1}$. HR-ESI-MS (positive ion mode) m/z: Calcd. For $C_{24}H_{29}N_2O_2Pd$ (M+H) 483.12584 found 483.12712.

1.11.3. Bis(4-((4-methylphenyl)amino)pent-3-en-2-one)palladium(II) complex (4c) [9,10]

Yield: 0.343 g (0.710 mmol, 92% based on **2c**). M. p.: 214 °C. IR (KBr, cm^{-1}): ν 2915 (m), 1617 (m), 1576 (s), 1513 (s), 1503 (s), 1400 (s), 1275 (m), 1203 (m), 1105 (m), 1016 (m), 947 (m), 873 (m), 756 (m), 625 (m) and 467 (m). ^{1}H NMR (500 MHz, $CDCl_3$): δ = 7.7 (d, J_{HH} = 12.0 Hz, 2H, Ph), 6.85 (d, J_{HH} = 7.7 Hz, 2H, Ph), 4.83 (s, 1H, CH NAcAc backbone), 2.31 (s, 3H, CH_3), 1.66 (s, 3H, CH_3), 1.40 (s, 3H, CH_3) ppm. ^{13}C{^{1}H} NMR (125 MHz, $CDCl_3$): δ = 176.2 (C=O), 162.9 (N-C=), 146.1 (*ipso*-Cph-N), 134.0 (*ipso*-Cph), 128.5 (CH), 125.9 (CH), 97.9 (CH NAcAc backbone), 23.9 (CH_3), 23.6 (CH_3), 21.1 (CH_3) ppm. $UV_{\lambda max}$ ($CHCl_3$) = 335 nm, ε = 12701 $Lmol^{-1}cm^{-1}$, 430 nm, ε = 615 $Lmol^{-1}cm^{-1}$. HR-ESI-MS positive ion mode) m/z: Calcd. For $C_{24}H_{29}N_2O_2Pd$ (M+H) 483.12584 found 483.12773.

1.11.4. Bis(4-((2,4-dimethylphenyl)amino)pent-3-en-2-one)palladium(II) complex (4d)

Yield: 0.306 g (0.600 mmol, 78% based on **2d**). M. p.: 184 °C. Anal. calcd. For $C_{26}H_{32}N_2O_2Pd$ (510.97): C, 61.12; H, 6.31; N, 5.48. Found; C, 61.20; H, 6.29; N, 5.55. IR (KBr, cm^{-1}): ν 3008 (m), 2963 (m), 2916 (m), 1615 (m), 1576 (s), 1510 (s), 1492 (s), 1405 (s), 1375 (s), 1274 (m), 1228 (m), 1124 (w), 1021 (m), 946 (m), 870 (m), 758 (m), 627 (m) and 478 (m). ^{1}H NMR (500 MHz, $CDCl_3$): δ = 6.95-6.92 (m, 2H, Ph), 6.78 (d, J_{HH} = 7.7 Hz, 1H, Ph), 4.83 (s, 1H, CH NAcAc backbone), 2.27 (s, 3H, CH_3), 2.21 (s, 3H, CH_3), 1.59 (s, 3H, CH_3), 1.40 (s, 3H, CH_3) ppm. ^{13}C{^{1}H} NMR (125 MHz, $CDCl_3$): δ = 176.4 (C=O), 162.7 (N-C=), 144.9 (*i*-Cph-CH_3), 134.2 (*ipso*-Cph-N), 132.8 (CH), 130.2 (*ipso*-Cph), 126.3 (CH), 125.6 (CH), 97.7 (CH NAcAc backbone), 23.6 (CH_3), 23.4 (CH_3), 21.1 (CH_3), 18.6 (CH_3) ppm. $UV_{\lambda max}$ ($CHCl_3$) = 337 nm, ε = 125198 $Lmol^{-1}cm^{-1}$, 420 nm, ε = 802 $Lmol^{-1}cm^{-1}$. HR-ESI-MS positive ion mode) m/z: Calcd. For $C_{26}H_{33}N_2O_2Pd$ (M+H) 511.15714 found 511.15588.

1.11.5. Bis(4-((2,6-dimethylphenyl)amino)pent-3-en-2-one)palladium(II) complex (4e)

Yield: 0.3048 g (0.596 mmol, 77% based on **2e**). M. p.: 250 °C. Anal. calcd. For $C_{26}H_{32}N_2O_2Pd$ (510.97): C, 61.12; H, 6.31; N, 5.48. Found; C, 61.23; H, 6.37; N, 5.57. IR (KBr, cm^{-1}): ν 3010 (m), 2967 (m), 2916 (m), 1579 (s), 1509 (s), 1468 (s), 1402 (s), 1373 (s), 1275 (m), 1257 (m), 1195 (m), 1090 (m), 1021 (m), 947 (m), 860 (m), 768 (m), 609 (m) and 463 (m). ^{1}H NMR (500 MHz, $CDCl_3$): δ = 6.99 (s, 3H, Ph), 4.85 (s, 1H, CH NAcAc backbone), 2.25 (s, 6H, CH_3), 1.53 (s, 3H, CH_3), 1.37 (s, 3H, CH_3) ppm. ^{13}C{^{1}H} NMR (125 MHz, $CDCl_3$): δ = 176.6 (C=O), 162.2 (N-C=), 146.4 (*ipso* -Cph-N), 132.7 (*ipso*-Cph), 127.3 (CH), 124.7 (CH), 97.5 (CH NAcAc backbone), 23.5 (CH_3), 22.6 (CH_3), 18.9 (CH_3) ppm. $UV_{\lambda max}$ ($CHCl_3$) = 336 nm, ε = 12203 $Lmol^{-1}cm^{-1}$, 420 nm, ε = 660 $Lmol^{-1}cm^{-1}$. HR-ESI-MS positive ion mode) m/z: Calcd. For $C_{26}H_{33}N_2O_2Pd$ (M+H) 511.15714 found 511.15555.

1.11.6. Bis(4-((3,5-dimethylphenyl)amino)pent-3-en-2-one)palladium(II) complex (4f)

Yield: 0.2155 g (0.422 mmol, 72% based on **2f**). M. p.: 174 °C. Anal. calcd. For $C_{26}H_{32}N_2O_2Pd$ (510.97): C, 61.12; H, 6.31; N, 5.48. Found; C, 61.19; H, 6.33; N, 5.46. IR (KBr, cm^{-1}): *ν* 2915 (m), 1615(s), 1585 (s), 1510 (s), 1408 (s), 1297 (m), 1274 (m), 1223 (m), 1157 (m), 1014 (m), 945 (w), 850 (w), 766 (m), 690 (m), 620 (m) and 472 (m). ^{1}H NMR (500 MHz, $CDCl_3$): δ = 6.77 (s, 1H, Ph), 6.58 (s, 2H, Ph), 4.82 (s, 1H, CH NAcAc backbone), 2.29 (s, 6H, CH_3, Ph), 1.67 (s, 3H, CH_3 NAcAc backbone), 1.41 (s, 3H, CH_3 NAcAc backbone) ppm. ^{13}C{^{1}H} NMR (125 MHz, $CDCl_3$): δ = 175.9 (C=O), 162.7 (N-C=), 148.4 (*ipso*-CPh-N), 137.2 (*ipso*-CPh), 126.2 (CH, Ph),

123.8 (CH, Ph), 97.9 (CH NAcAc backbone), 23.8 (CH_3 NAcAc backbone), 23.7 (CH_3 NAcAc backbone), 21.4 (CH_3-Ph) ppm. $UV_{\lambda max}$ ($CHCl_3$) = 342 nm, ε = 10297 $Lmol^{-1}cm^{-1}$, 427 nm, ε = 864 $Lmol^{-1}cm^{-1}$. HR-ESI-MS positive ion mode) m/z: Calcd. For $C_{26}H_{33}N_2O_2Pd$ (M+H) 511.15714 found 511.15553.

1.11.7. Bis(4-((2,4,6-trimethylphenyl)amino)pent-3-en-2-one)palladium(II) complex (4g)

Yield: 0.3221 g (0.598 mmol, 78% based on **2g**). M. p.: 233 °C. Anal. calcd. For $C_{28}H_{36}N_2O_2Pd$ (539.03): C, 62.39; H, 6.73; N, 5.20. Found; C, 62.45; H, 6.63; N, 5.26. IR (KBr, cm^{-1}): *ν* 2994 (m), 2914 (m), 1616 (s), 1577 (s), 1503 (s), 1448 (s), 1401 (s), 1369 (s), 1270 (m), 1234 (m), 1201 (m), 1151 (m), 1021 (m), 945 (m), 858 (m), 761 (m), 624 (m) and 474 (m). ^{1}H NMR (500 MHz, $CDCl_3$): δ = 6.80 (s, 2H, Ph), 4.83 (s, 1H, CH NAcAc backbone), 2.23 (s, 3H, CH_3), 2.19 (s, 6H, CH_3), 1.52 (s, 3 H, CH_3), 1.39 (s, 3H, CH_3) ppm. $^{13}C\{^1H\}$ NMR (500 MHz, $CDCl_3$): δ = 176.6 (C=O), 162.3 (N-C=), 143.8 (*ipso*-CPh-N), 133.9 (*ipso*-CPh), 132.4 (*ipso*-CPh), 128.0 (CH, Ph), 97.5 (CH NAcAc backbone), 23.5 (CH_3 NAcAc backbone), 22.5 (CH_3 NAcAc backbone), 21.1 (CH_3-Ph), 18.9 (CH_3-Ph) ppm. $UV_{\lambda max}$ ($CHCl_3$) = 342 nm, ε = 9828 $Lmol^{-1}cm^{-1}$, 420 nm, ε = 630 $Lmol^{-1}cm^{-1}$. HR-ESI-MS positive ion mode) m/z: Calcd. For $C_{28}H_{37}N_2O_2Pd$ (M+H) 539.18844 found 539.18940.

1.11.8. Bis(4-((3,4-dimethylphenyl)amino)pent-3-en-2-one)palladium(II) complex (4h)

Yield: 0.2538 g (0.496 mmol, 64% based on **2h**). M. p.: 186 °C. Anal. calcd. For $C_{26}H_{32}N_2O_2Pd$ (510.97): C, 61.12; H, 6.31; N, 5.48. Found; 61.21; H, 6.36; N, 5.41. IR (KBr, cm^{-1}): *ν* 2918 (m), 1576 (s), 1510 (s), 1495 (s), 1404 (s), 1272 (m), 1199 (m), 1157 (m), 1000 (m), 949 (m), 876 (w), 756 (m), 646 (m) and 478 (m). ^{1}H NMR (500 MHz, $CDCl_3$): δ = 7.01 (d, J_{HH} = 7.8 Hz 1H, Ph), 6.74 (s, 1H, Ph), 6.68 (d, J_{HH} = 7.8 Hz, 1H, Ph), 4.82 (s, 1H, CH NAcAc backbone), 2.24 (s, 3H, CH_3, Ph), 2.21 (s, 3H, CH_3, Ph), 1.67 (s, 3H, CH_3 NAcAc backbone), 1.40 (s, 3H, CH_3 NAcAc backbone) ppm. $^{13}C\{^1H\}$ NMR (500 MHz, $CDCl_3$): δ = 176.1 (C=O), 162.8 (N-C=), 146.2 (*ipso*-Cph-N), 135.7 (*ipso*-Cph), 132.6 (CH), 129.0 (*ipso*-Cph), 127.3 (CH), 123.3 (CH), 97.9 (CH NAcAc backbone), 23.9 (CH_3), 23.7 (CH_3), 19.9 (CH_3), 19.4 (CH_3) ppm. $UV_{\lambda max}$ ($CHCl_3$) = 335 nm, ε = 12334 $Lmol^{-1}cm^{-1}$, 408 nm, ε = 1598 $Lmol^{-1}cm^{-1}$. HR-ESI-MS positive ion mode) m/z: Calcd. For $C_{26}H_{33}N_2O_2Pd$ (M+H) 511.15714 found 511.15782.

1.11.9. Bis(4-((2,5-dimethylphenyl)amino)pent-3-en-2-one)palladium(II) complex (4i)

Yield: 0.283 g (0.553 mmol, 72% based on **2i**). M. p.: 174 °C. Anal. calcd. For $C_{26}H_{32}N_2O_2Pd$ (510.97): C, 61.12; H, 6.31; N, 5.48. Found; C, 61.25; H, 6.35; N, 5.62. IR (KBr, cm^{-1}): ν 2948

(m), 2918 (m), 1615 (m), 1577 (s), 1510 (s), 1407 (s), 1275 (m), 1254 (m), 1127 (m), 1027 (m), 948 (m), 801 (m), 773 (m), 619 (m) and 453 (m). ^{1}H NMR (500 MHz, $CDCl_3$): δ =6.99 (d, J_{HH} = 7.6 Hz, 2H, Ph), 6.87 (d, J_{HH} = 7.7 Hz, 1H, Ph), 6.71 (s, 1H, Ph), 4.83 (s, 1H, CH NAcAc backbone), 2.30 (s, 3H, CH_3), 2.20 (s, 3H, CH_3), 1.59 (s, 3H, CH_3), 1.39 (s, 3H, CH_3) ppm. ^{13}C{^{1}H} NMR (125 MHz, $CDCl_3$): δ = 176.3 (C=O), 162.5 (N-C=), 147.2 (*ipso*-Cph-N), 135.1 (*ipso*-Cph), 130.0 (*ipso*-Cph), 129.3 (*i*-Cph), 126.4 (CH), 125.6 (CH), 97.7 (CH NAcAc backbone), 23.6 (CH_3), 23.4 (CH_3), 21.1 (CH), 18.3 (CH) ppm. $UV_{\lambda max}$ ($CHCl_3$) = 335 nm, ε = 13336 $Lmol^{-1}cm^{-1}$, 428 nm, ε = 741 $Lmol^{-1}cm^{-1}$. HR-ESI-MS positive ion mode) m/z: Calcd. For $C_{26}H_{33}N_2O_2Pd$ (M+H) 511.15714 found 511.15810.

1.11.10. Bis(4-((4-chloro-2-methylphenyl)amino-3-penten-2-one)palladium(II) complex (4j)

Yield: 0.469 g (0.766 mmol, 91% based on **2j**). M. p.: 207 °C-decomposition. Anal. calcd. For $C_{24}H_{26}Cl_2N_2O_2Pd$ (551.80): C, 52.24; H, 4.75; N, 5.08. Found; 52.31; H, 4.69; N, 5.12. IR (KBr, cm^{-1}): *v* 2919 (w), 1637 (s), 1617 (vs), 1575 (m), 1508 (s), 1478 (m), 1402 (s), 1271 (w), 1186 (m), 1118 (w), 1089 (w), 1024 (w), 949 (w), 880 (w), 768 (w), 620 (m) and 476 (m). ^{1}H NMR (500 MHz, $CDCl_3$): δ = 7.12 (s, 1H, Ph), 7.09 (d, J_{HH} = 7.7 Hz, 1H, Ph), 6.82 (dd, J_{HH} = 7.7 Hz, 4.7 Hz, 1H, Ph), 4.86 (s, 1H, CH NAcAc backbone), 2.21 (s, 3H, CH_3), 1.59 (s, 3H, CH_3), 1.41 (s, 3H, CH_3) ppm. ^{13}C{^{1}H} NMR (125 MHz, $CDCl_3$): δ = 176.9 (CO), 162.8 (N-C=), 146.0 (*ipso*-CPh), 135.3 (*ipso*-CPh), 130.0 (CH, Ph), 129.3 (*ipso*-CPh), 127.2 (CH, Ph), 125.8 (CH, Ph), 97.9 (CH NAcAc backbone), 23.8 (CH_3 NAcAc backbone), 23.5 (CH_3 NAcAc backbone) ppm, 18.6 (CH_3-Ph) ppm. $UV_{\lambda max}$ ($CHCl_3$) = 324 nm, ε = 15505 $Lmol^{-1}cm^{-1}$, 402 nm, ε = 640 $Lmol^{-1}cm^{-1}$. HR-ESI-MS (positive ion mode) m/z: Calcd. For $C_{24}H_{27}Cl_2N_2O_2Pd$ (M+H) 552.08032 found 552.04377.

Table S1. IR (KBr) data for **3a–j** and **4a–j**.

Ligand	ν (cm^{-1})		Complex	ν (cm^{-1})
	ν H-N	ν C=C, C=O, C=N		ν C=C, ν C=O, ν C=N
3a	3422	1618 (s), 1580 (m), 1506 (m)	**4a**	1578 (s), 1510 (s), 1484 (s)
3b	3415	1617 (s), 1576 (m), 1491 (m)	**4b**	1585 (s), 1508 (s), 1405 (s)
3c	3417	1609 (s), 1565 (s), 1520 (m)	**4c**	1576 (s), 1513 (s), 1503 (s)
3d	3416	1611 (s), 1563 (s), 1512 (m)	**4d**	1576 (s), 1510 (s),1492 (s)
3e	3454	1615 (s), 1552 (s), 1500 (m)	**4e**	1579 (s), 1509 (s), 1468 (s)
3f	3419	1612 (s), 1569 (s), 1507 (m)	**4f**	1585 (s), 1510 (s), 1408 (s)
3g	3414	1614 (s), 1570 (s), 1481 (m)	**4g**	1577(s), 1503 (s), 1448 (m)
3h	3417	1611 (s), 1568 (s), 1508 (m)	**4h**	1576 (s), 1510 (s), 1495 (s)
3i	3419	1614 (s), 1575 (m), 1513 (m)	**4i**	1577 (s), 1510 (s), 1407 (s)
3j	3414	1611 (s) , 1559 (s), 1507 (m)	**4j**	1637 (s), 1617 (vs), 1576(m), 1508(s), 1478 (s),

Table S2. NMR (^{1}H, $^{13}C\{^{1}H\}$) data for **3a–j**.

ligand	^{1}H NMR ($CDCl_3$)	^{13}C NMR ($CDCl_3$)
	δ (ppm)	δ (ppm)
3a	12.33 (s, 1H, NH), 7.22 (d, J_{HH} = 7.3 Hz, 1H, CH), 7.15 (dq, J_{HH} = 13.7, 6.9 Hz, 2H, CH), 7.07 (d, J_{HH} = 7.6 Hz, 1H, CH), 5.19 (s, 1H, CH nacac backbone), 2.27 (s, 3H, CH_3), 2.09 (s, 3H, CH_3), 1.86 (s, 3H, CH_3).	196.1(CO), 161.3 (N-C=), 137.5 (*i*-Cph-NH), 133.7 (*i*-Cph), 130.8 (CH), 126.5 (CH), 126.4 (CH), 126.3 (CH), 97.1 (CH nacac backbone), 29.1 (CH_3), 19.6 (CH_3), 18.1 (CH_3).
3b	12.45 (s, 1H, NH), 7.19 (t, J = 7.7 Hz, 1H, CH), 6.97 (d, J_{HH} = 8.2 Hz, 1H, CH), 6.89 (bs, 1H, CH), 6.88 (bs, 1H, CH), 5.16 (s, 1H, CH nacac backbone), 2.31 (s, 3H, CH_3), 2.08 (s, 3H, CH_3), 1.96 (s, 3H, CH_3).	195.9(CO), 160.3 (N-C=), 139.0 (*i*-Cph-NH), 138.5 (*i*-Cph), 128.8 (CH), 126.3 (CH), 125.3 (CH), 121.6 (CH), 97.4 (CH nacac backbone), 29.0 (CH_3), 21.2 (CH_3), 19.8 (CH_3).
3c	12.39 (s, 1H, NH), 7.12 (d, J_{HH} = 7.9 Hz, 2H, CH), 6.97 (d, J_{HH} = 7.9 Hz, 2H, CH), 5.15 (s, 1H, CH nacac backbone), 2.32 (s, 3H, CH_3), 2.07 (s, 3H, CH_3), 1.94 (s, 3H, CH_3).	195.8(CO), 160.6 (N-C=), 136.0 (*i*-Cph-NH), 135.4 (*i*-Cph), 129.6 (CH), 124.8 (CH), 97.2 (CH nacac backbone), 29.1 (CH_3), 20.9 (CH_3), 19.7 (CH_3).
3d	12.23 (s, 1H, NH), 7.03 (s, 1H, CH), 6.95 (m, 2H, CH), 5.17 (s, 1H, CH nacac backbone), 2.30 (s, 3H, CH_3-Ph), 2.22 (s, 3H, CH_3-Ph), 2.09 (s, 3H, CH_3), 1.82 (s, 3H, CH_3).	195.8(CO), 161.6 (N-C=), 136.3 (*i*-Cph), 134.9 (*i*-Cph-NH), 133.6 (CH), 131.5 (*i*-Cph), 127.0 (CH), 126.3 (CH), 96.7 (CH nacac backbone), 29.1 (CH_3), 20.9 (CH_3), 19.6 (CH_3), 18.0 (CH_3).
3e	11.92 (s, 1H, NH), 7.10 (m, 3H, CH), 5.20 (s, 1H, CH nacac backbone), 2.19 (s, 6H, CH_3-Ph), 2.10 (s, 3H, CH_3), 1.62 (s, 3H, CH_3).	196.1(CO), 163.0 (N-C=), 136.6 (*i*-Cph-NH), 136.2 (*i*-Cph), 128.3 (CH), 127.5 (CH), 95.9 (CH nacac backbone), 29.1 (CH_3), 18.9 (CH_3), 18.3 (CH_3).
3f	12.49 (s, 1H, NH), 6.88 (s, 1H, CH), 6.78 (s, 2H, CH), 5.21 (s, 1H, CH nacac backbone), 2.35 (s, 6H, CH_3), 2.14 (s, 3H, CH_3), 2.04 (s, 3H, CH_3).	195.8 (CO), 160.7 (N-C=), 138.8 (*i*-Cph-NH), 127.3 (*i*-Cph), 122.5 (CH), 113.1 (*i*-Cph), 97.3 (CH nacac backbone), 29.1 (CH_3), 21.2 (CH_3), 19.8 (CH_3).
3g	11.84 (s, 1H, NH), 6.89 (s, 2H, CH), 5.18 (s, 1H, CH nacac backbone), 2.27 (s, 3H, CH_3), 2.14 (s, 6H, CH_3), 2.09 (s, 3H, CH_3), 1.61 (s, 3H, CH_3).	195.9 (CO), 163.2 (N-C=), 137.1 (*i*-Cph-NH), 135.8 (*i*-Cph), 134.0 (*i*-Cph), 129.0 (CH), 95.7 (CH nacac backbone), 29.1 (CH_3), 21.0 (CH_3), 18.9 (CH_3), 18.2 (CH_3).
3h	12.39 (s, 1H, NH), 7.07 (d, J_{HH} = 8.1 Hz, 1H, CH), 6.88 (s, 1H, CH), 6.83 (d, J_{HH} = 8.3 Hz, 1H, CH), 5.14 (s, 1H, CH nacac backbone), 2.23 (s, 6H, CH_3), 2.08 (s, 3H, CH_3), 1.95 (s, 3H, CH_3).	195.8 (CO), 160.9 (N-C=), 137.5 (*i*-Cph-NH), 136.3 (*i*-Cph), 134.3 (*i*-Cph), 130.1 (CH), 126.2 (CH), 122.3 (CH), 97.1 (CH nacac backbone), 29.1 (CH_3), 19.8 (CH_3), 19.3 (CH_3), 17.6 (CH_3).
3i	12.28 (s, 1H, NH), 7.10 (d, J_{HH} = 7.7 Hz, 1H, CH), 6.95 (d, J_{HH} = 7.7 Hz, 1H, CH), 6.89 (s, 1H, CH), 5.18 (s, 1H, CH nacac backbone), 2.30 (s, 3H, CH_3), 2.22 (s, 3H, CH_3-Ph), 2.09 (s, 3H, CH_3), 1.85 (s, 3H, CH_3).	195.5 (CO), 161.0 (N-C=), 137.0 (*i*-Cph-NH), 135.8 (*i*-Cph), 130.3 (CH), 130.2 (*i*-Cph), 127.0 (CH), 126.6 (CH), 96.6 (CH nacac backbone), 28.7 (CH_3), 20.6 (CH_3) 19.3 (CH_3), 17.3 (CH_3-Ph).
3j	12.25 (s, 1H, NH), 7.21 (s, 1H, Ph), 7.14 (d, J_{HH}= 8.4 Hz, 1H, Ph), 6.99 (d, J_{HH}= 8.3 Hz, 1H, Ph), 5.20 (s, 1H, CH nacac backbone), 2.24 (s, 3H, CH_3), 2.09 (s, 3H, CH_3), 1.84 (s, 3H, CH_3) .	196.5 (CO), 160.8 (N-C=), 136.2 (ipso-Cph), 135.6 (*i*-Cph), 131.7 (*i*-Cph), 130.7 (CH, Ph), 127.4 (CH, Ph), 126.5 (CH, Ph), 97.6 (CH nacac backbone), 29.2 (CH_3), 19.7 (CH_3), 18.1 (CH_3).

Table S3. NMR (^{1}H, $^{13}C\{^{1}H\}$) data for **4a–j**.

Complex	^{1}H NMR ($CDCl_3$)	^{13}C NMR ($CDCl_3$)
	δ (ppm)	δ (ppm)
4a	7.12 (t, J_{HH} = 7.5, 2H, Ph), 7.06 (d, J_{HH} = 7.1, 1H, Ph), 6.91 (t, J_{HH} = 7.5 Hz, 1H, Ph), 4.85 (s, 1H, CH nacac backbone), 2.26 (s, 3H, CH_3), 1.59 (s, 3H, CH_3), 1.37 (s, 3H, CH_3).	176.4 (C=O), 162.6 (N-C=), 147.6 (*i*-Cph-N), 133.3 (*i*-Cph), 129.5 (CH, Ph), 125.8 (CH, Ph), 125.7 (CH, Ph), 124.9 (CH, Ph), 97.7 (CH nacac backbone), 23.5 (CH_3), 23.4 (CH_3), 18.7 (CH_3).
4b	7.13 (t, J_{HH} = 7.6 Hz, 1H, Ph), 6.94 (d, J_{HH} = 7.6 Hz, 1H, Ph), 6.79 (s, 1H, Ph), 6.76 (d, J_{HH} = 7.8 Hz, 1H, Ph), 4.83 (s, 1H, CH nacac backbone), 2.33 (s, 3H, CH_3), 1.66 (s, 3H, CH_3), 1.39 (s, 3H, CH_3).	176.1 (C=O), 162.8 (N-C=), 148.6 (*i*-Cph-N), 137.5 (*i*-Cph), 127.7 (CH, Ph), 126.8 (CH, Ph), 125.4 (CH, Ph), 123.1 (CH, Ph), 97.9 (CH nacac backbone), 23.9 (CH_3), 23.7 (CH_3), 21.4 (CH_3).
4c	7.7 (d, J_{HH} = 12.0 Hz, 2H, Ph), 6.85 (d, J_{HH} = 7.7 Hz, 2H, Ph), 4.83 (s, 1H, CH nacac backbone), 2.31 (s, 3H, CH_3), 1.66 (s, 3H, CH_3), 1.40 (s, 3H, CH_3).	176.2 (C=O), 162.9 (N-C=), 146.1 (*i*-Cph-N), 134.0 (*i*-Cph), 128.5 (CH), 125.9 (CH), 97.9 (CH nacac backbone), 23.9 (CH_3), 23.6 (CH_3), 21.1 (CH_3).
4d	6.95-6.92 (m, 2H, Ph), 6.78 (d, J_{HH} = 7.8 Hz, 1H, Ph), 4.83 (s, 1H, CH nacac backbone), 2.27 (s, 3H, CH_3), 2.21 (s, 3H, CH_3), 1.59 (s, 3H, CH_3), 1.40 (s, 3H, CH_3).	176.4 (C=O), 162.7 (N-C=), 144.9 (*i*-Cph-CH_3), 134.2 (*i*-Cph-N), 132.8 (CH), 130.2 (*i*-Cph), 126.3 (CH), 125.6 (CH), 97.7 (CH nacac backbone), 23.6 (CH_3), 23.4 (CH_3), 21.1 (CH_3), 18.6 (CH_3).
4e	6.93 (bs, 3H, Ph), 4.85 (s, 1H, CH nacac backbone), 2.25 (s, 6H, CH_3), 1.53 (s, 3H, CH_3), 1.37 (s, 3H, CH_3).	176.6 (C=O), 162.2 (N-C=), 146.4 (*i*-Cph-N), 132.7 (*i*-Cph), 127.3 (CH), 124.7 (CH), 97.5 (CH nacac backbone), 23.5 (CH_3), 22.6 (CH_3), 18.9 (CH_3).
4f	6.77 (s, 1H, Ph), 6.58 (s, 2H, Ph), 4.82 (s, 1H, CH nacac backbone), 2.29 (s, 6H, CH_3, Ph), 1.67 (s, 3H, CH_3), 1.41 (s, 3H, CH_3).	175.9 (C=O), 162.7 (N-C=), 148.4 (*i*-Cph-N), 137.2 (*i*-Cph), 126.2 (CH), 123.8 (CH), 97.9 (CH nacac backbone), 23.8 (CH_3), 23.7 (CH_3), 21.4 (CH_3).
4g	6.80 (s, 2H, Ph), 4.83 (s, 1H, CH nacac backbone), 2.23 (s, 3H, CH_3), 2.19 (s, 6H, CH_3), 1.52 (s, 3 H, CH_3), 1.39 (s, 3H, CH_3).	176.6 (C=O), 162.3 (N-C=), 143.8 (*i*-Cph-N), 133.9 (*i*-Cph), 132.4 (*i*-Cph), 128.0 (CH), 97.5 (CH nacac backbone), 23.5 (CH_3), 22.5 (CH_3), 21.1 (CH_3), 18.9 (CH_3).
4h	7.00 (d, J_{HH} = 7.8 Hz 1H, Ph), 6.73 (s, 1H, Ph), 6.68 (d, J_{HH} = 8.0 Hz, 1H, Ph), 4.81 (s, 1H, CH nacac backbone), 2.23 (s, 3H, CH_3), 2.20 (s, 3H, CH_3), 1.66 (s, 3H, CH_3), 1.39 (s, 3H, CH_3).	176.1 (C=O), 162.8 (N-C=), 146.2 (*i*-Cph-N), 135.7 (*i*-Cph), 132.6 (CH), 129.0 (*i*-Cph), 127.3 (CH), 123.3 (CH), 97.9 (CH nacac backbone), 23.9 (CH_3), 23.7 (CH_3), 19.9 (CH_3), 19.4 (CH_3).
4i	6.99 (d, J_{HH} = 7.6 Hz, 2H, Ph), 6.87 (d, J_{HH} = 7.7 Hz, 1H, Ph), 6.71 (s, 1H, Ph), 4.83 (s, 1H, CH nacac backbone), 2.30 (s, 3H, CH_3), 2.20 (s, 3H, CH_3), 1.59 (s, 3H, CH_3), 1.39 (s, 3H, CH_3).	176.3 (C=O), 162.5 (N-C=), 147.2 (*i*-Cph-N), 135.1 (*i*-Cph), 130.0 (*i*-Cph), 129.3 (*i*-Cph), 126.4 (CH), 125.6 (CH), 97.7 (CH nacac backbone), 23.6 (CH_3), 23.4 (CH_3), 21.1 (CH), 18.3 (CH).
4j	7.12 (s, 1H, Ph), 7.09 (d, J_{HH} = 7.7 Hz, 1H, Ph), 6.82 (dd, J_{HH} = 7.7 Hz, 4.7 Hz, 1H, Ph), 4.86 (s, 1H, CH nacac backbone), 2.21 (s, 3H, CH_3), 1.59 (s, 3H, CH_3), 1.41 (s, 3H, CH_3).	176.9 (CO), 162.8 (N-C=), 146.0 (ipso-Cph), 135.3 (*i*-Cph), 130.0 (CH), 129.3 (*i*-Cph), 127.2 (CH), 125.8 (CH), 97.9 (CH nacac backbone), 23.8 (CH_3), 23.5 (CH_3) ppm, 18.6 (CH_3) ppm.

Table S4. Analysis for each peak observed from HRMS for complexes **4a–j**.

4a				
Pd Isotope	**#^{13}C**	**Calculated [M+H]$^+$**	**Observed m/z**	**Notes**
^{102}Pd	0	479.12800	479.32101	Monoisotopic ^{102}Pd
^{104}Pd	0	481.12640	481.12341	Monoisotopic ^{104}Pd
^{105}Pd	0	482.12750	482.12474	Monoisotopic ^{105}Pd
^{106}Pd	0	483.12590	483.12391	Monoisotopic ^{106}Pd
^{106}Pd	1	484.12923	484.12635	^{13}C satellite ^{106}Pd
^{108}Pd	0	485.12630	485.12397	Monoisotopic ^{108}Pd
^{108}Pd	1	486.12963	486.12744	^{13}C satellite ^{108}Pd
^{110}Pd	0	487.12760	487.12509	Monoisotopic ^{110}Pd
^{110}Pd	1	488.13093	488.12815	^{13}C satellite / adduct
4b				
Pd Isotope	**#^{13}C**	**Calculated [M+H]$^+$**	**Observed m/z**	**Notes**
^{102}Pd	0	479.12800	479.12567	Monoisotopic ^{102}Pd
^{102}Pd	1	480.13133	480.12567	^{13}C satellite ^{102}Pd
^{104}Pd	0	481.12640	481.12737	Monoisotopic ^{104}Pd
^{105}Pd	0	482.12750	482.12684	Monoisotopic ^{105}Pd
^{106}Pd	0	483.12590	483.12749	Monoisotopic ^{106}Pd
^{106}Pd	1	484.12923	484.34503	^{13}C satellite ^{106}Pd
^{108}Pd	0	485.12630	485.16542	Monoisotopic ^{108}Pd
^{108}Pd	1	486.12963	485.30033	^{13}C satellite ^{108}Pd
^{108}Pd	1	486.12963	486.16587	^{13}C satellite ^{108}Pd
^{110}Pd	0	487.12760	487.12509	Monoisotopic ^{110}Pd
^{110}Pd	1	488.13093	488.12815	^{13}C satellite ^{110}Pd
^{110}Pd	2	~489.13426	489.18050	2 ^{13}C satellite
^{110}Pd	2	~489.13426	489.31050	2 ^{13}C satellite / adduct
4c				
Pd Isotope	**#^{13}C**	**Calculated [M+H]$^+$**	**Observed m/z**	**Notes**
^{102}Pd	0	479.12800	479.10229	Monoisotopic ^{102}Pd
^{102}Pd	1	480.13133	480.12567	^{13}C satellite ^{102}Pd
^{104}Pd	0	481.12640	481.15242	Monoisotopic ^{104}Pd
^{105}Pd	0	482.12750	482.12684	Monoisotopic ^{105}Pd
^{106}Pd	0	483.12590	483.34186	Monoisotopic ^{106}Pd
^{106}Pd	1	484.12923	484.12457	^{13}C satellite ^{106}Pd
^{108}Pd	0	485.12630	485.07917	Monoisotopic ^{108}Pd
^{108}Pd	1	486.12963	486.08154	^{13}C satellite ^{108}Pd
^{110}Pd	0	487.12760	487.07277	Monoisotopic ^{110}Pd
^{110}Pd	1	488.13093	488.12815	^{13}C satellite ^{110}Pd
4d				
Pd Isotope	**#^{13}C**	**Calculated [M+H]$^+$ (5 decimals)**	**Observed m/z**	**Notes**
^{102}Pd	1	507.15933	507.15841	^{13}C satellite ^{102}Pd
^{104}Pd	0	508.15440	508.12540	Monoisotopic ^{104}Pd
^{105}Pd	0	509.15550	509.15539	Monoisotopic ^{105}Pd
^{106}Pd	0	510.15390	510.15676	Monoisotopic ^{106}Pd
^{106}Pd	1	511.15723	511.15586	^{13}C satellite ^{106}Pd
^{108}Pd	0	512.15430	512.15874	Monoisotopic ^{108}Pd
^{108}Pd	1	513.15763	513.15567	^{13}C satellite ^{108}Pd
^{110}Pd	0	514.15560	514.15919	Monoisotopic ^{110}Pd
^{110}Pd	1	515.15893	515.15781	^{13}C satellite ^{110}Pd
^{110}Pd	2	516.16226	516.16017	2 ^{13}C satellite / minor peak
4e				
Pd Isotope	**#^{13}C**	**Calculated [M+H]$^+$ (5 decimals)**	**Observed m/z**	**Notes**
^{105}Pd	0	509.15550	509.15482	Monoisotopic ^{105}Pd
^{106}Pd	0	510.15390	510.15602	Monoisotopic ^{106}Pd
^{106}Pd	1	511.15723	511.15555	^{13}C satellite ^{106}Pd
^{108}Pd	0	512.15430	512.15794	Monoisotopic ^{108}Pd
^{108}Pd	1	513.15763	513.15536	^{13}C satellite ^{108}Pd
^{110}Pd	0	514.15560	514.15856	Monoisotopic ^{110}Pd
^{110}Pd	1	515.15893	515.15726	^{13}C satellite ^{110}Pd
^{110}Pd	2	516.16226	516.16193	2 ^{13}C satellite / minor peak
4f				
Pd Isotope	**#^{13}C**	**Calculated [M+H]$^+$**	**Observed m/z**	**Notes**
^{102}Pd	1	507.15933	507.15921	^{13}C satellite ^{102}Pd
105Pd	0	509.15550	509.15636	Monoisotopic ^{105}Pd

106Pd	0	510.15390	510.15747	Monoisotopic ^{106}Pd
106Pd	1	511.15723	511.15553	^{13}C satellite ^{106}Pd
108Pd	0	512.15430	512.15997	Monoisotopic ^{108}Pd
108Pd	1	513.15763	513.15566	^{13}C satellite ^{108}Pd
110Pd	0	514.15560	514.16123	Monoisotopic ^{110}Pd
110Pd	1	515.15893	515.15950	^{13}C satellite ^{110}Pd
110Pd	2	516.16226	516.16123	2 ^{13}C satellite / minor peak

4g

Pd Isotope	**#^{13}C**	**Calculated [M+H]$^+$**	**Observed m/z**	**Notes**
^{102}Pd	1	535.19353	535.19205	^{13}C satellite ^{102}Pd
^{104}Pd	0	536.18860		Monoisotopic ^{104}Pd
^{105}Pd	0	537.18970	537.18911	Monoisotopic ^{105}Pd
^{106}Pd	0	538.19010	538.19063	Monoisotopic ^{106}Pd
^{108}Pd	0	540.19050	540.19310	Monoisotopic ^{108}Pd
^{108}Pd	1	541.19383	541.18896	^{13}C satellite ^{108}Pd
^{110}Pd	0	542.19180	542.19407	Monoisotopic ^{110}Pd
^{110}Pd	1	543.19513	543.19194	^{13}C satellite ^{110}Pd
^{110}Pd	2	544.19846	544.19522	2 ^{13}C satellite / minor peak

4h

Pd Isotope	**#^{13}C**	**Calculated [M+H]$^+$**	**Observed m/z**	**Notes**
^{105}Pd	0	509.15550	509.15749	Monoisotopic ^{105}Pd
^{106}Pd	0	510.15390	510.15824	Monoisotopic ^{106}Pd
^{106}Pd	1	511.15723	511.15782	^{13}C satellite ^{106}Pd
^{108}Pd	0	512.15430	512.16075	Monoisotopic ^{108}Pd
^{108}Pd	1	513.15763	513.15770	^{13}C satellite ^{108}Pd
^{110}Pd	0	514.15560	514.16140	Monoisotopic ^{110}Pd
^{110}Pd	1	515.15893	515.15976	^{13}C satellite ^{110}Pd
^{110}Pd	2	516.16226	516.16182	2 ^{13}C satellite / minor peak

4i

Pd Isotope	**#^{13}C**	**Calculated [M+H]$^+$**	**Observed m/z**	**Notes**
^{105}Pd	0	509.15550	509.15735	Monoisotopic ^{105}Pd
^{106}Pd	0	510.15390	510.15930	Monoisotopic ^{106}Pd
^{106}Pd	1	511.15723	511.15810	^{13}C satellite ^{106}Pd
^{108}Pd	0	512.15430	512.16103	Monoisotopic ^{108}Pd
^{108}Pd	1	513.15763	513.15819	^{13}C satellite ^{108}Pd
^{110}Pd	0	514.15560	514.16262	Monoisotopic ^{110}Pd
^{110}Pd	1	515.15893	515.16063	^{13}C satellite ^{110}Pd
^{110}Pd	2	516.16226	516.16278	2 ^{13}C satellite / minor peak
^{110}Pd	2	516.16226	517.36075	Likely adduct or combined isotopic contribution

4j

Pd isotope	**Cl isotope**	**#^{13}C**	**Calculated [M+H]$^+$**	**Observed m/z**	**Notes**
^{102}Pd	^{35}Cl$_2$	0.00000	549.04296	549.04296	Monoisotopic ^{102}Pd + ^{35}Cl$_2$
^{102}Pd	^{35}Cl$_2$	1.00000	550.04631	550.04581	^{13}C satellite
^{102}Pd	^{35}Cl^{37}Cl	0.00000	551.03991	551.04546	Cl M+2
^{104}Pd	^{35}Cl$_2$	0.00000	551.04033	550.04581	^{104}Pd monoisotopic (overlaps with ^{13}C peak)
^{105}Pd	^{35}Cl$_2$	0.00000	552.04140	552.04377	^{105}Pd monoisotopic
^{106}Pd	^{35}Cl$_2$	0.00000	553.03950	553.04397	^{106}Pd monoisotopic
^{108}Pd	^{35}Cl$_2$	0.00000	555.03900	555.31421	^{108}Pd monoisotopic
^{108}Pd	^{35}Cl$_2$	1.00000	556.04235	556.31741	^{108}Pd + ^{13}C (also small Cl contribution)
^{102}Pd	^{37}Cl$_2$	0.00000	553.03500	553.04397	^{102}Pd + ^{37}Cl$_2$
^{105}Pd	^{35}Cl^{37}Cl	0.00000	554.03805	554.04579	^{105}Pd + ^{35}Cl^{37}Cl
^{106}Pd	^{35}Cl^{37}Cl	0.00000	555.03615	555.31421	^{106}Pd + ^{35}Cl^{37}Cl
^{110}Pd	^{35}Cl$_2$	0.00000		556.31741	^{110}Pd + ^{35}Cl$_2$

Table S5. Crystal data and structure refinement for compound **4c**.

	4c
Empirical formula	$C_{24}H_{28}N_2O_2Pd$
Formula weight	482.88
Temperature	120.02(10) K
Wavelength	1.54184 Å
Crystal system	Triclinic
Space group	*P -1*
Unit cell dimensions	
A	7.4798(3) Å
B	7.8326(3) Å
C	9.4659(4) Å
α	78.533(3)°
β	86.809(3)°
γ	85.861(3)°
Volume	541.60(4)Å^3
Z	1
Density (calculated)	1.481 Mg/m^3
Absorption coefficient	7.077 mm^{-1}
F(000)	248
Crystal size	366 · 0.256 · 0.102 mm^3
Theta range for data collection	4.771 to 66.475°
Index ranges	–8<= *h* <=8, –8<= *k* <=9, –9<= l <=11
Reflections collected	7423
Independent reflections	1900 (R_{int} = 0.0662)
Completeness to (theta) =	(66.475) 99.7 %
Absorption correction	Gaussian
Max. and min. transmission	1.00000 and 0.176
Refinement method	Full-matrix least-squares on F^2
Data / restraints / parameters	1900 / 0 / 136
Goodness-of-fit on F^2	1.089
Final *R* indices [*I*>2sigma(*I*)]	*R*1 = 0.0389, *wR*2 = 0.0979
R indices (all data)	*R*1 = 0.0389, *wR*2 = 0.0979+
Largest diff. peak and hole	2.015 and -1.426 e·Å^{-3}

Table S6. Selected experimental and calculated bond distances (Å) for compounds **4c**. Calculations performed at the PBE0/def2-TZVP/CPCM (chloroform) level of theory.

	4c [Å] Exp.	**4c [Å] Cal.**
C(1)-C(2)	1.501(5)	1.501
C(2)-O(1)	1.272(5)	1.276
C(2)-C(3)	1.380(6)	1.381
C(3)-C(4)	1.417(5)	1.411
C(4)-N(1)	1.308(5)	1.313
C(4)-C(5)	1.521(5)	1.505
C(6)-N(1)	1.437(4)	1.423
O(1)-Pd(1)	1.991(3)	1.983
Pd(1)-N(1)	2.031(3)	2.040

Table S7. Selected experimental and calculated bond angles (°) for compounds **4c**. Calculations performed at the PBE0/def2-TZVP/CPCM (chloroform) level of theory.

	4c [º]	Calculated **4c [º]**
O(1)-C(2)-C(3)	126.6(3)	126.40
O(1)-C(2)-C(1)	113.8(3)	114.00
C(3)-C(2)-C(1)	119.5(3)	119.54
C(2)-C(3)-C(4)	126.6(4)	126.87
N(1)-C(4)-C(3)	124.9(3)	124.49
N(1)-C(4)-C(5)	119.8(3)	119.67
C(3)-C(4)-C(5)	115.4(3)	115.85
C(2)-O(1)-Pd(1)	125.4(2)	126.02
O(1)-Pd(1)-N(1)	92.50(12)	92.11
C(4)-N(1)-C(6)	118.2(3)	117.93
C(4)-N(1)-Pd(1)	123.7(2)	124.11
C(6)-N(1)-Pd(1)	118.1(2)	117.97
N(1)-Pd(1)-N(1)1	180	197.98
O(1)-Pd(1)-O(1)1	180	180

Table S8. Interaction topology energy table for **4c** at the HF/3-21G level of theory.

[a]C	[b]N	[c]Symop	[d]R	[e]Electron Density	E_{ele}	E_{pol}	E_{dis}	E_{rep}	E_{tot}
	2	x, y, z	15.88	HF/3-21G	-0.1	0	-4.8	1.2	-3.5
	2	x, y, z	11.22	HF/3-21G	-1.5	-0.3	-25.7	9.9	-16.9
	2	x, y, z	9.46	HF/3-21G	-3.6	-0.7	-33	12.8	-23.5
	2	x, y, z	7.49	HF/3-21G	-8.1	-3.5	-64.5	30.3	-44.1
	2	x, y, z	11.74	HF/3-21G	-0.3	-0.1	-8.6	2.8	-5.9
	2	x, y, z	13.42	HF/3-21G	-4.7	-1.9	-34.8	18.1	-22.8
	2	x, y, z	7.84	HF/3-21G	-14.2	-3.6	-66.5	32.3	-50.6

[a]Color codes indicate the molecule with the crystal structures, as shown in **Figure 4**. [b] N represents the number of molecules. [c] Symop is the relational symmetry operation to the ventral molecule. [d] R is the distance between the molecular centroids

Table S9. Absolute HOMO and LUMO energies and the HOMO-LUMO gap for **3a**–**j** calculated at PBE0/def2-TZVP/CPCM (chloroform). All energy units are given in eV.

Compounds			**Energy/eV**	**HL gap/eV**
3a	H	50.0	-6.031	4.8014
	L	51.0	-1.229	
3b	H	50.0	-6.025	4.7979
	L	51.0	-1.228	
3c	H	50.0	-5.957	4.7573
	L	51.0	-1.199	
3d	H	54.0	-5.936	4.7677
	L	55.0	-1.168	
4f	H	54.0	-6.230	5.3493
	L	55.0	-0.881	
3h	H	54.0	-5.994	4.7996
	L	55.0	-1.194	
3i	H	58.0	-6.207	5.3505
	L	59.0	-0.857	
3g	H	54.0	-5.946	4.8081
	L	55.0	-1.138	
3e	H	54.0	-5.995	4.7986
	L	55.0	-1.196	
3j	H	63.0	-7.214	7.0044
	L	64.0	-0.210	

Table S10. Absolute HOMO and LUMO energies and the HOMO-LUMO gap for **4a-j** calculated at PBE0/def2-TZVP/CPCM (chloroform). All energy units are given in eV.

Compounds			Energy/eV	HL gap/eV
4a	H-1	108	-7.5905	6.8995
	H	109	-6.9694	
	L	110	-0.0699	
	L+1	111	0.1691	
4b	H-1	108	-7.5907	6.8769
	H	109	-6.9455	
	L	110	-0.0686	
	L+1	111	0.1937	
4c	H-1	108	-7.5841	6.9135
	H	109	-6.9394	
	L	110	-0.0259	
	L+1	111	0.2028	
4d	H-1	116	-7.493	6.9286
	H	117	-6.9355	
	L	118	-0.0069	
	L+1	119	0.2023	
4e	H-1	116	-7.5972	6.915
	H	117	-6.967	
	L	118	-0.052	
	L+1	119	0.1628	
4f	H-1	116	-7.5689	6.8811
	H	117	-6.9226	
	L	118	-0.0415	
	L+1	119	0.2142	
4g	H-1	124	-7.3019	6.5697
	H	125	-6.7124	
	L	126	-0.1427	
	L+1	127	0.0888	
4h	H-1	116	-7.5345	6.9171
	H	117	-6.916	
	L	118	0.0011	
	L+1	119	0.2246	
4i	H-1	116	-7.5522	6.888
	H	117	-6.9417	
	L	118	-0.0537	
	L+1	119	0.195	
4j	H-1	124	-7.7994	7.4741
	H	125	-7.6695	
	L	126	-0.1954	
	L+1	127	-0.0811	

Table S11. Experimental and calculated [TD-CAM-B3LYP/def2-TZVP/CPCM(chloroform)] UV–Vis absorption bands of ligands **3a-j** in chloroform solvent.

Compound	Experimental UV-Vis bands		Calculated (TD-DFT) UV-Vis bands			
	λ_{max} (nm)	ε (× 10^4 $M^{-1}cm^{-1}$) [Conc. (mol/L)]	State	λ_{max} (nm)	Oscillator strength (*f*)	Major contribution (Coefficient)
3a	318	2.9 [2.9 × 10^{-5}]	S_1	298.1	0.640	H → L (0.930)
3b	325	2.9 [3.0× 10^{-5}]	S_1	297.4	0.712	H → L (0.946)
3c	323	2.7 [2.7× 10^{-5}]	S_1	298.7	0.763	H → L (0.941)
3d	318	3.4 [2.5 × 10^{-5}]	S_1	299.2	0.684	H → L (0.924)
3e	310	3.1 [2.5 × 10^{-5}]	S_2	268.8	0.571	H → L (0.968)
3f	327	2.0 [2.8 × 10^{-5}]	S_1	297.2	0.716	H → L (0.940)
3g	312	1.5 [4.7 × 10^{-5}]	S_2	268.9	0.591	H → L (0.968)
3h	322	3.3 [2.8 × 10^{-5}]	S_1	295.7	0.738	H → L (0.930)
3i	317	3.0 [2.6 × 10^{-5}]	S_1	298.1	0.645	H → L (0.923)
3j	309	1.7 [4.5 × 10^{-5}]	S_1	297.9	0.665	H → L (0.904)

Table S12. Experimental and calculated [TD-CAM-B3LYP/def2-TZVP/CPCM(chloroform)] UV–Vis absorption bands of complexes **4a-j** in chloroform as the solvent.

	Experimental UV-Vis bands				**Calculated (TD-DFT) UV-Vis bands**			
Compound	**λ_{max} (nm)**	**ε (× 10^4 $M^{-1}cm^{-1}$) [Conc. (mol/L)]**	**λ_{max} (nm)**	**ε ($M^{-1}cm^{-1}$)**	**State**	**λ_{max} (nm)**	**Oscillator strength (*f*)**	**Major contribution (Coefficient)**
4a	339	1.0 [4.3 × 10^{-5}]	400	1905	S_5	315.3	0.361	H-1 → L+1 (0.748)
4b	341	1.2 [6.4 × 10^{-5}]	420	1087	S_5	315.3	0.382	H-1 → L+1 (0.755)
4c	335	1.3 [6.5 × 10^{-5}]	430	615	S_5	315.4	0.374	H-1 → L+1 (0.752)
4d	337	1.3 [6.0 × 10^{-5}]	420	802	S_5	315.6	0.360	H-1 → L+1 (0.742)
4e	336	1.2 [5.9 × 10^{-5}]	420	660	S_5	315.9	0.341	H-1 → L+1 (0.746)
4f	342	1.0 [6.0 × 10^{-5}]	427	864	S_5	315.3	0.391	H-1 → L+1 (0.751
4g	342	0.98 [7.6 × 10^{-5}]	420	630	S_5	29 6.2	0.331	H-1 → L+1 (0.739)
4h	335	1.2 [5.9 × 10^{-5}]	408	1598	S_5	315.5	0.380	H-1 → L+1 (0.750)
4i	335	1.3 [5.9 × 10^{-5}]	428	741	S_5	315.4	0.365	H-1 → L+1 (0.743)
4j	324	1.6 [5.4 × 10^{-5}]	402	640	S_5	295.7	0.382	H → L+1 (0.742)

Table S13. TGA data of **4a–j.**

Compound	25-220 °C	220-325 °C	325-900 °C	%Ash
4a	0	67	9	24
4b	0	62	12	26
4c	0.1	60	13	27
4d	0	61	12	27
4e	0	61	12	28
4f	0	74	4	21
4g	0	75	1	24
4h	0	54	13	34
4i	1	67	9	23
4j	0	75	7	18

Table S14. Chemosensitivity results of complexes **4** and **5** against fibroblast, MCF-7 and HCT-116. Values are stated as 50% inhibitory concentrations (IC_{50}) ± Standard Deviation (SD) and are triplicate repeats.

		IC50 against fibroblast		IC50 against MCF7		IC50 against HCT				IC50 against fibroblast		IC50 against MCF7		IC50 against HCT	
Comp.	Substituent	cell viability data	Mean±SD	cell viability data	Mean ±SD	cell viability data	Mean ±SD	**Comp.**	Substituent	cell viability data	Mean ±SD	cell viability data	Mean ±SD	cell viability data	Mean ±SD
4a	2-Me	121.1; 116.4; 142.5	126.7±11.36	112.4; 118.3; 135.4	122.03±9.75	106.3; 114.3; 132.4	117.67 ±10.92	**5a**	2-Cl	32.42; 28.18; 30.31	30.30 ±1.73	48.57; 28.58; 32.56	36.57 ±8.64	25.79; 42.48; 61.13	43.13 ±14.43
4b	3-Me	35.88; 41.94; 37.09	38.30±2.62	13.61; 19.40; 10.47	14.49 ±3.70	36.02; 36.88; 35.41	36.10 ±0.60	**5b**	3-Cl	35.84; 27.08; 29.68	30.90 ±3.67	16.88; 14.62; 17.67	16.39 ±1.29	75.47; 76.63; 75.20	75.765 ±0.615
4c	4-Me	116.4; 101.7; 106.9	108.4±6.08	43.38; 59.22; 46.65	49.75 ±6.83	141.5; 135.2; 144.8	140.5 ±3.98	**5c**	4-Cl	11.26; 6.107; 11.98	9.78± 2.62	4.917; 5.904; 9.305	6.71± 1.88	115.2; 103.2; 119.7	112.7 ±6.96
4d	2,4-diMe	9.48; 13.84; 8.12	10.48±2.44	21.76; 17.11; 13.79	17.55 ±3.27	21.75; 42.26; 21.22	28.41 ±9.80	**5d**	2,4-Cl	107.5; 132.4; 145.5	128.5 ±15.76	106.9; 114.8; 133.7	118.47 ±11.24	98.10; 98.6; 91.2	95.93 ±3.329
4e	2,6-Me	55.07; 97.83; 72.01	74.97±17.58	48.50; 80.31; 59.48	62.76 ±13.19	65.81; 96.29; 88.89	83.66 ±12.98	**5e**	2,6-Cl	107.4; 115.7; 113.8	112.3 ±3.55	108.3; 119.2; 114.1	113.9 ±4.45	111.5; 115.8; 102.3	109.9 ±5.63
4f	3,5-Me	51.21; 47.31; 49.71	49.41±1.6	53.61; 50.70; 50.21	51.51 ±1.50	76.26; 71.19; 75.45	74.3± 2.2	**5f**	3,5-diCl	66.44; 93.92; 80.12	80.16 ±11.22	134.5; 122.8; 104.3	120.5 ±12.43	56.75; 38.70; 81.01	58.82 ±17.33
4g	2,4,6-Me	105.3; 109.5; 115.5	110.1±4.19	110.2; 121.5; 132.5	121.4 ±9.10	101.2; 104.5; 111.8	105.83 ±4.43	**5g**	2,4,6-Cl	117.7; 80.76; 94.96	97.81 ±15.21	126.2; 115.7; 102.3	114.7 ±9.78	153.5; 114.2; 123.7	130.5 ±16.74
4h	3,4-Me	162.18; 134.30; 145.81	147.4±11.41	11.73; 12.17; 17.02	13.64 ±2.40	37.57; 43.45; 39.94	40.32 ±2.42	**5h**	2,3-Cl comp	181.4; 103.8; 146.8	144.0 ±31.74	147.2; 125.9; 116.2	129.8 ±12.95	145.8; 154.9; 113.2	137.97 ±17.90
4i	2,5-Me	61.92; 39.75; 32.52	44.73±12.51	5.455; 5.954; 4.851	5.42± 0.45	10.95; 10.27; 30.38	17.20 ±9.32	**5i**	2,4,5-Cl	111.2; 149.5; 106.2	122.30 ±19.34	108.7; 115.8; 121.5	115.33 ±5.24	126.2; 167.5; 121.8	138.5 ±20.58
4j	4-Cl-2-Me	105.67; 107.54; 112.59	108.5±2.9	5.94; 7.47; 6.69	6.70± 0.62	115.5; 132.5; 101.2	116.4 ±12.79								
Cisplatin	Positive control	51.13; 53.79; 57.14	54.02±2.46	3.91; 6.07; 4.12	4.70± 0.97	13.08; 17.88; 12.18	14.38 ±2.50								

Table S15. Chemosensitivity results of ligands against fibroblast, MCF-7 and HCT-116. Values are stated as 50% inhibitory concentrations (IC_{50}) ± Standard Deviation (SD) and are triplicate repeats.

	IC50 against fibroblast		IC50 against MCF7		IC50 against HCT			IC50 against fibroblast		IC50 against MCF7		IC50 against HCT	
Substitue nt	cell viability data	Mean± SD	cell viability data	Mean± SD	cell viability data	Mean±SD	**Substitue nt**	cell viability data	Mean ±SD	cell viability data	Mean± SD	cell viability data	Mean±SD
2-Me lig	131.4; 172.7; 127.0	143.7± 20.58	111.0; 112.3; 106.6	109.97 ±2.43	122.6; 142.3;104 .6	123.17±15. 40	2-Cl lig	111.64; 112.17; 114.93	112.9 ±1.45	71.40; 71.29; 71.18	71.29± 0.089	39.99; 78.51; 71.03	63.18±16. 68
3-Me lig	109.1; 176.8; 113.1	133.0± 31.01	123.7; 141.7; 113.0	126.13 ±11.84	131.7; 116.3; 110.4	119.45±8.9 8	3-Cl lig	115.78; 116.40; 111.25	114.4 ±2.30	169.1; 120.6; 85.76	125.15 ±34.18	174.0; 115.5; 100.6	130.0±31. 68
4-Me lig	19.93; 18.32; 18.09	18.78± 0.819	14.84; 19.48; 15.67	16.66± 2.02	37.71; 55.84; 47.73	47.09±7.42	4-Cl lig	119.97; 159.38; 172.6	150.6 ±22.3 8	55.3; 62.99; 47.49	55.26± 6.33	42.28; 31.73; 36.92	36.98±4.3 1
2,4-diMe lig	67.14; 57.87; 66.64	63.88± 4.26	57.99; 66.3; 65.03	63.11± 3.65	77.95; 70.26; 50.22	66.14±11.6 8	2,4-Cl lig	102.8; 101.2; 11.4	105.1 3±4.4 8	113.4; 121.1; 130.9	121.8± 7.16	102.8; 101.2; 99.4	101.13±1. 39
2,6-diMe lig	49.34; 54.79; 67.26	57.13± 7.50	100.2; 99.03; 101.3	100.17 ±0.93	36.27; 33.08; 27.33	32.22±3.69	2,6-Cl lig	100.2; 100.5; 105.1	101.9 3±2.2 4	45.3; 48.2; 46.1	46.53± 1.22	110.2; 108.2; 111.6	110.0±1.3 40
3,5-diMe lig	51.10; 41.01; 54.31	48.81± 5.67	44.65; 33.90; 53.19	43.91± 7.89	18.38; 26.18; 11.43	18.66±6.03	3,5-diCl ligand	66.02; 60.90l; 61.90	62.94 ±2.22	134.0; 111.9; 114.2	120.03 ±9.92	29.31; 29.79; 29.70	29.6±0.21
2,4,6-Me	130.1; 156.1; 116.4	134.2± 16.46	123.3; 152.1; 140.3	138.57 ±11.82	150.7; 111.6; 137.3	133.2±16.2 2	2,4,6-triCl lig	43.09; 44.18; 45.33	44.2± 0.91	22.16; 26.77; 25.74	24.8±1 .97	26.13; 41.24; 60.87	42.7±14.2
3,4-diMe lig	40.08; 77.61; 60.17	59.285 ±15.33 5	103.5 ; 69.75 ;82.88	85.37± 13.89	28.11; 28.02; 16.08	24.07±5.65	2,3-Cl lig	107.2; 105.8; 106.9	106.6 ±0.60	111.2; 114.0; 115.1	113.43 ±1.64	106.0; 101.3; 103.9	103.73±1. 92
2,5-diMe lig	56.1; 42.29; 48.03	48.81± 5.66	41.44 ;54.58 ;35.71	43.91± 7.89	12.67; 26.90; 16.40	18.66±6.02	2,4,5-Cl lig	82.3; 83.5;79. 10	81.6± 1.85	60.3; 63.2; 55.1	59.5±3 .35	58.3; 55.4; 60.1	57.9±1.93
4-Cl-2-Me	130.7; 133.3; 121.3	128.4± 5.15	123.6; 139.7; 124.6	129.3± 7.37	139.4; 147.4; 111.6	132.8±15.3 4							

Table S16. Chemosensitivity results of complexes **6** and **7**, against HT 116 and MCF-7. Values are stated as 50 % inhibitory concentrations (IC_{50}) ± Standard Deviation (SD) and are triplicate repeats.[45,46]

Compound No.	Substituent	HCT 116	MCF-7	Compound No.	Substituent	HCT 116	MCF-7
6a	2-Me	3.45±0.20	35.61±0.16	**7a**	2-Cl	55.36±0.15	> 100
6b	3-Me	41.68±0.22	> 100	**7b**	3-Cl	14.16±0.15	> 100
6c	4-Me	1.73±0.22	> 100	**7c**	4-Cl	0.452±0.24	49.62±0.17
6d	2,4-Me	39.39±0.22	> 100	**7d**	2,4-Cl	13.35±0.16	61.95±0.12
6e	2,6-Me	24.97±0.23	> 100	**7e**	NA	NA	NA
8f	NA	NA	NA	**7f**	3,5-Cl	23.9±0.17	> 100
6g	2,4,6-Me	> 400	> 400	**7g**	NA	NA	NA
6h	3,4-Me	> 400	> 400	**7h**	3,4-Cl	48.01±0.16	> 100
6i	2,5-Me	>400	> 400	**7i**	NA	NA	NA
6j	4-Cl-2-Me	> 400	> 400	**7j**	NA	NA	NA
6k	NA	NA	NA	**7k**	2,3-Cl	34.83±0.16	> 100
6l	NA	NA	NA	**7l**	2,4,5-Cl	3.62±0.18	33.88±0.16
6m	NA	NA	NA	**7m**	H	6.91±0.21	81.05±0.09
6n	2-Et	> 400	> 400	**7n**	NA	NA	NA
Cisplatin	Positive control	14.38±2.5	4.7± 0.97				

Table S17. Lowest Binding Energy Values of Methyl- and Chloride-substituted Pd(II) Complexes with Targeted Proteins in MCF-7 (Breast Cancer).

Pd(II) Complex	Binding Affinity Scores (kcal/mol)	
	PIK3CA-E545K	ERBB4-Y1242C
4a (2-Me-C_6H_4)	–7.416	–5.967
4b (3-Me-C_6H_4)	–7.640	–7.849
4c (4-Me-C_6H_4)	–8.162	–7.937
4d (2,4-Me-C_6H_3)	–7.467	–6.019
4e (2,6-Me-C_6H_3)	–6.498	–4.623
4f (3,5-Me-C_6H_3)	–6.914	–6.279
4g (2,4,6-Me-C_6H_2)	–6.373	–4.386
4h (3,4-Me-C_6H_3)	–7.393	–8.059
4i (2,5-Me-C_6H_3)	–6.591	–4.672
4j (4-Cl-2-Me-C_6H_3)	–7.639	–6.253
5a (2-Cl-C_6H_4)	–7.591	–6.216
5b (3-Cl-C_6H_4)	–7.893	–8.245
5c (4-Cl-C_6H_4)	–8.469	–8.245
5d (2,4-Cl-C_6H_3)	–7.925	–6.599
5e (2,6-Cl-C_6H_3)	–6.870	–4.925
5f (3,5-Cl-C_6H_3)	–7.474	–6.773
5g (2,4,6-Cl-C_6H_2)	–7.119	–4.970
5h (2,3-Cl-C_6H_3)	–7.950	–6.332
5i (2,4,5-Cl-C_6H_2)	–6.847	–5.520

Table S18. Lowest Binding Energy Values of Methyl- and Chloride-substituted Pd(II) Complexes with Targeted Proteins in HCT-116 (Colon Cancer).

Pd(II) Complex	Binding Affinity Scores (kcal/mol)		
	KRAS-G13D	PIK3CA-H1047R	ATM-A112V
4a (2-Me-C_6H_4)	–5.589	–5.530	–7.324
4b (3-Me-C_6H_4)	–6.593	–6.651	–7.641
4c (4-Me-C_6H_4)	–6.870	–6.222	–7.383
4d (2,4-Me-C_6H_3)	–5.608	–5.078	–6.624
4e (2,6-Me-C_6H_3)	–4.960	–4.514	–6.394
4f (3,5-Me-C_6H_3)	–6.142	–5.770	–6.848
4g (2,4,6-Me-C_6H_2)	–5.197	–4.578	–6.283
4h (3,4-Me-C_6H_3)	–6.792	–6.030	–6.527
4i (2,5-Me-C_6H_3)	–5.180	–5.839	–6.592
4j (4-Cl-2-Me-C_6H_3)	–5.763	–5.358	–6.684
5a (2-Cl-C_6H_4)	–5.896	–6.094	–7.451
5b (3-Cl-C_6H_4)	–6.998	–6.764	–7.915
5c (4-Cl-C_6H_4)	–7.253	–6.414	–7.546
5d (2,4-Cl-C_6H_3)	–6.410	–5.594	–7.126
5e (2,6-Cl-C_6H_3)	–5.312	–4.884	–6.993
5f (3,5-Cl-C_6H_3)	–6.758	–5.896	–7.513
5g (2,4,6-Cl-C_6H_2)	–5.699	–5.156	–6.987
5h (2,3-Cl-C_6H_3)	–6.082	–5.660	–7.347
5i (2,4,5-Cl-C_6H_2)	–6.628	–5.668	–6.946

Table S19. List of qPCR primers.

Gene name	*Primer (5' to 3' direction)*
Bcl-2	F: GGACAACATCGCCCTGTGGA
	R: TCCACAAAGGCATCCCAGCC
18S rRNA	F: AGAAACGGCTACCACATCCA
	R: TACAGGGCCTCGAAAGAGTC
Bax	F: GGTCCGGGGAGCAGC
	R: GATCCTGGATGAAACCCTGAAG

Table S20. Bax:Bcl-2 ratio in different cell types after treatment with different concentration of compounds.

Cell line	Compound Concentration (µM)	$\Delta\Delta Ct_{Bax}$ ± SD	$\Delta\Delta Ct_{BcL2}$ ± SD	$\Delta\Delta Ct_{Bax}$: $\Delta\Delta Ct_{BcL2}$ Ratio
Fibroblast (4h)	294.86	0.07 ± 0.03	1.22 ± 0.45	0.06
	147.43	0.31 ± 0.03	0.71± 0.20	0.43
Fibroblast (4a)	294.86	1.59 ± 0.20	0.98 ± 0.24	1.62
	147.43	0.83 ± 0.25	1.14 ± 0.35	0.72
MCF-7 (4h)	27.2	2.59 ± 0.16	0.21 ± 0.09	12.3
	13.6	2.25 ± 0.09	0.87 ± 0.05	2.58
MCF-7 (4a)	27.2	0.65 ± 0.02	0.43 ± 0.00	1.51
	13.6	0.46 ± 0.16	0.35 ± 0.10	1.31
HCT116 (4h)	80.6	2.36 ± 0.31	0.41 ± 0.02	5.75
	40.3	1.26 ± 0.18	0.36 ± 0.15	3.50
HCT116 (4a)	80.6	1.03 ± 0.26	1.42 ± 0.40	0.72
	40.3	1.02 ± 0.11	1.40 ± 0.06	1.02

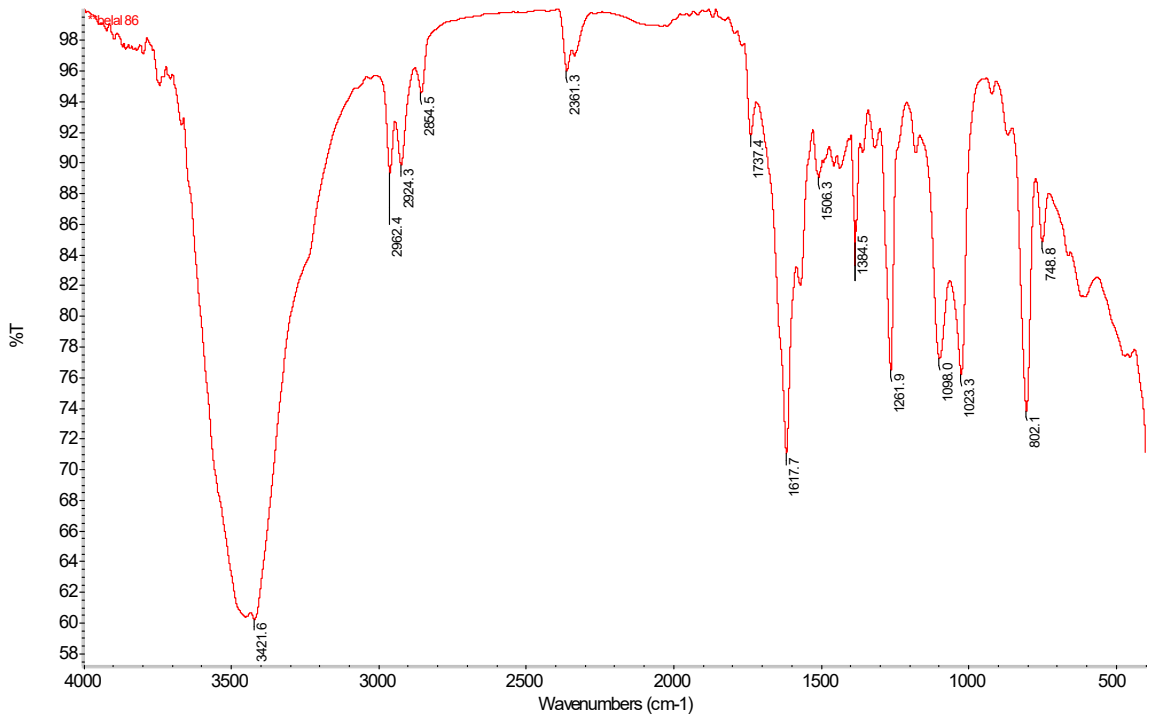

Figure S1. Infrared spectrum (KBr) of **3a.**

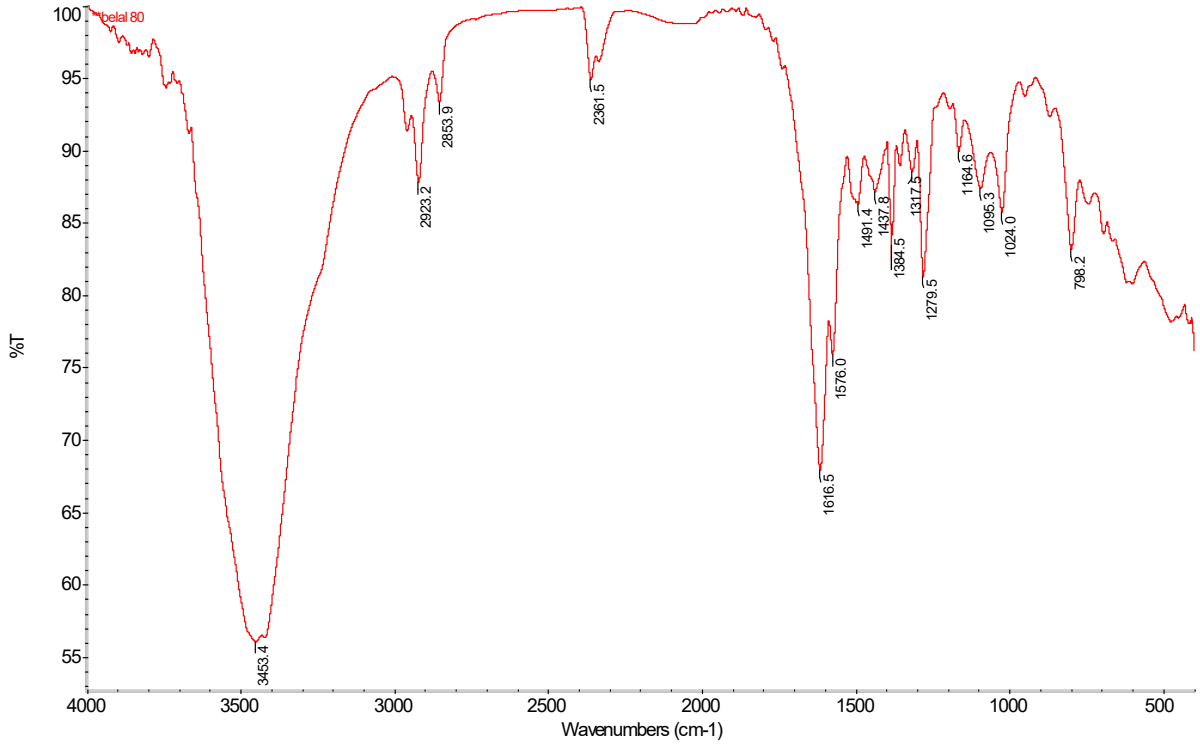

Figure S2. Infrared spectrum (KBr) of **3b.**

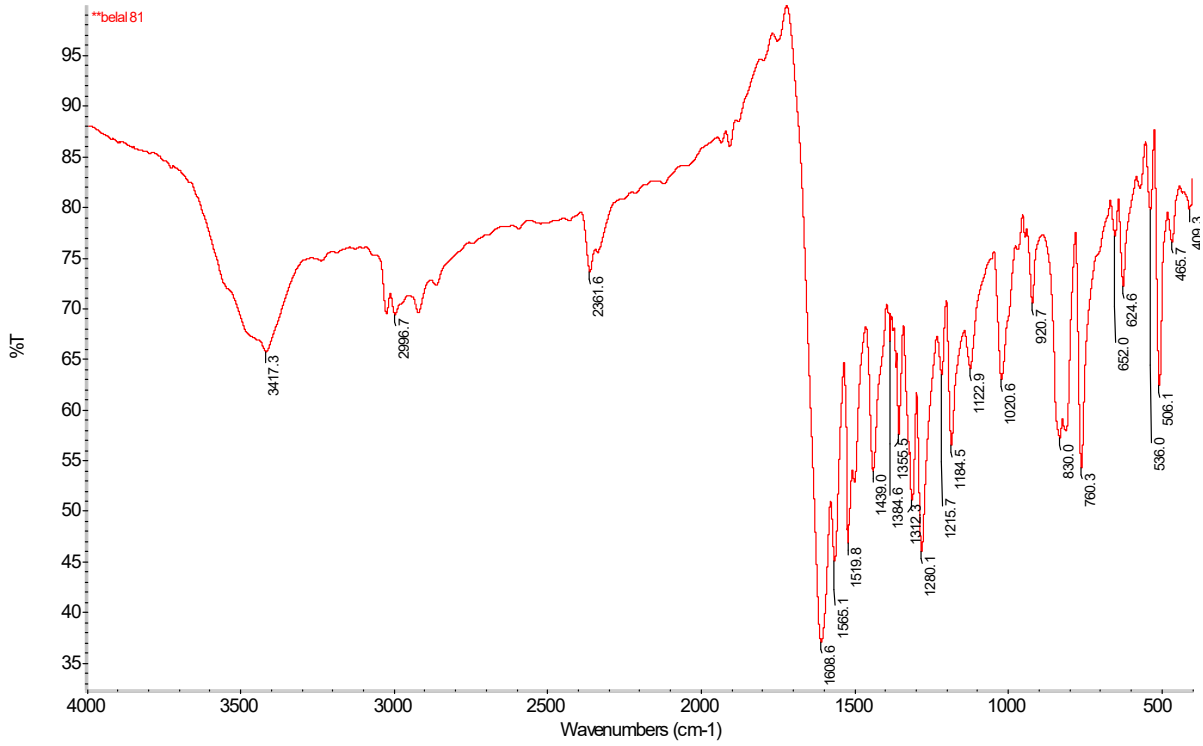

Figure S3. Infrared spectrum (KBr) of **3c.**

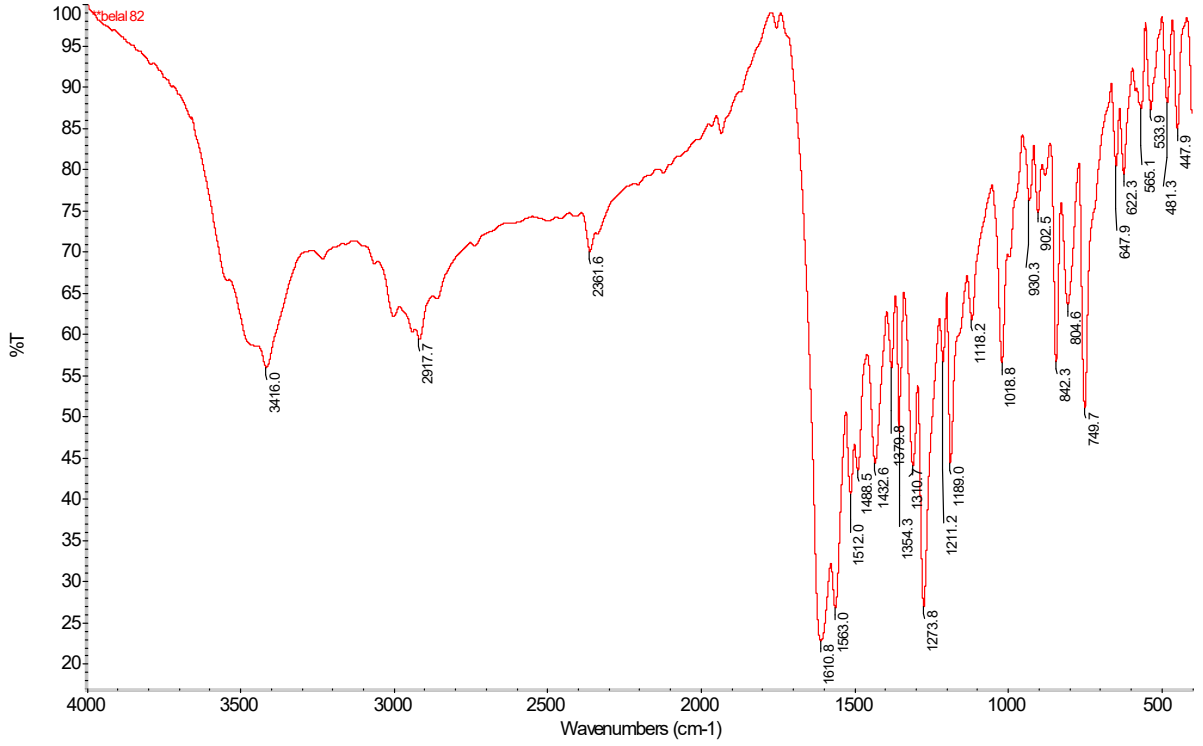

Figure S4. Infrared spectrum (KBr) of **3d.**

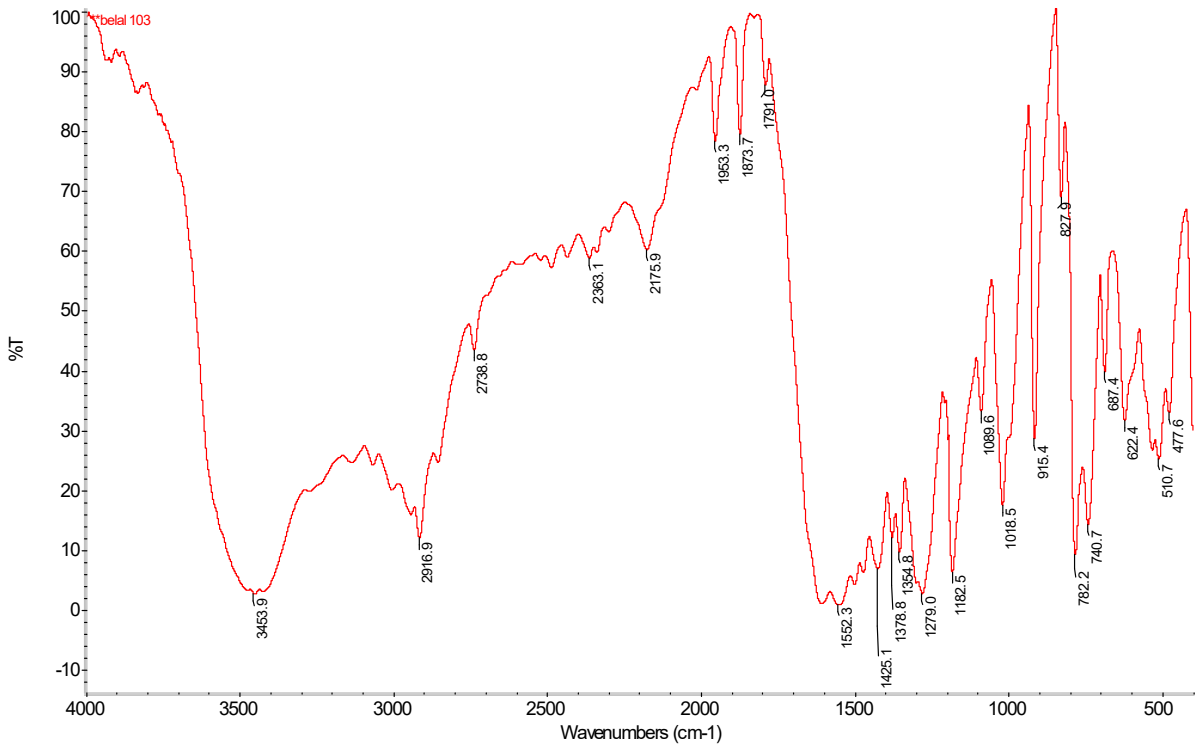

Figure S5. Infrared spectrum (KBr) of **3e.**

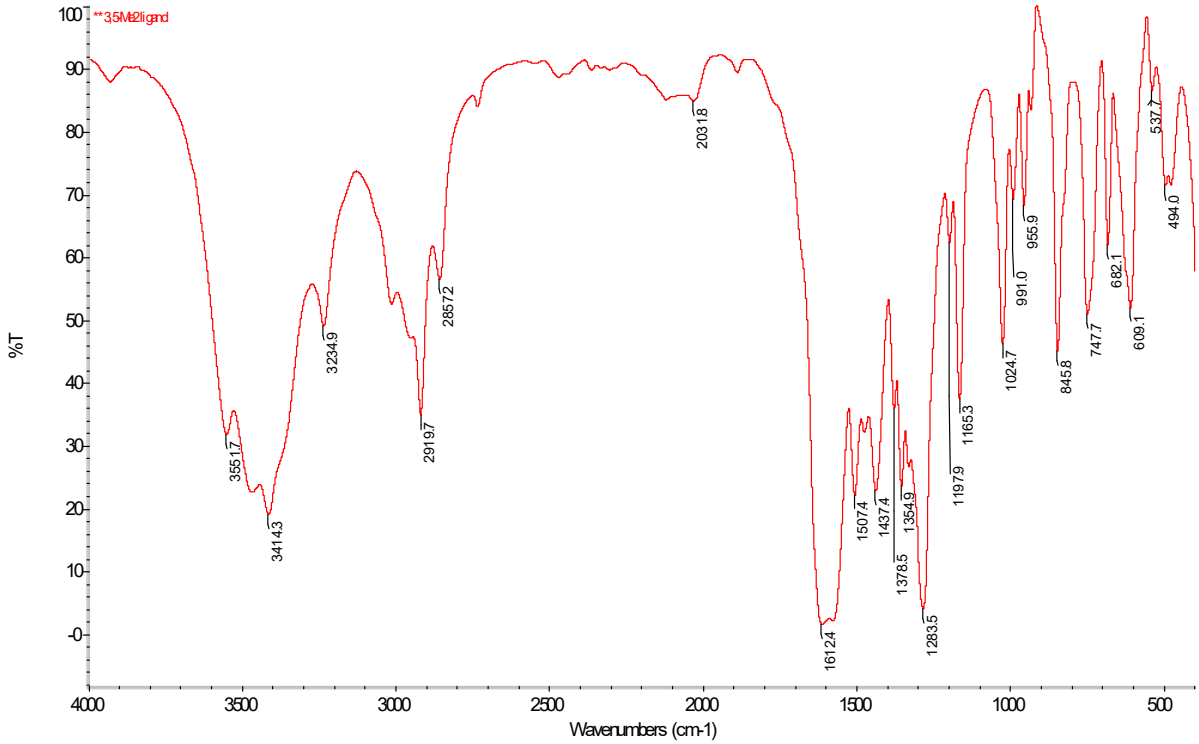

Figure S6. Infrared spectrum (KBr) of **3f.**

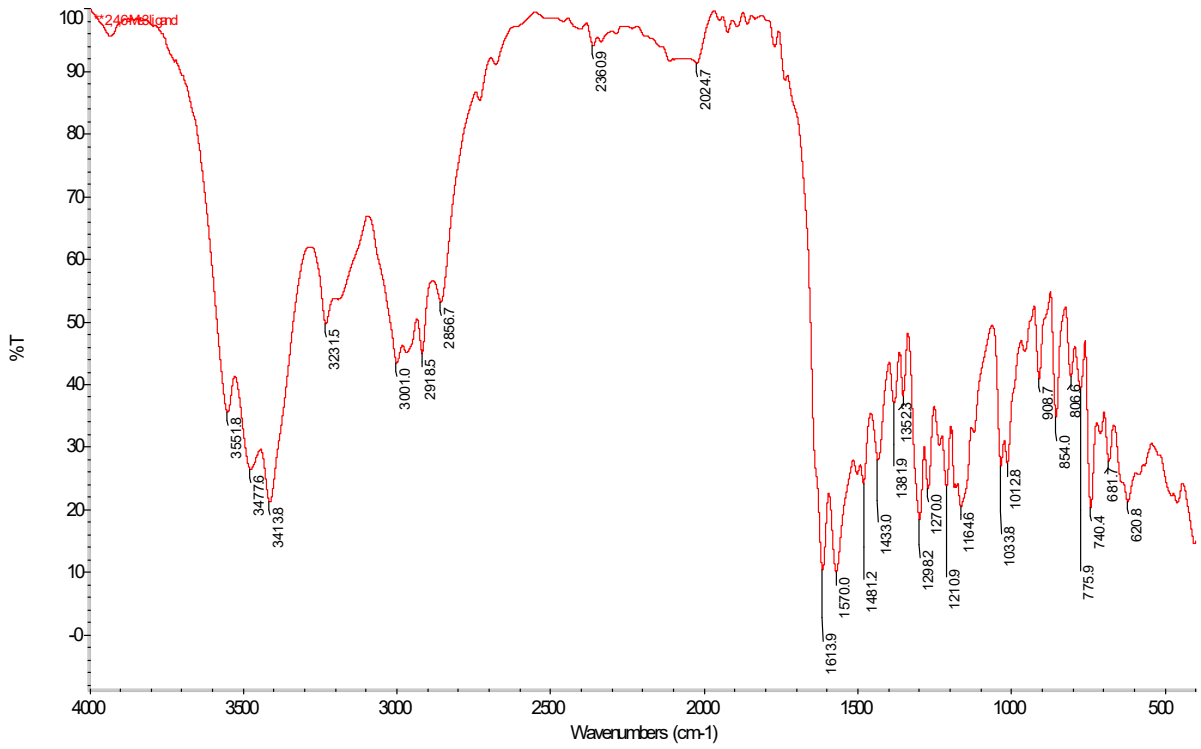

Figure S7. Infrared spectrum (KBr) of **3g.**

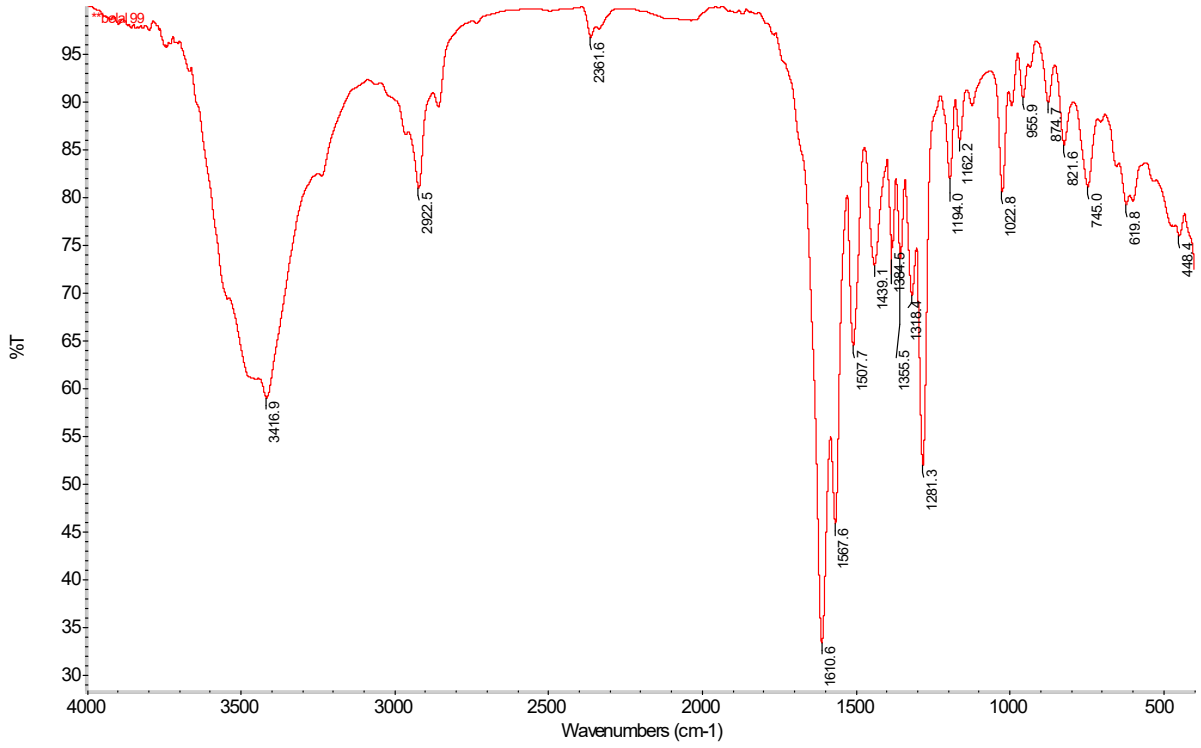

Figure S8. Infrared spectrum (KBr) of **3h.**

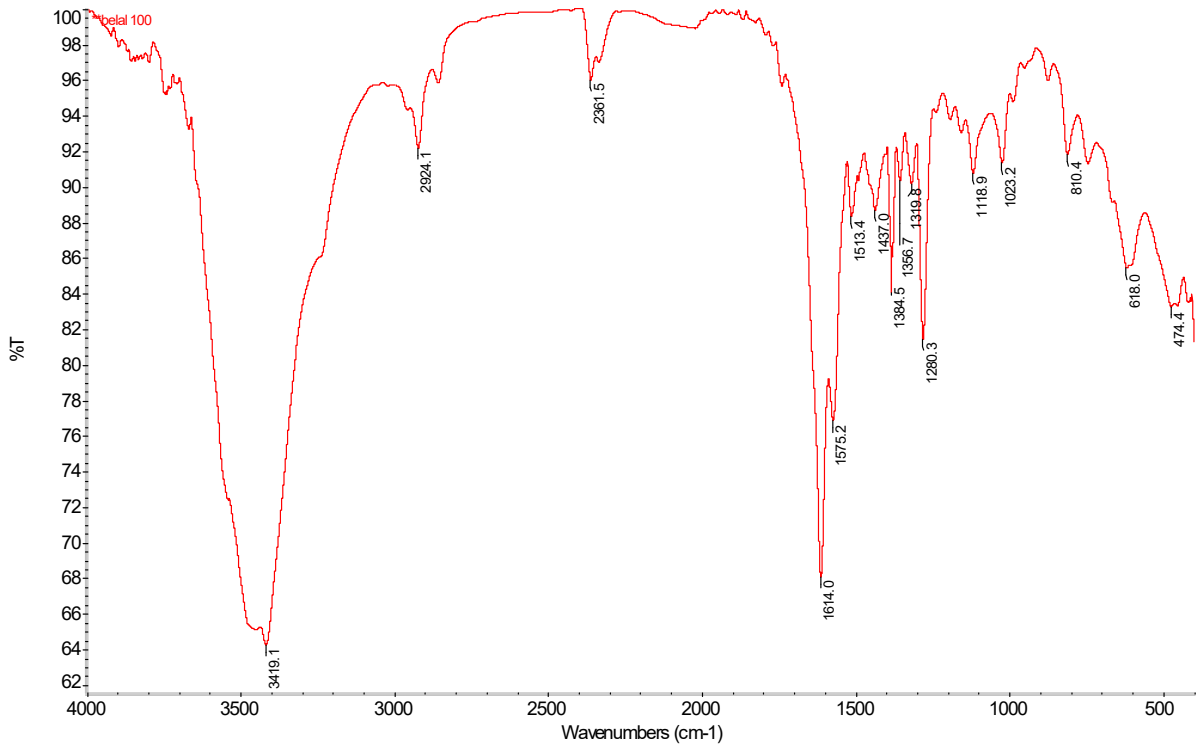

Figure S9. Infrared spectrum (KBr) of **3i**.

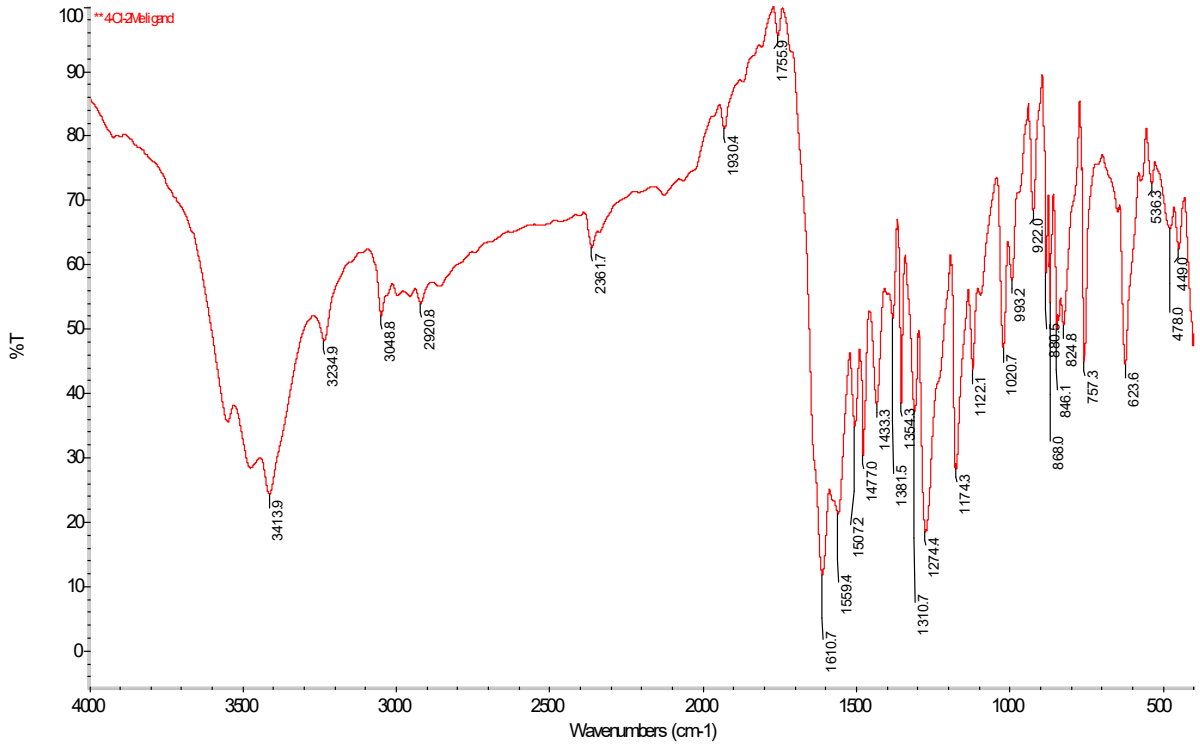

Figure S10. Infrared spectrum (KBr) of **3j.**

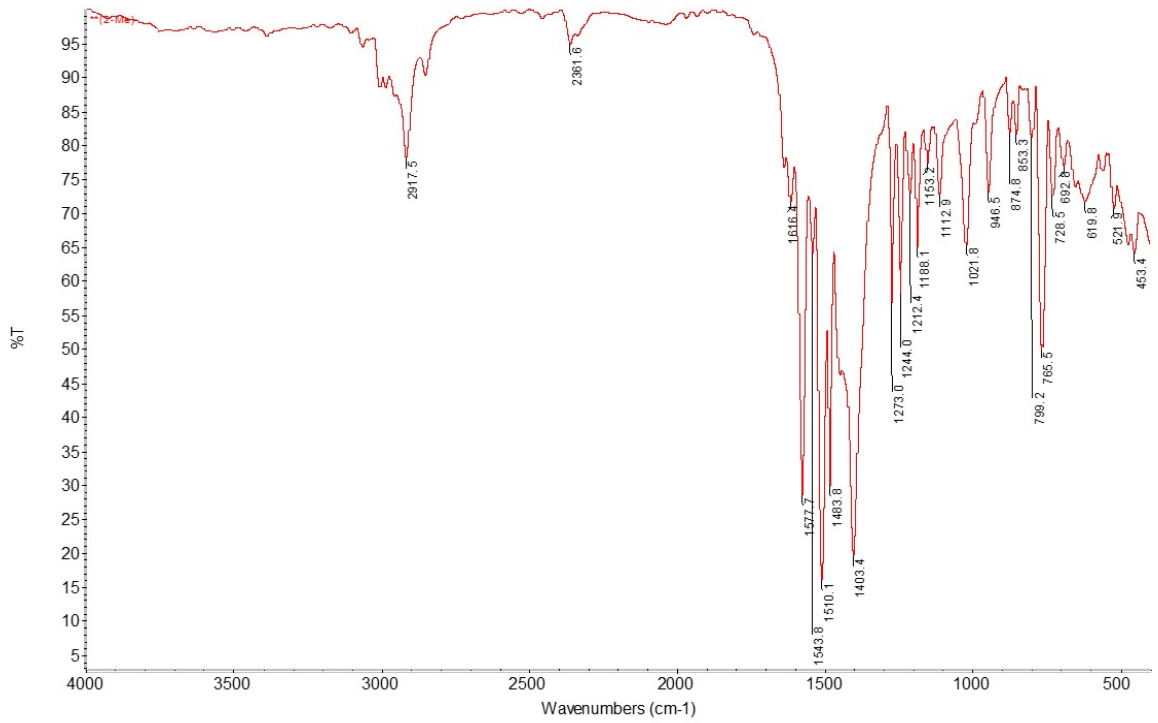

Figure S11. Infrared spectrum (KBr) of **4a.**

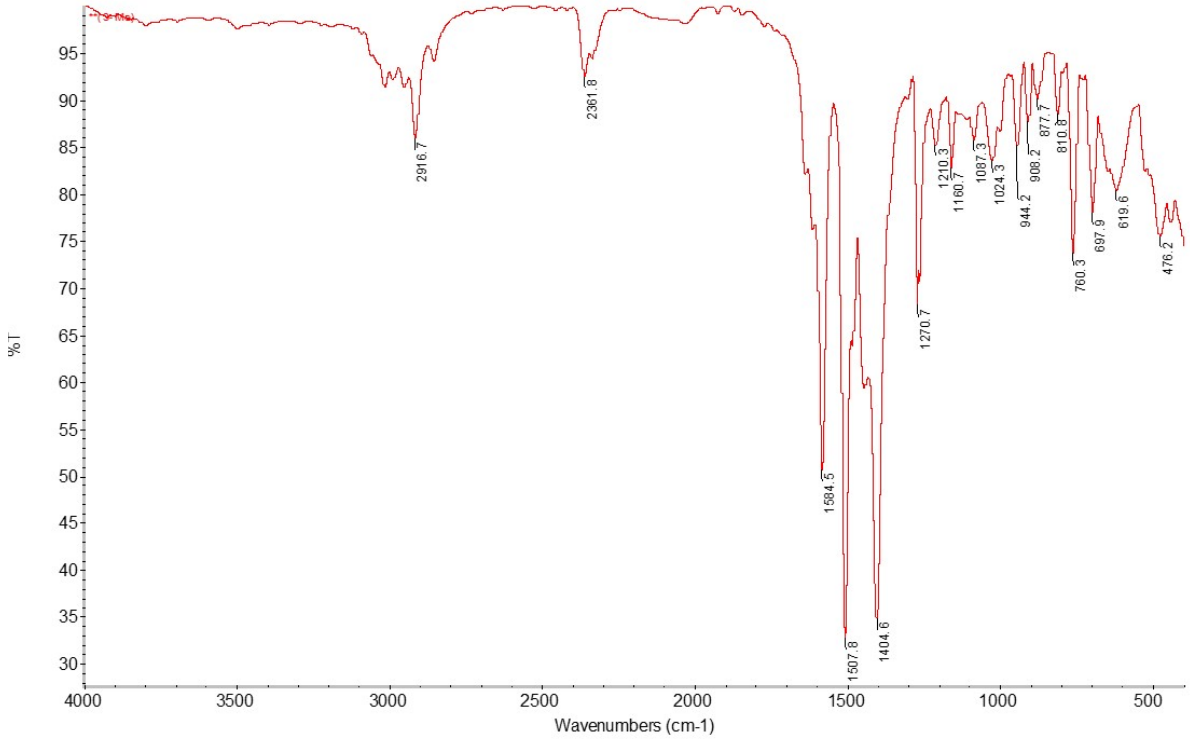

Figure S12. Infrared spectrum (KBr) of **4b.**

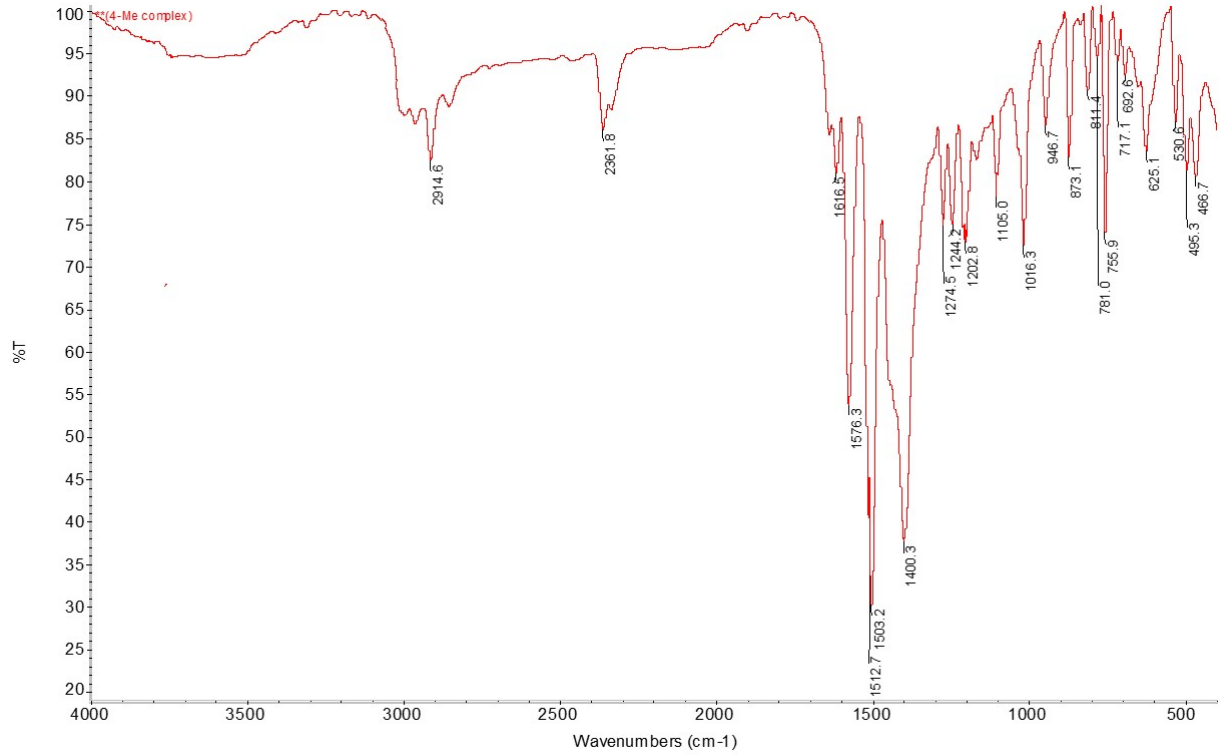

Figure S13. Infrared spectrum (KBr) of **4c**

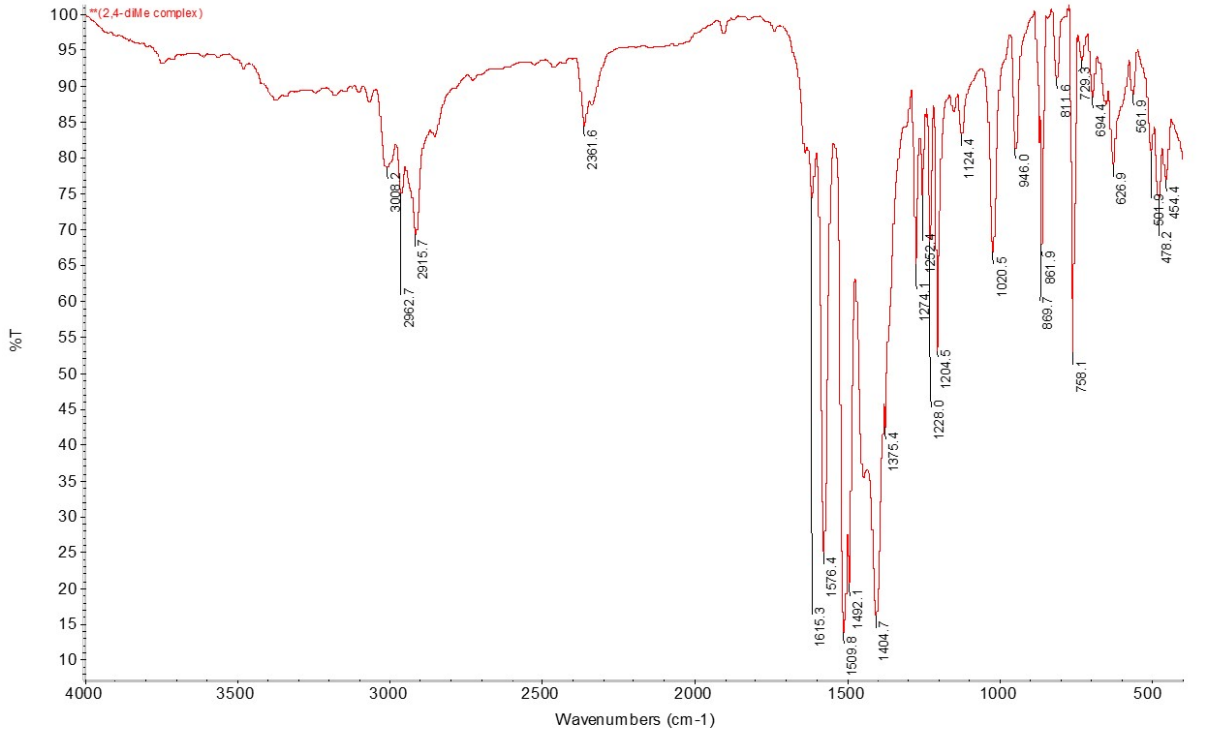

Figure S14. Infrared spectrum (KBr) of **4d.**

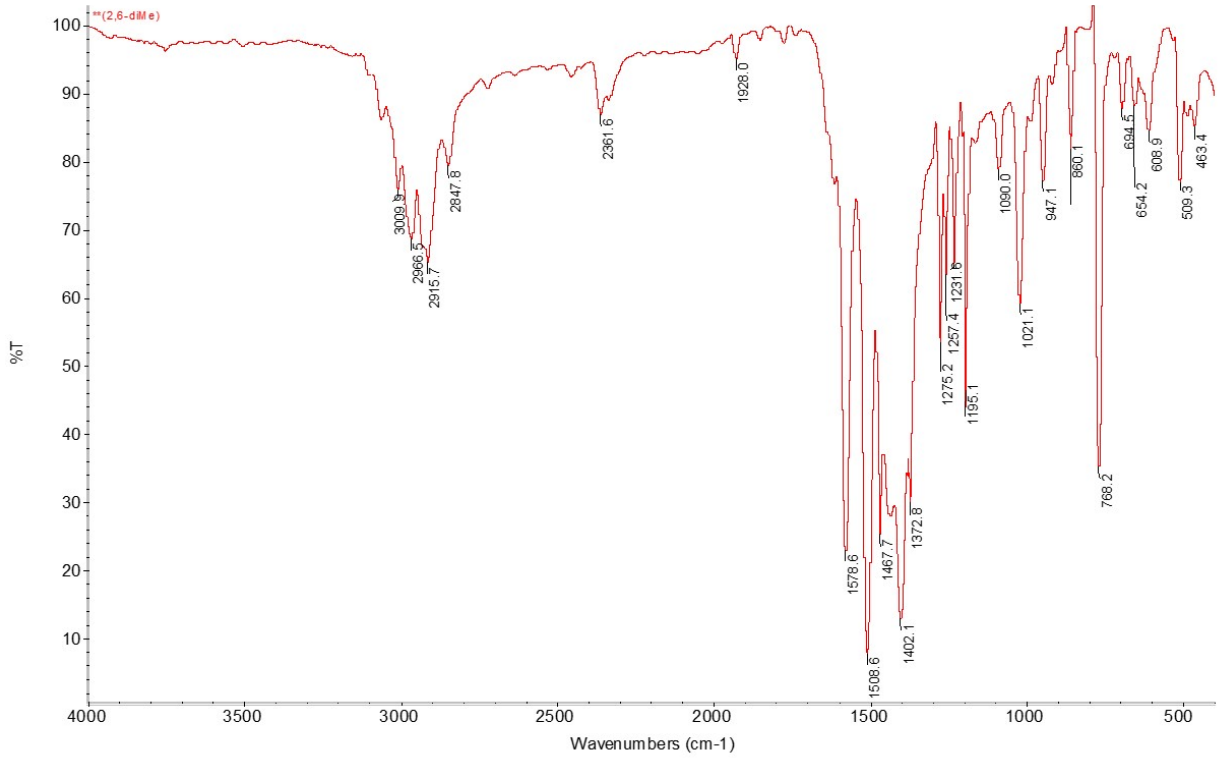

Figure S15. Infrared spectrum (KBr) of **4e.**

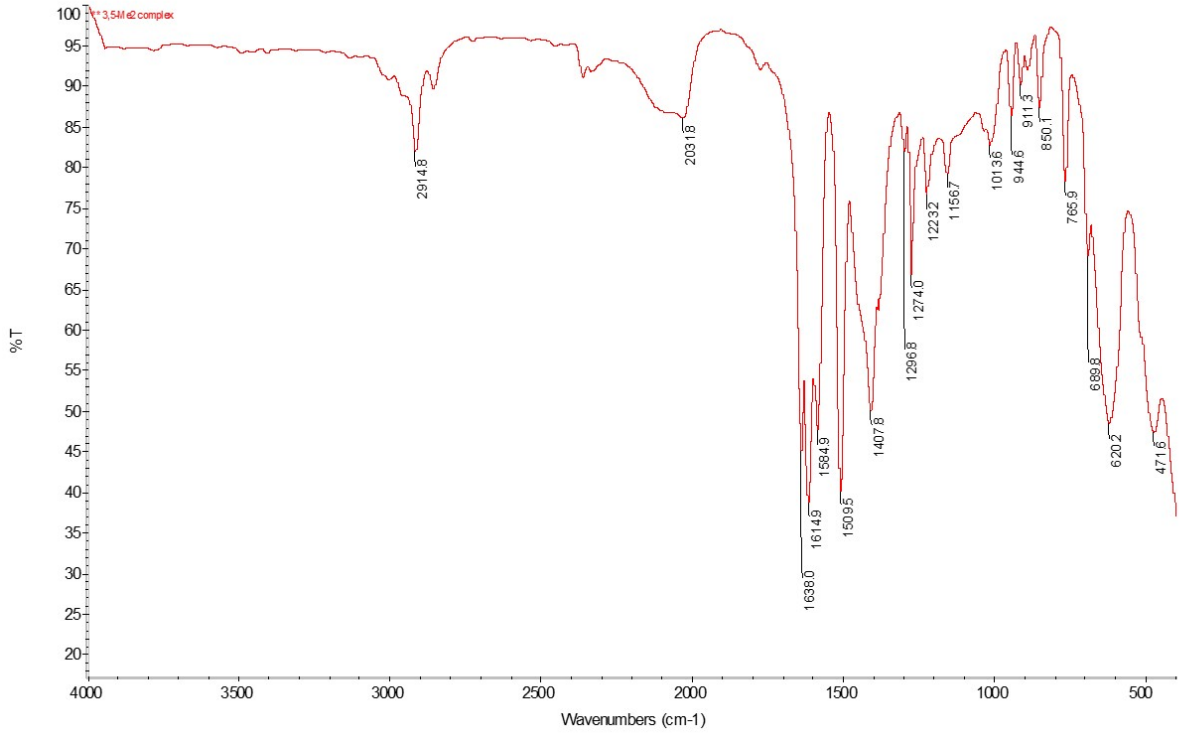

Figure S16. Infrared spectrum (KBr) of **4f.**

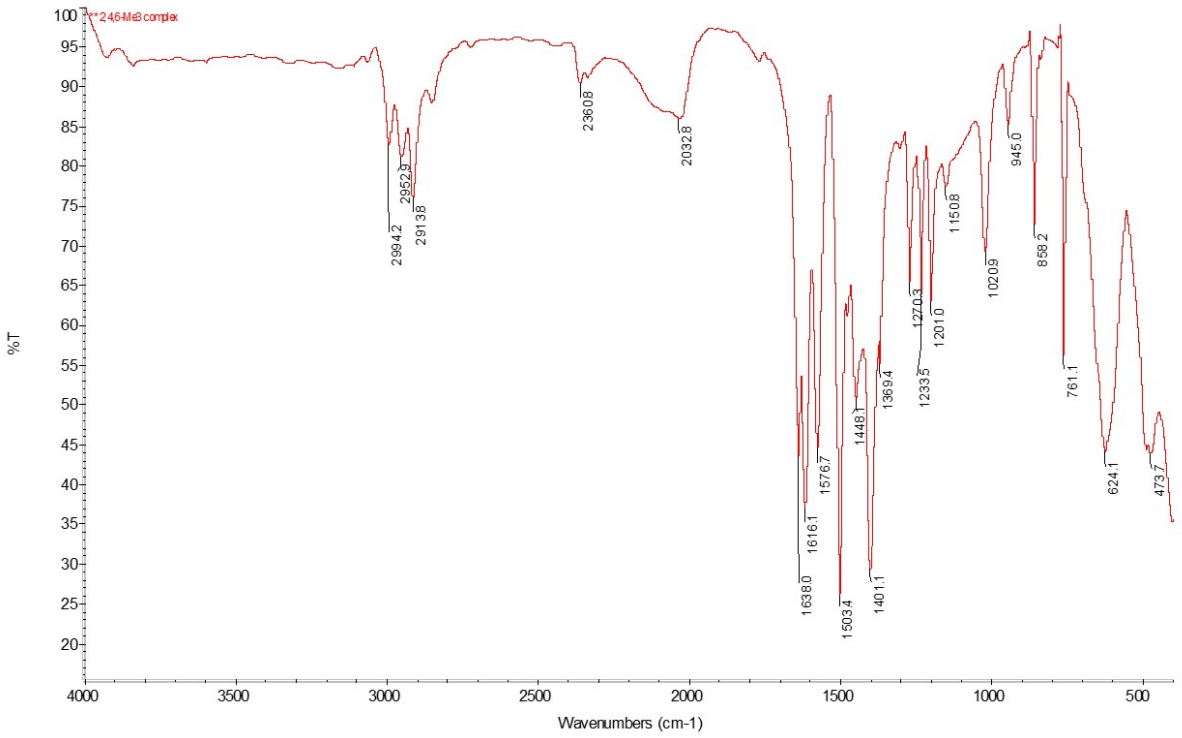

Figure S17. Infrared spectrum (KBr) of **4g.**

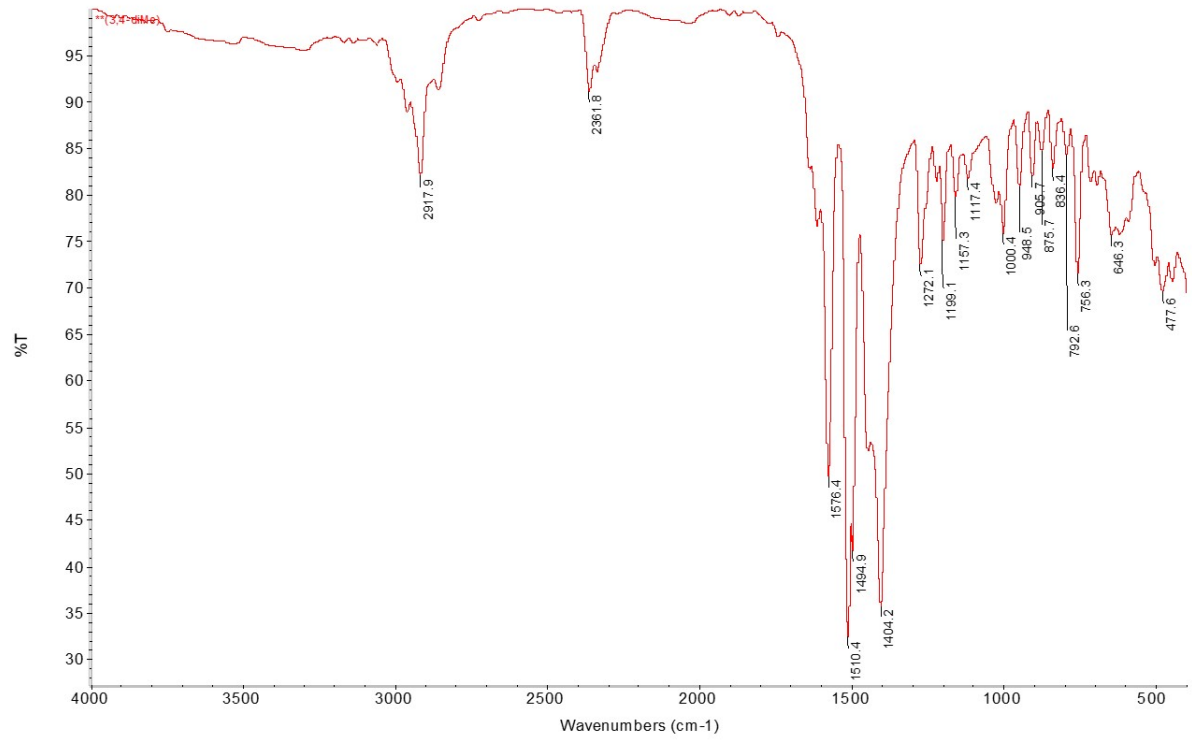

Figure S18. Infrared spectrum (KBr) of **4h.**

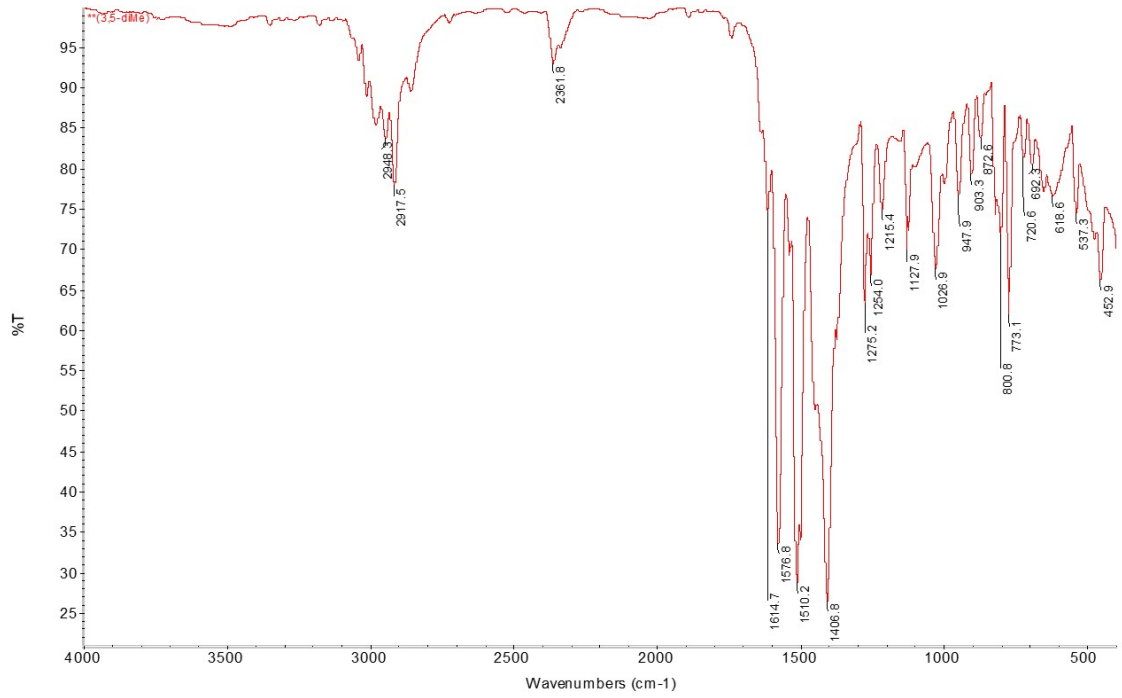

Figure S19. Infrared spectrum (KBr) of **4i**.

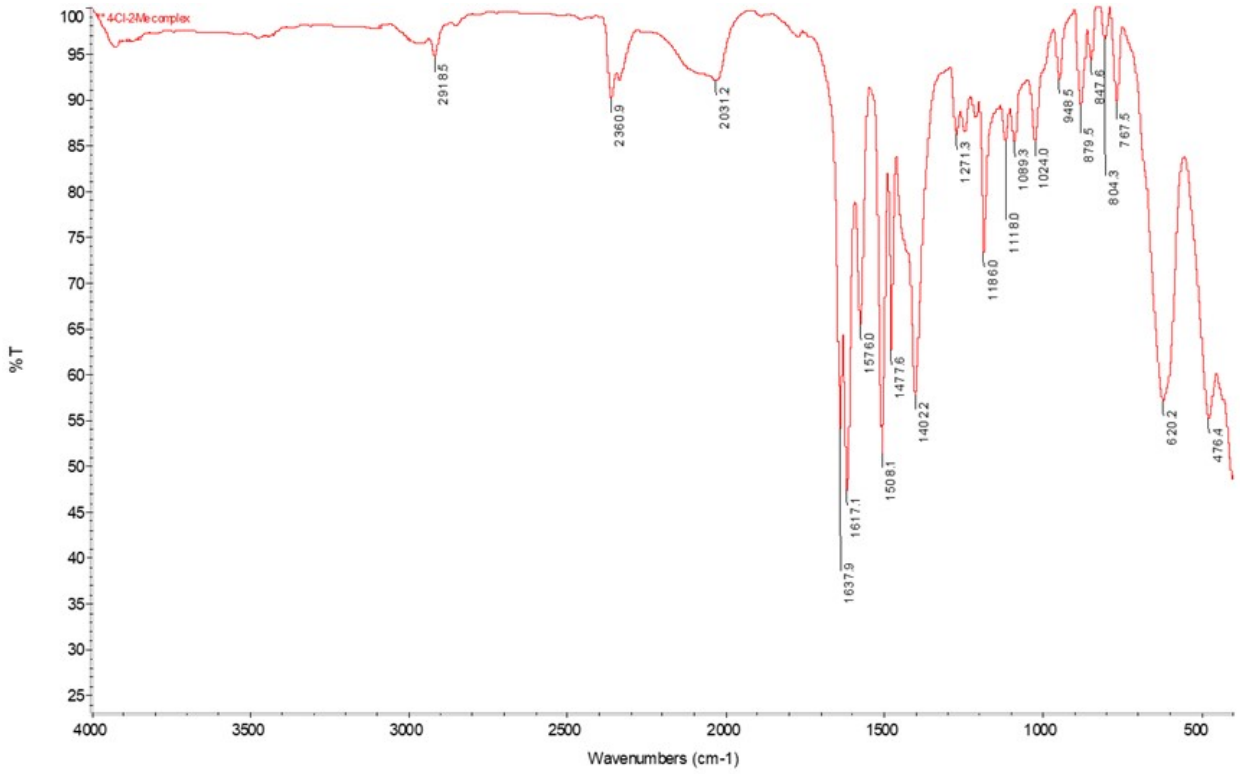

Figure S20. Infrared spectrum (KBr) of **4j.**

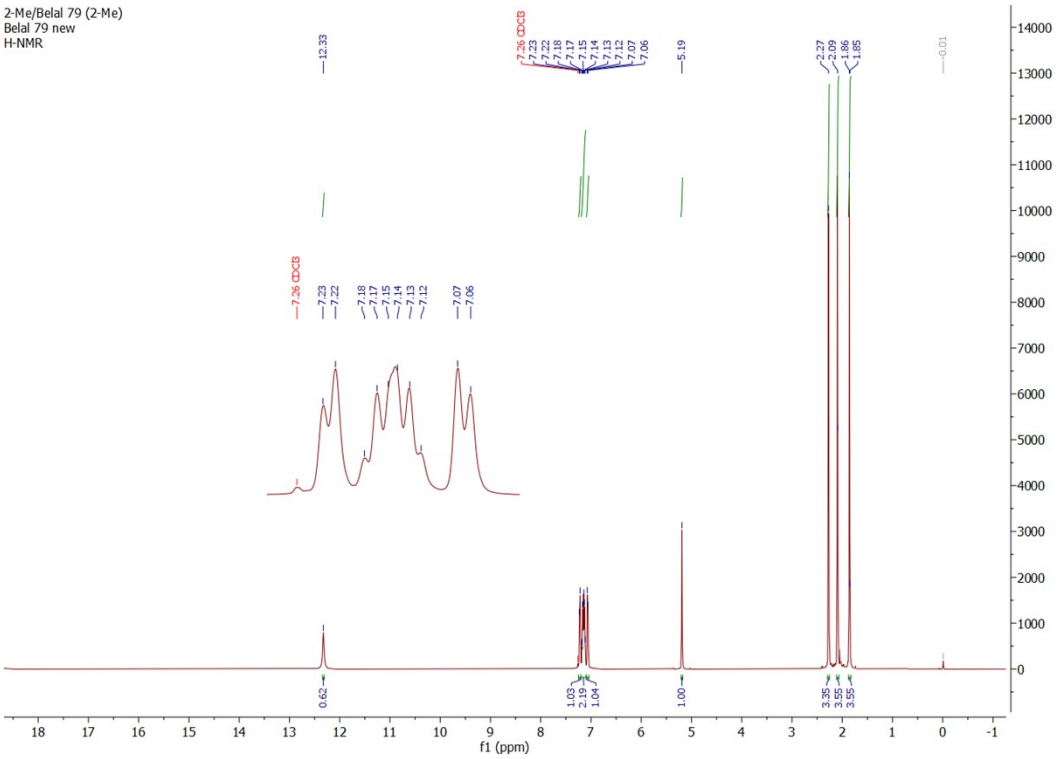

Figure S21. ^{1}H NMR spectrum ($CDCl_3$, 25 ^{o}C, 500.303 MHz) of **3a**.

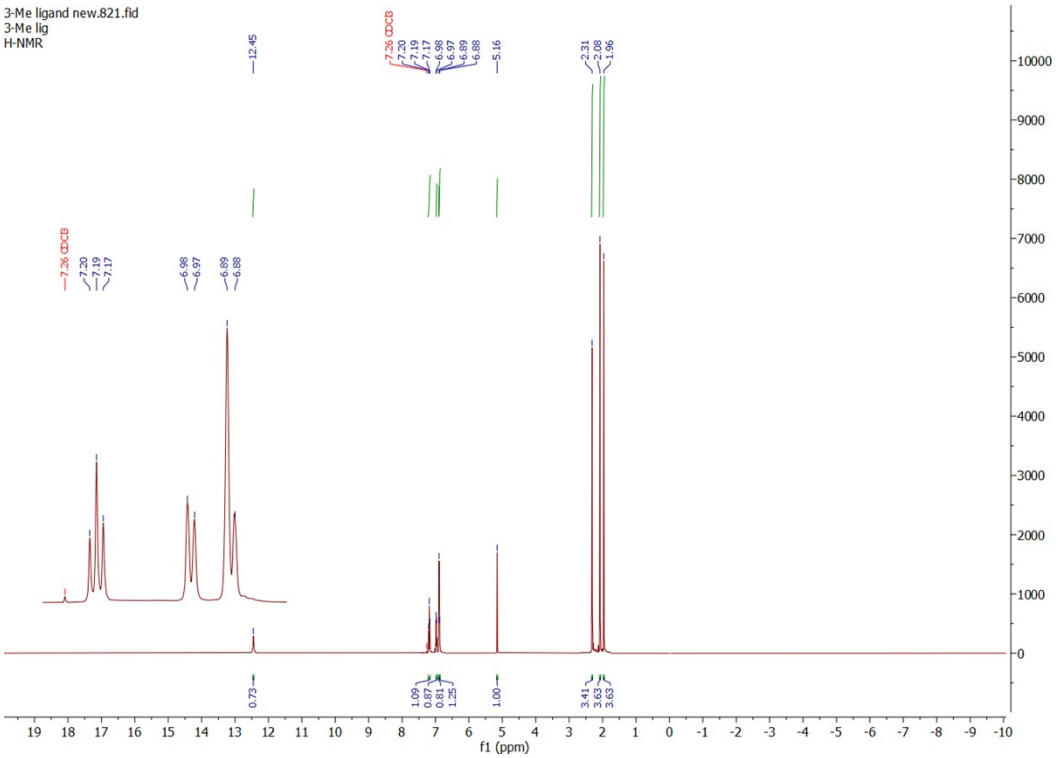

Figure S22. ^{1}H NMR spectrum ($CDCl_3$, 25 ^{o}C, 500.303 MHz) of **3b**.

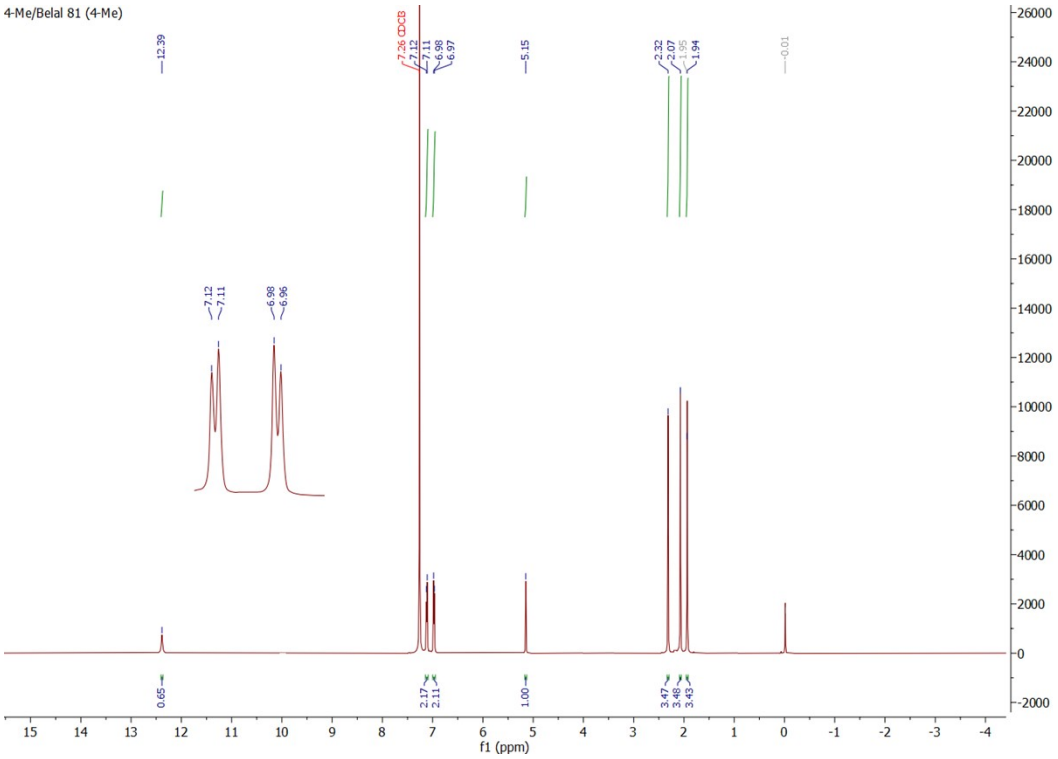

Figure S23. ^{1}H NMR spectrum ($CDCl_3$, 25 ^{o}C, 500.303 MHz) of **3c**.

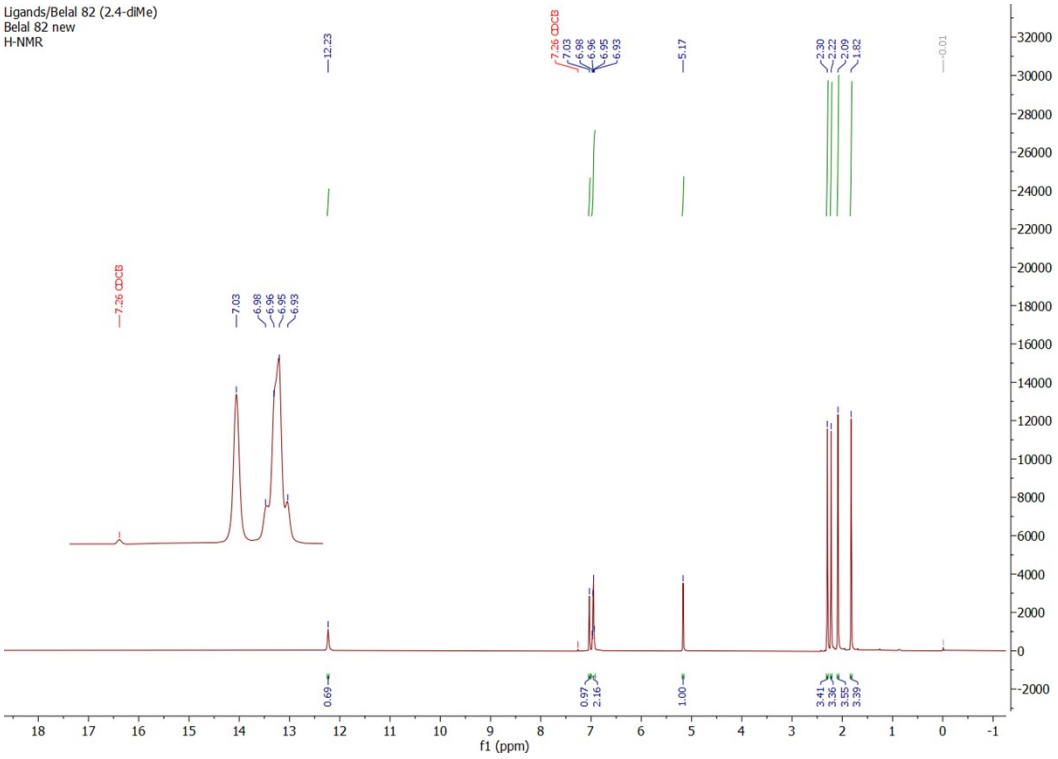

Figure S24. ^{1}H NMR spectrum ($CDCl_3$, 25 ^{o}C, 500.303 MHz) of **3d**.

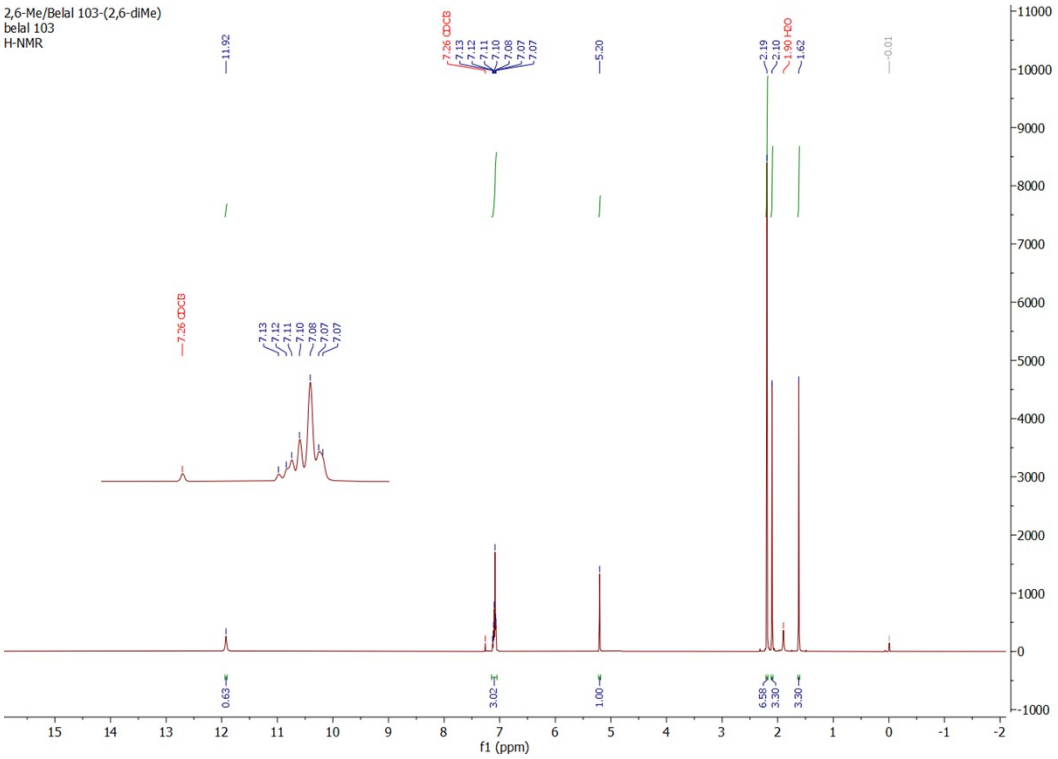

Figure S25. ^{1}H NMR spectrum ($CDCl_3$, 25 ^{o}C, 500.303 MHz) of **3e**.

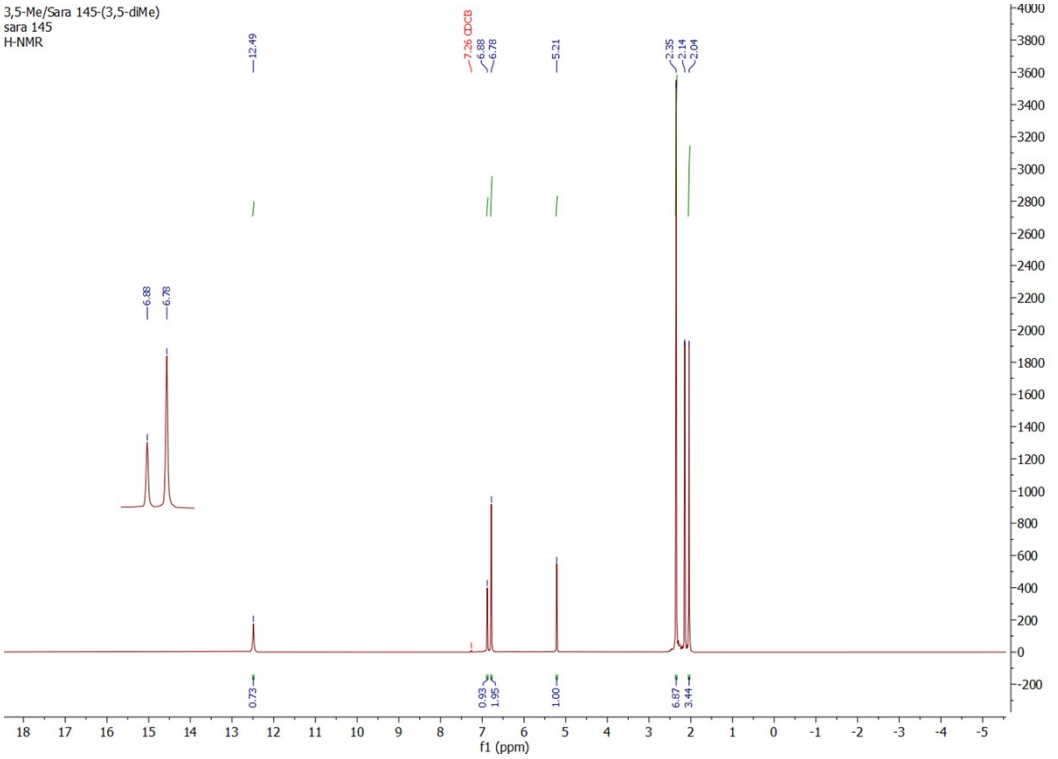

Figure S26. ^{1}H NMR spectrum ($CDCl_3$, 25 ^{o}C, 500.303 MHz) of **3f**.

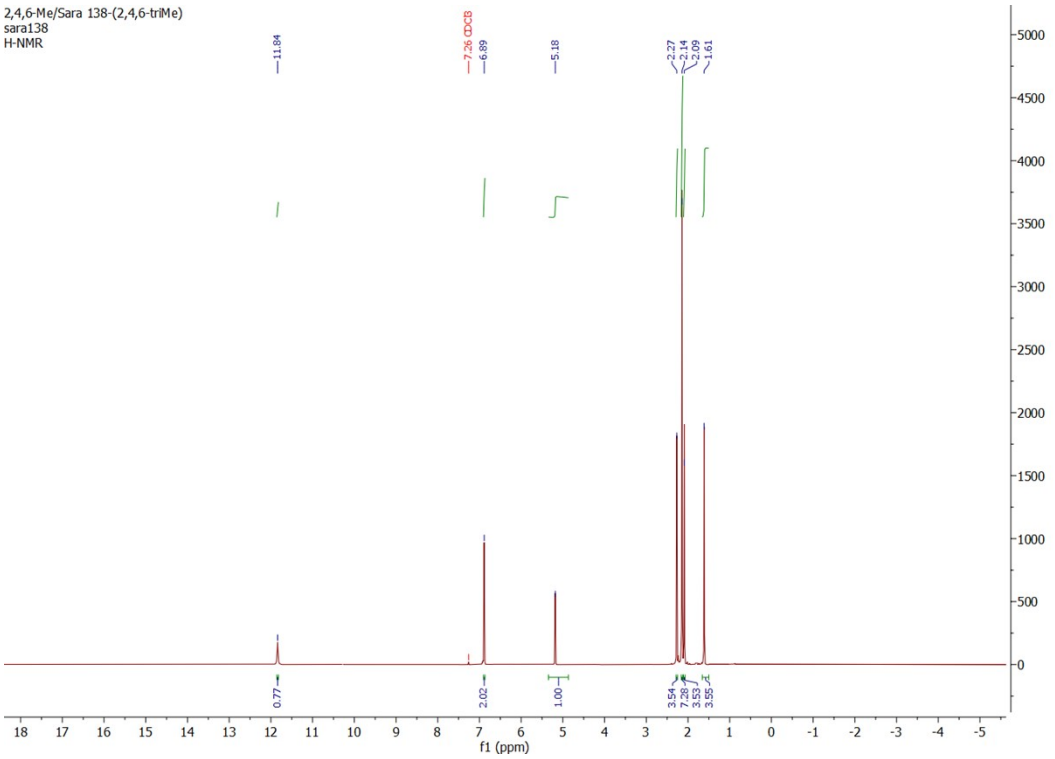

Figure S27. ^{1}H NMR spectrum ($CDCl_3$, 25 ^{o}C, 500.303 MHz) of **3g**.

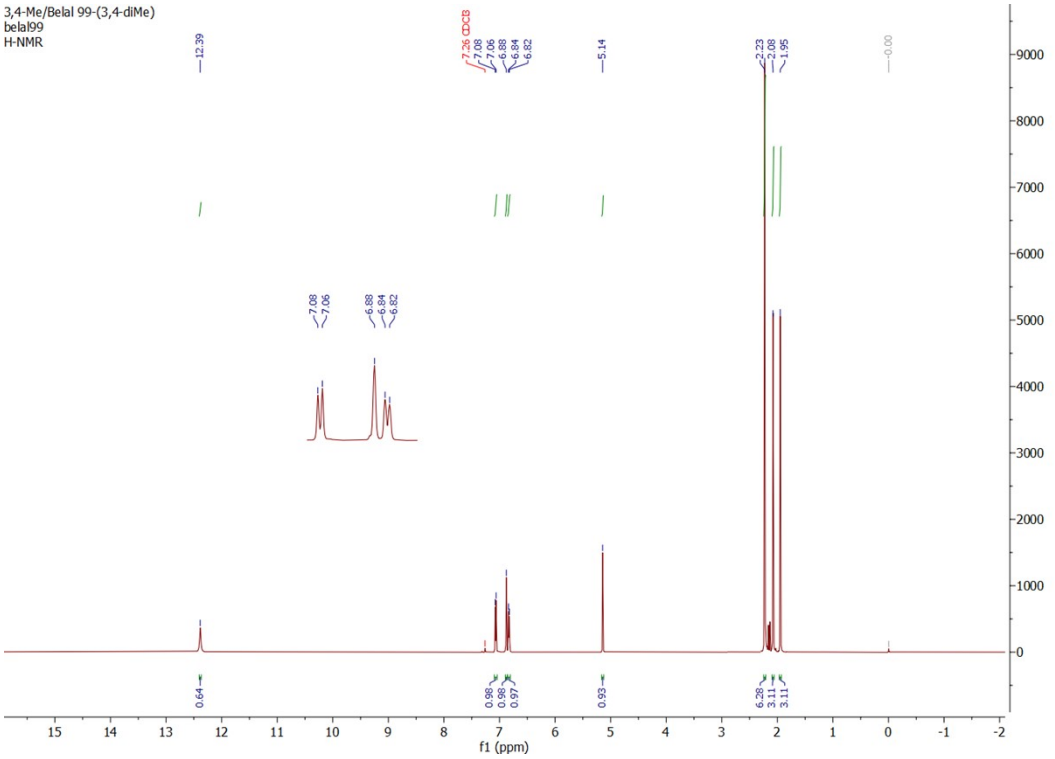

Figure S28. ^{1}H NMR spectrum ($CDCl_3$, 25 ^{o}C, 500.303 MHz) of **3h**.

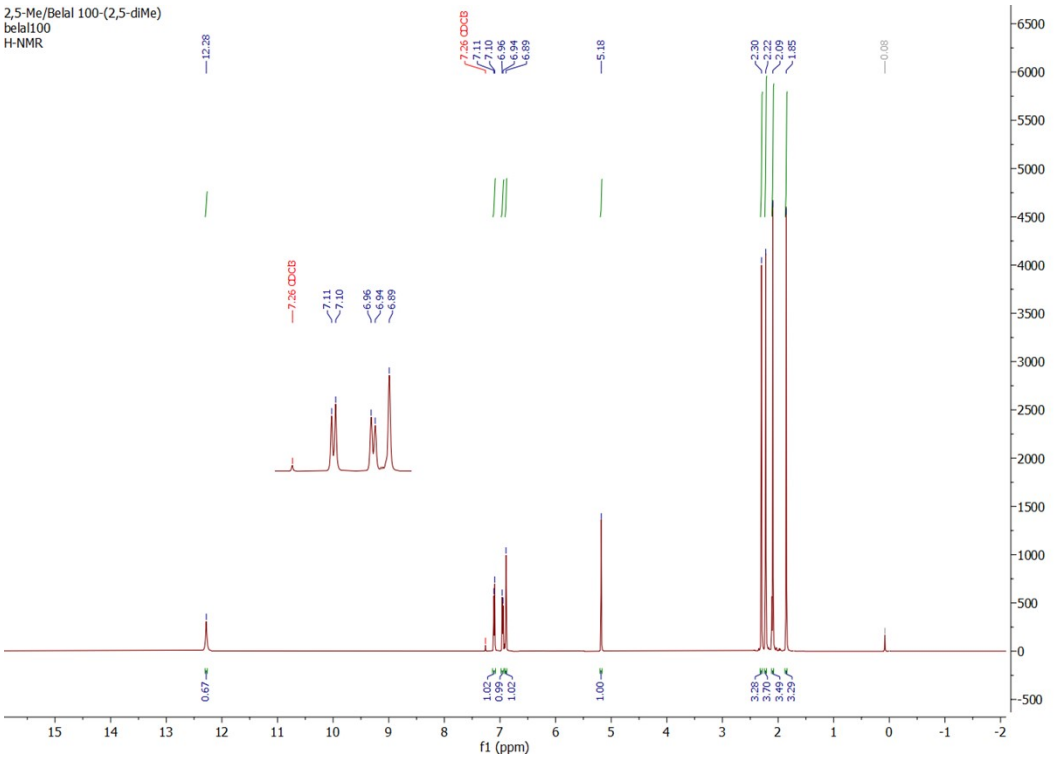

Figure S29. ^{1}H NMR spectrum ($CDCl_3$, 25 ^{o}C, 500.303 MHz) of **3i**.

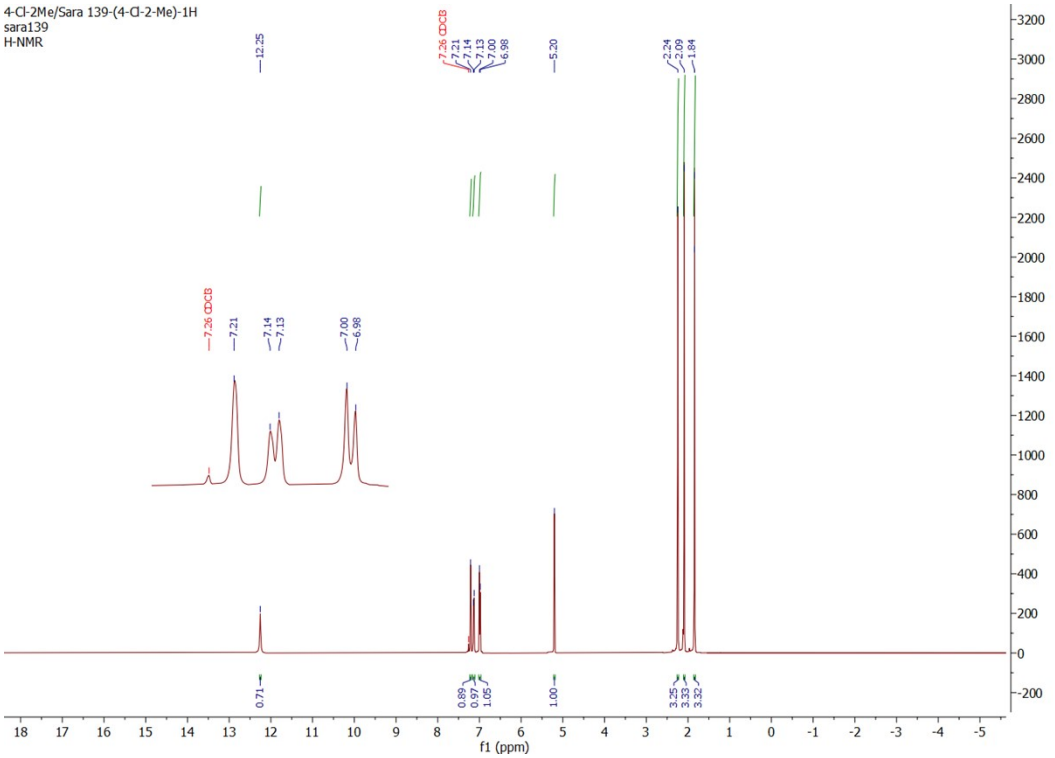

Figure S30. ^{1}H NMR spectrum ($CDCl_3$, 25 ^{o}C, 500.303 MHz) of **3j**.

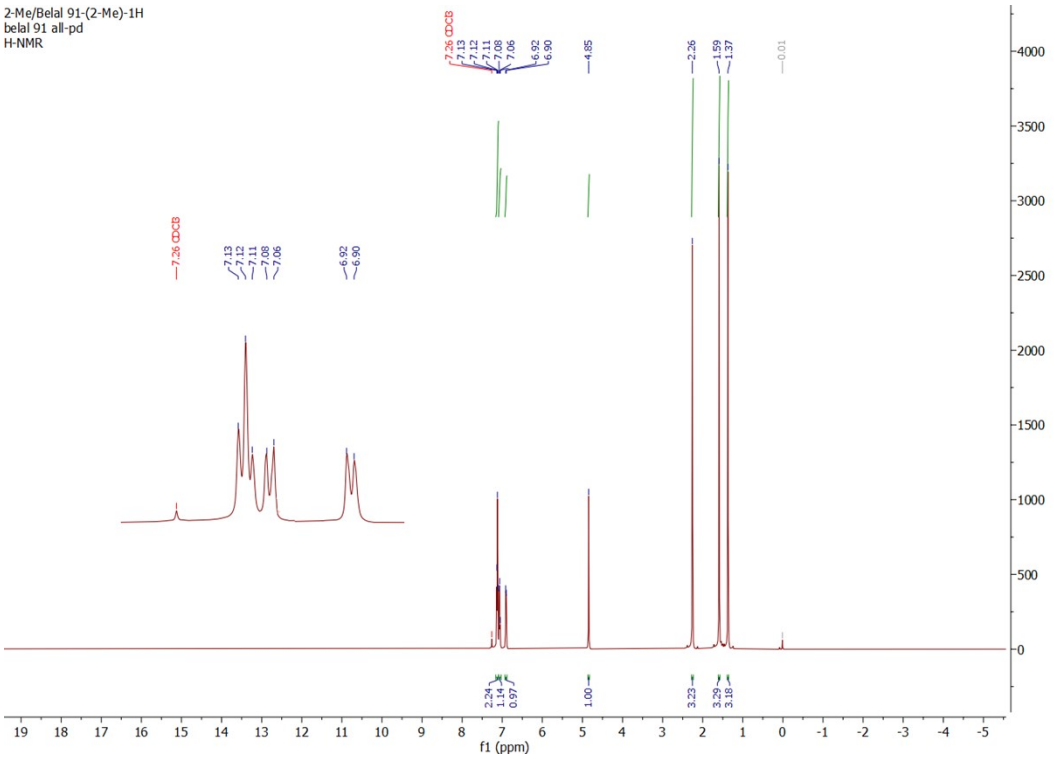

Figure S31. ^{1}H NMR spectrum ($CDCl_3$, 25 °C, 500.303 MHz) of **4a**.

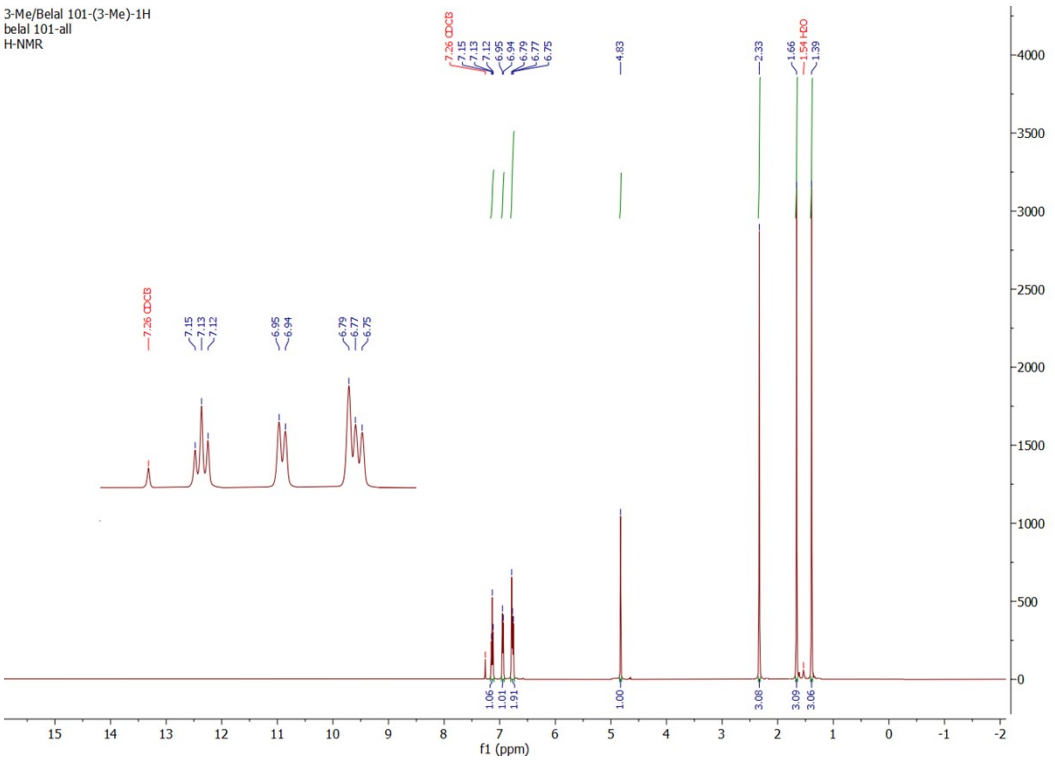

Figure S32. ^{1}H NMR spectrum ($CDCl_3$, 25 °C, 500.303 MHz) of **4b**.

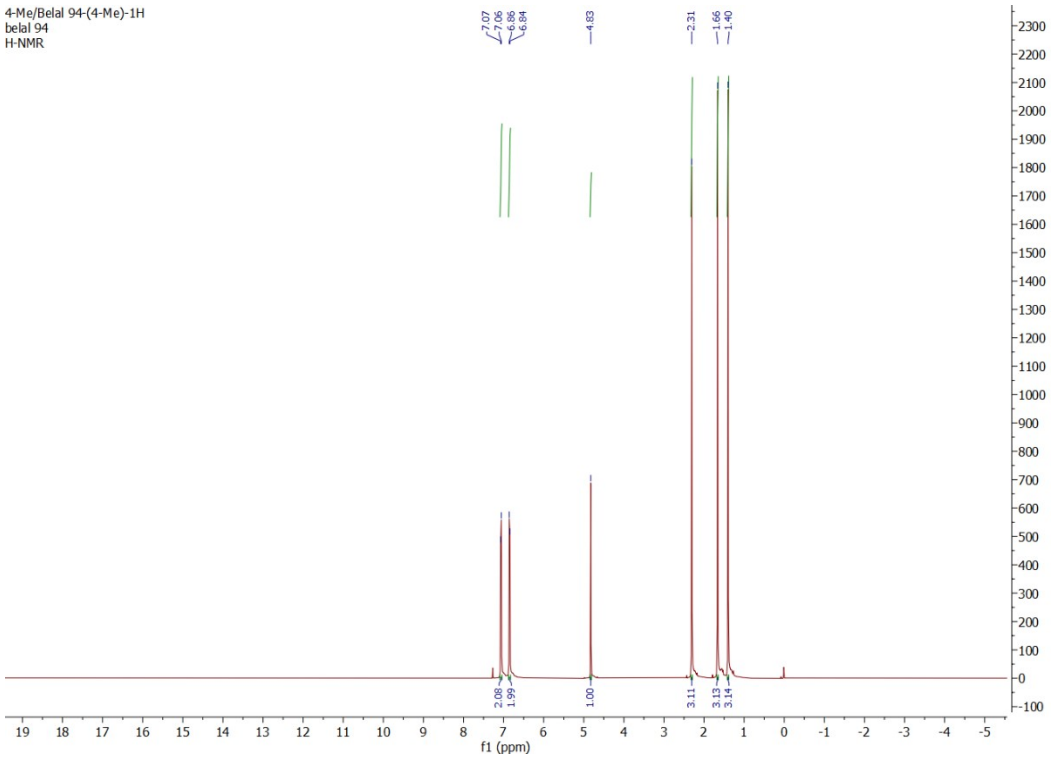

Figure S33. ^{1}H NMR spectrum ($CDCl_3$, 25 ^{o}C, 500.303 MHz) of **4c**.

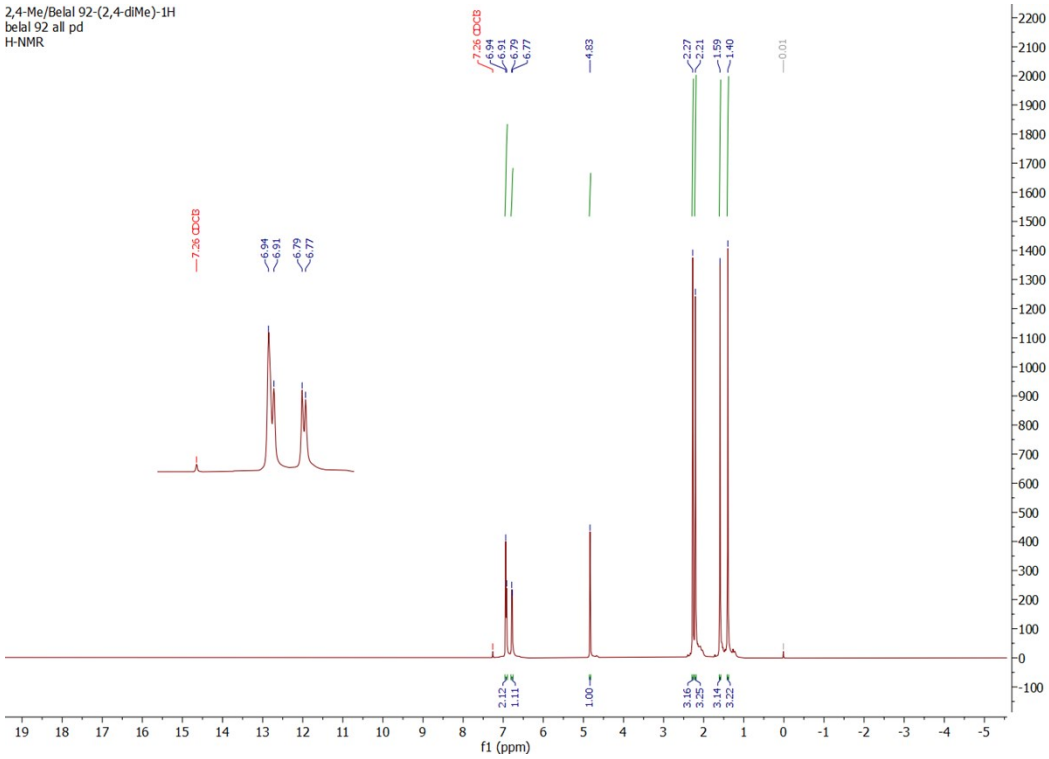

Figure S34. ^{1}H NMR spectrum ($CDCl_3$, 25 ^{o}C, 500.303 MHz) of **4d**.

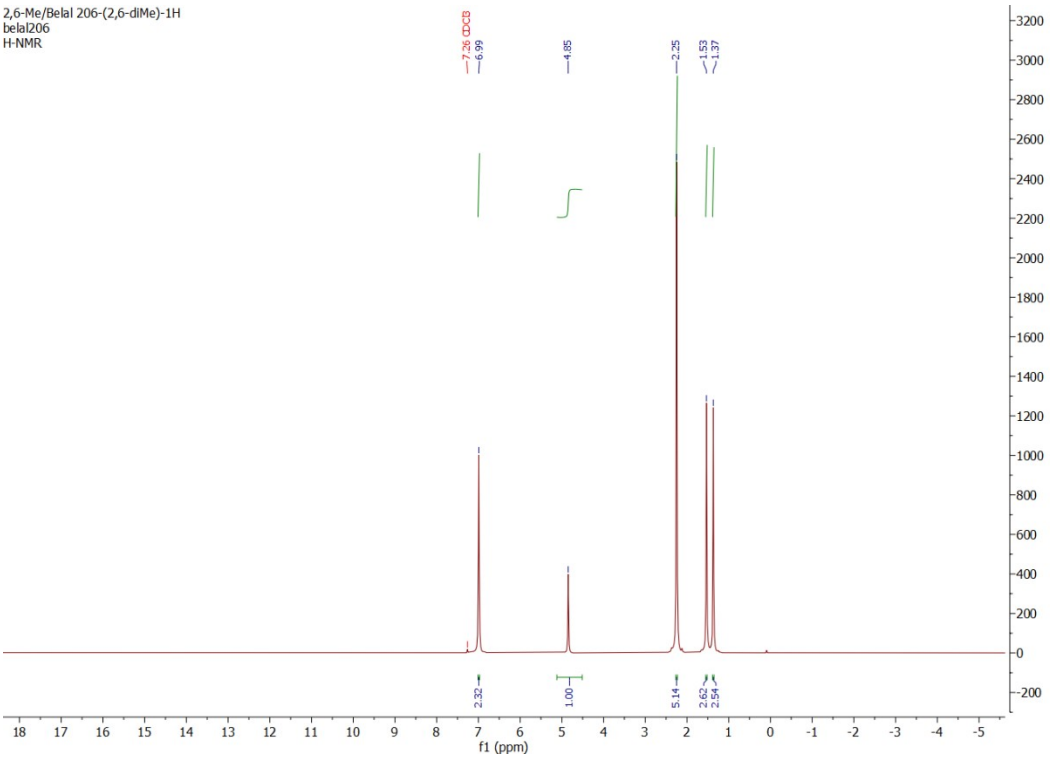

Figure S35. ^{1}H NMR spectrum ($CDCl_3$, 25 ^{o}C, 500.303 MHz) of **4e**.

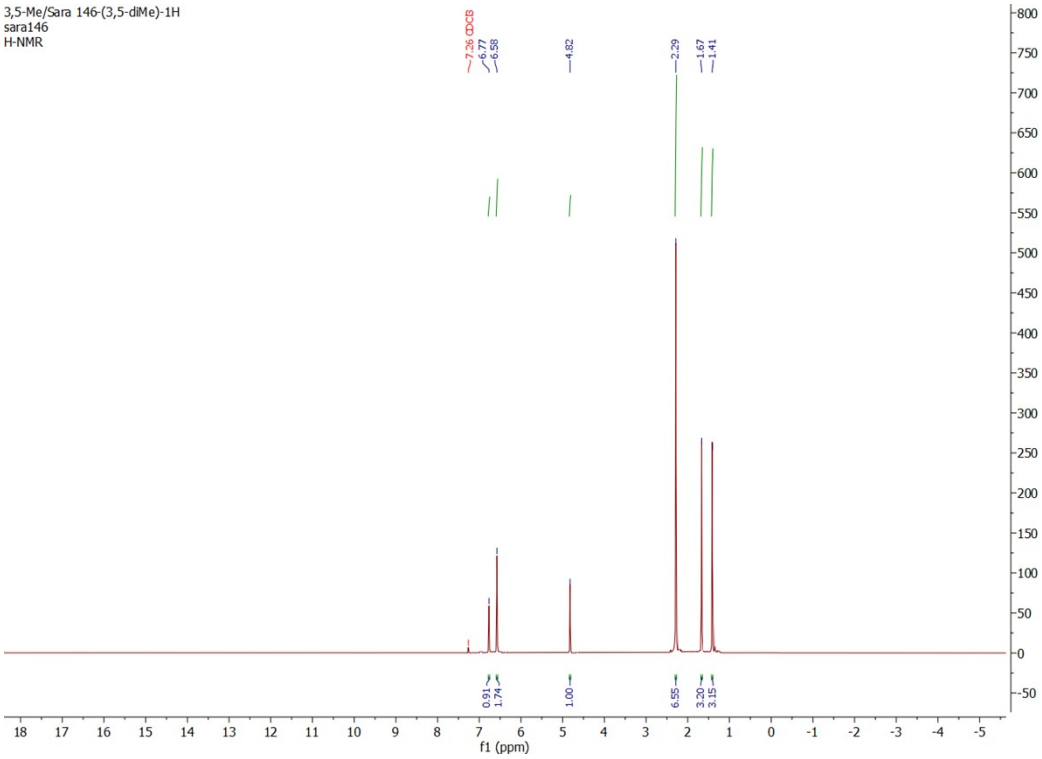

Figure S36. ^{1}H NMR spectrum ($CDCl_3$, 25 ^{o}C, 500.303 MHz) of **4f**.

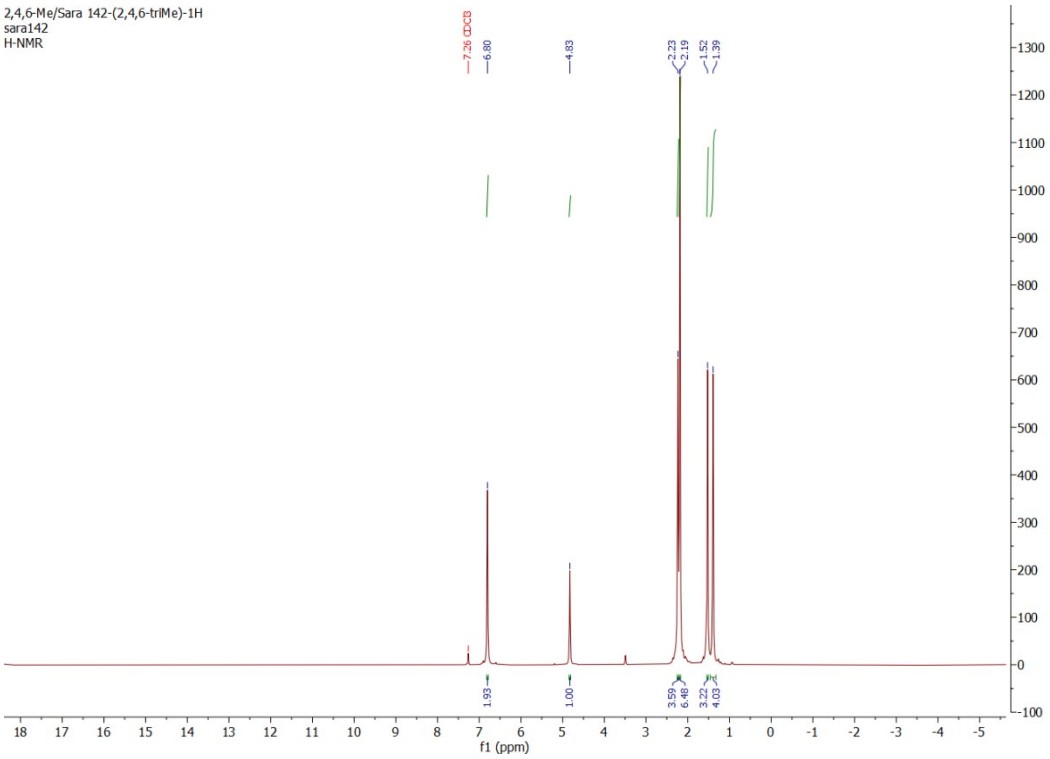

Figure S37. ^{1}H NMR spectrum ($CDCl_3$, 25 ^{o}C, 500.303 MHz) of **4g**.

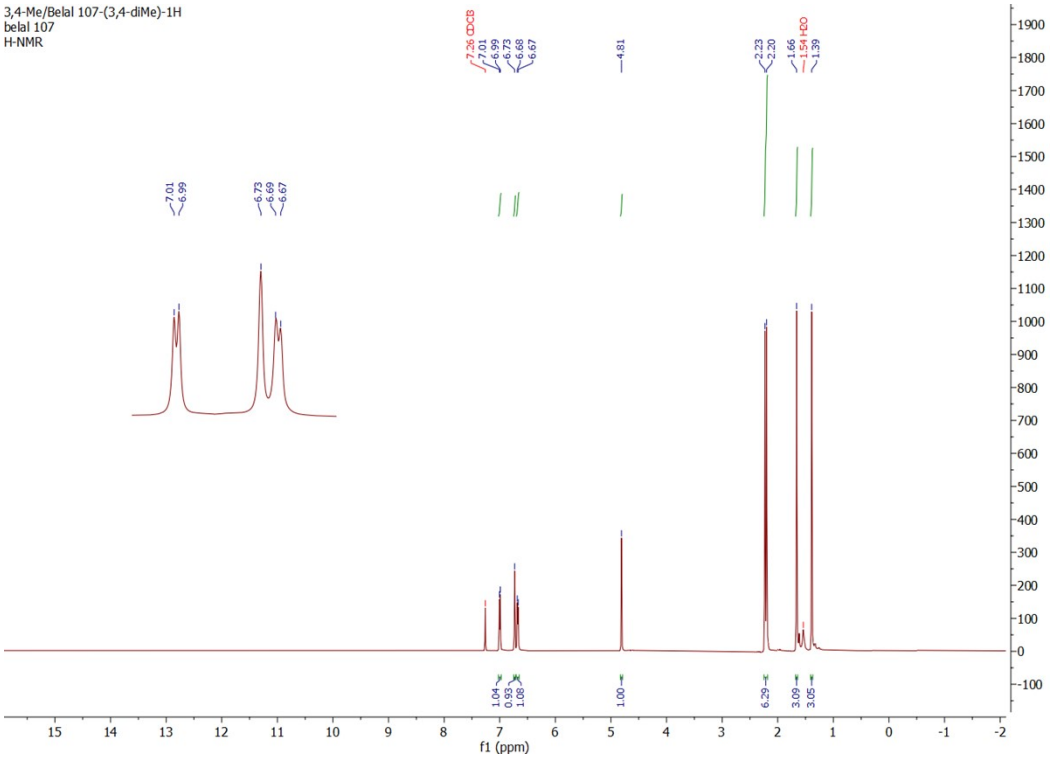

Figure S38. ^{1}H NMR spectrum ($CDCl_3$, 25 ^{o}C, 500.303 MHz) of **4h**.

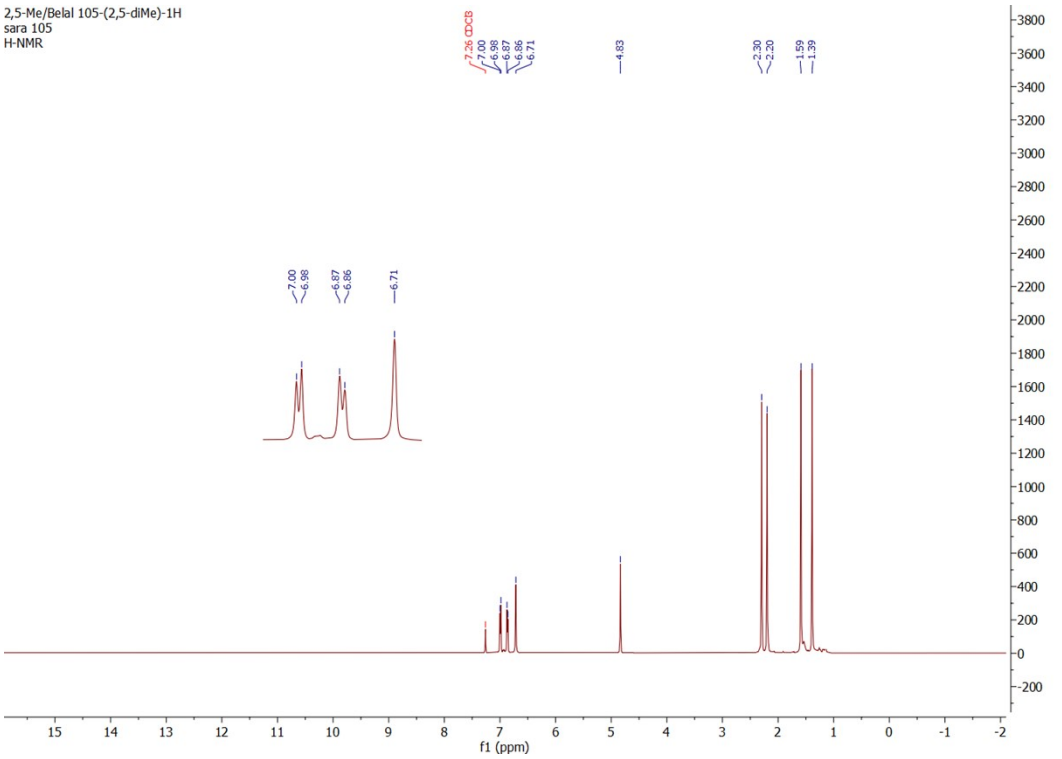

Figure S39. ^{1}H NMR spectrum ($CDCl_3$, 25 °C, 500.303 MHz) of **4i**.

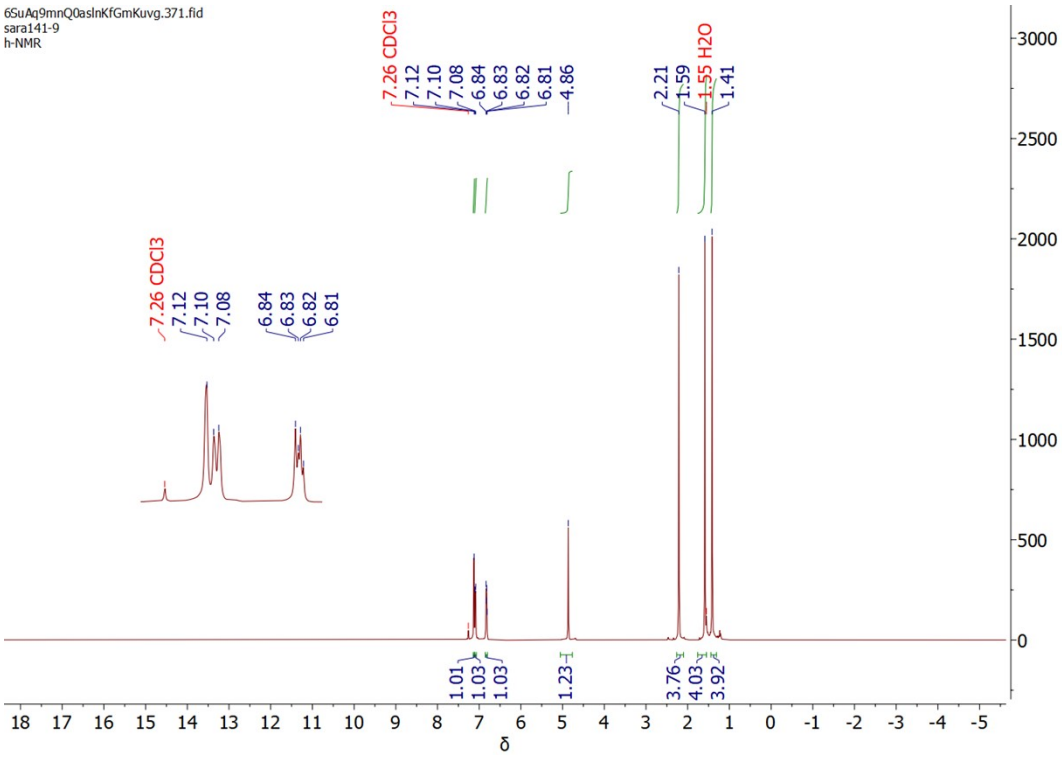

Figure S40. ^{1}H NMR spectrum ($CDCl_3$, 25 °C, 500.303 MHz) of **4j**.

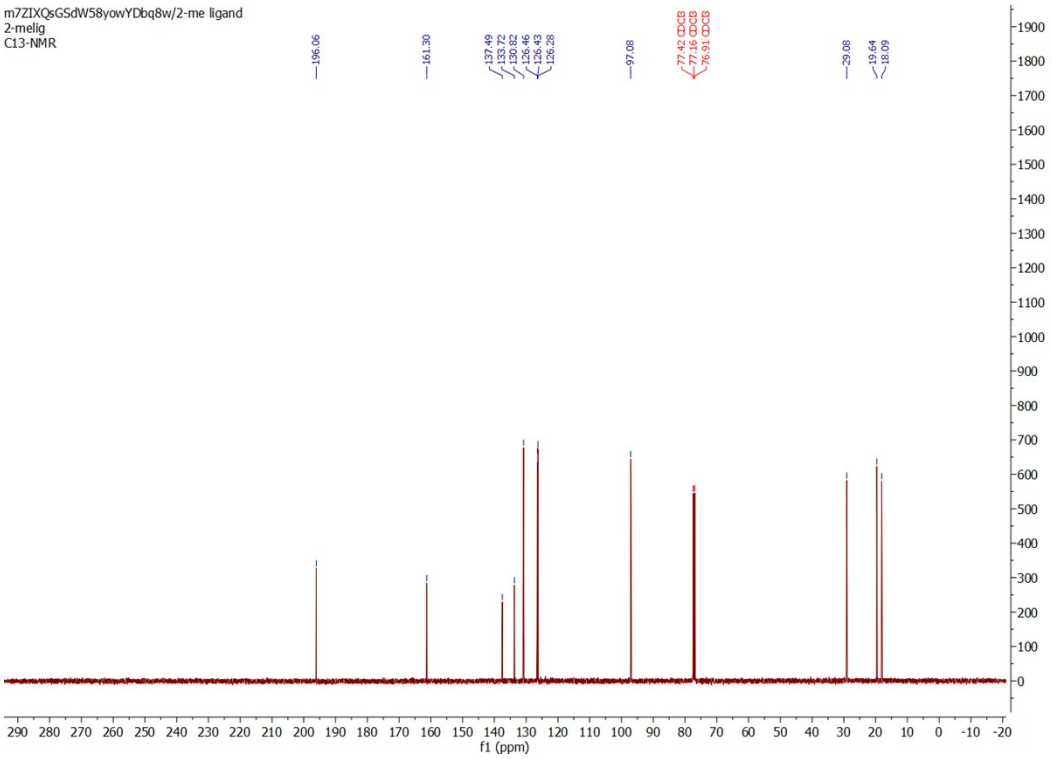

Figure S41. $^{13}C\{^{1}H\}$ NMR spectrum ($CDCl_3$, 25 °C, 125.813 MHz MHz) of **3a**.

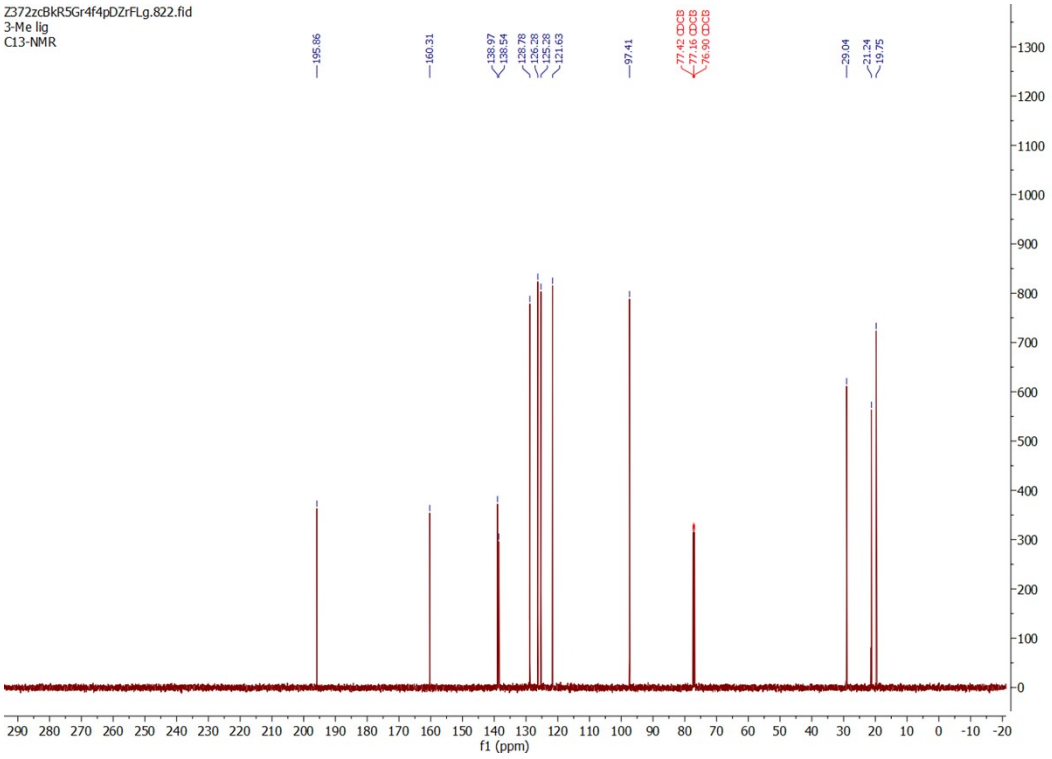

Figure S42. $^{13}C\{^{1}H\}$ NMR spectrum ($CDCl_3$, 25 °C, 125.813 MHz MHz) of **3b**.

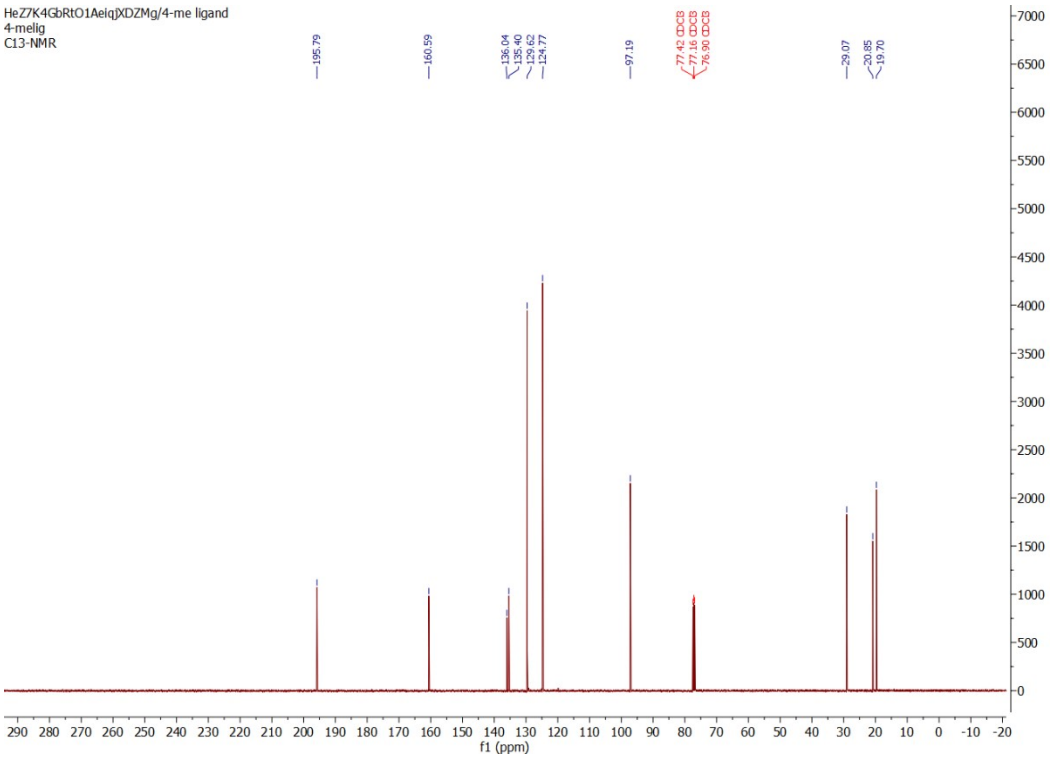

Figure S43. $^{13}C\{^{1}H\}$ NMR spectrum ($CDCl_3$, 25 °C, 125.813 MHz MHz) of **3c**.

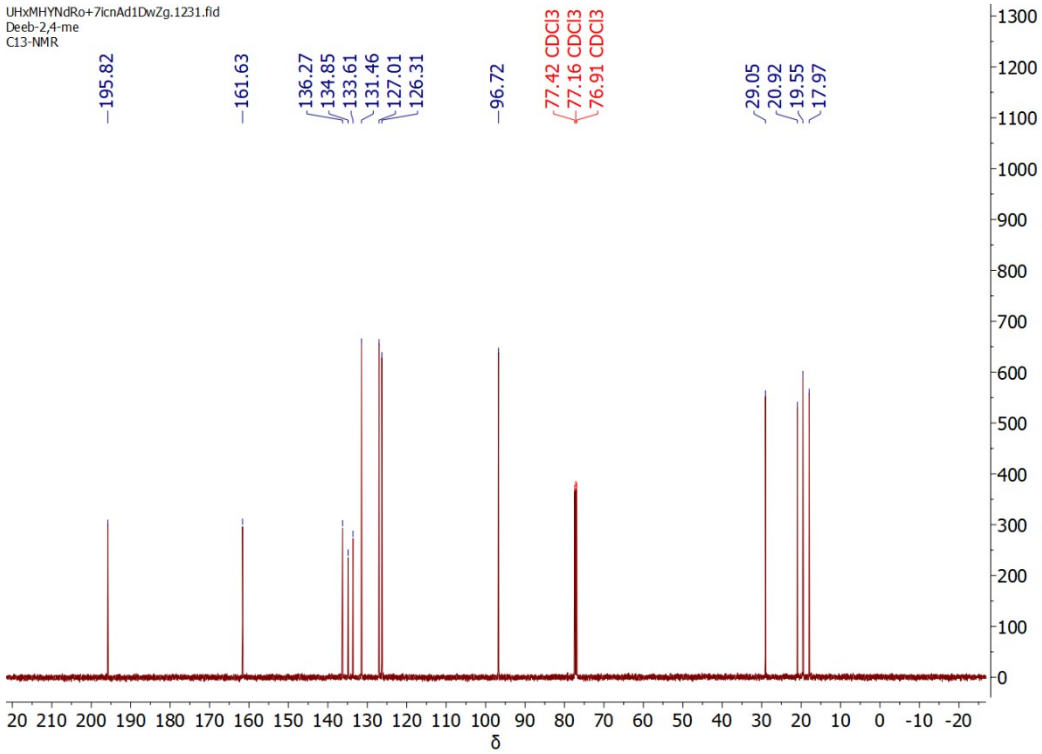

Figure S44. $^{13}C\{^{1}H\}$ NMR spectrum ($CDCl_3$, 25 °C, 125.813 MHz MHz) of **3d**.

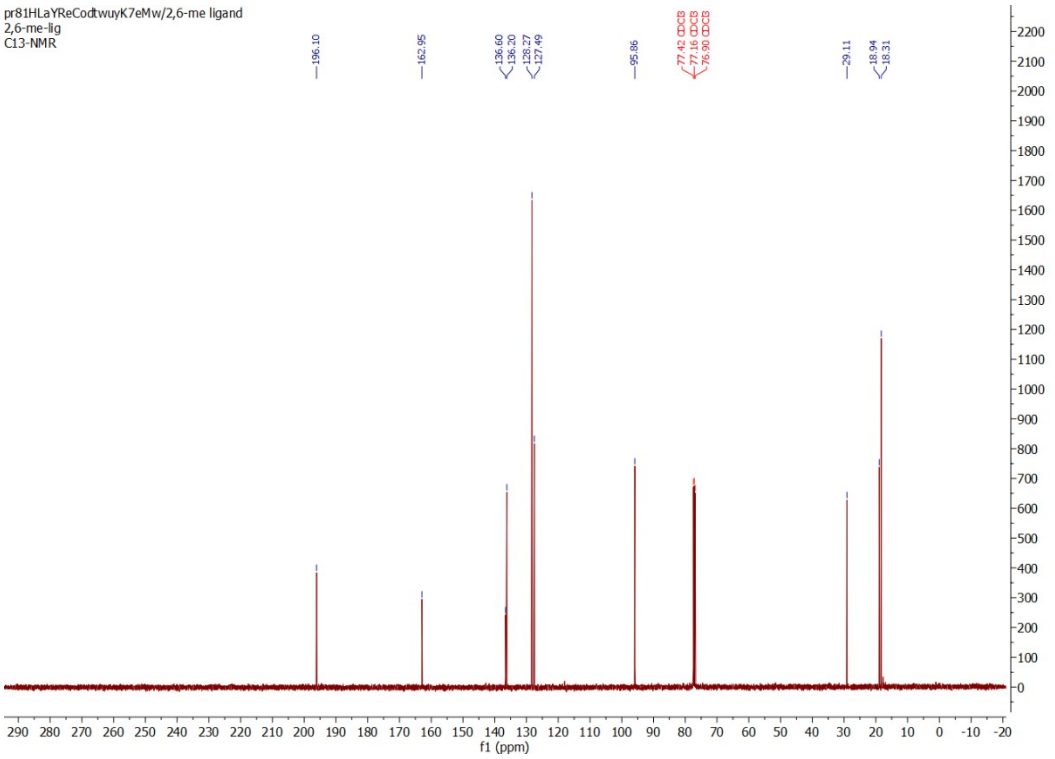

Figure S45. $^{13}C\{^{1}H\}$ NMR spectrum ($CDCl_3$, 25 °C, 125.813 MHz MHz) of **3e**.

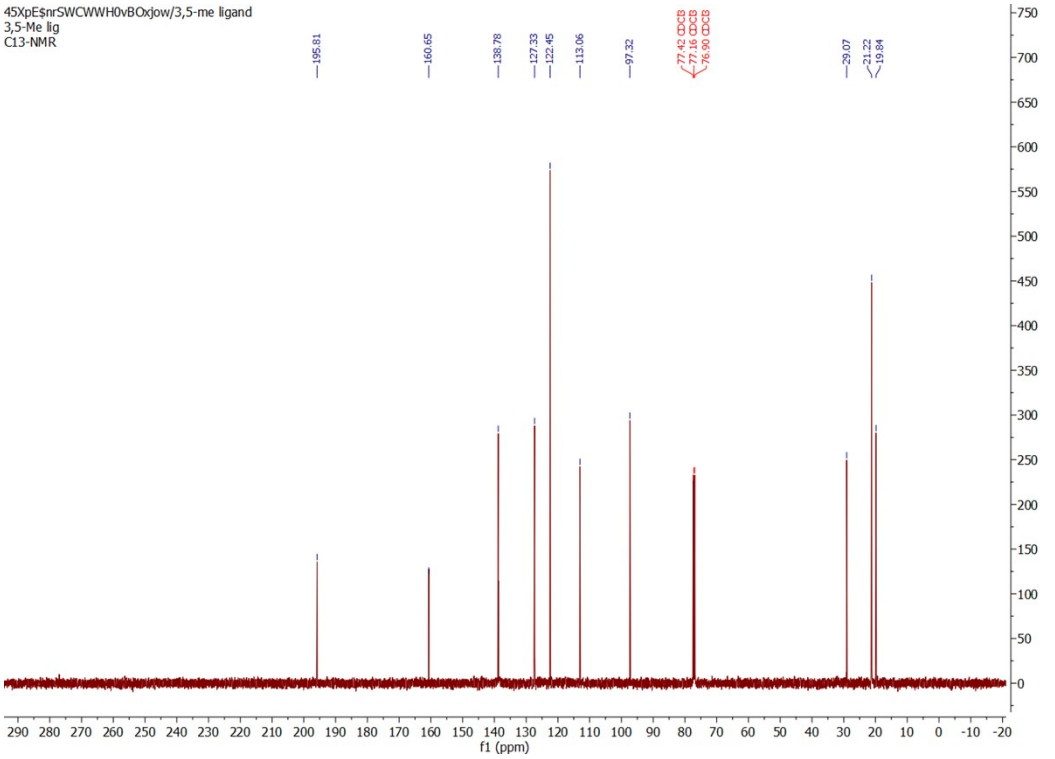

Figure S46. $^{13}C\{^{1}H\}$ NMR spectrum ($CDCl_3$, 25 °C, 125.813 MHz MHz) of **3f**.

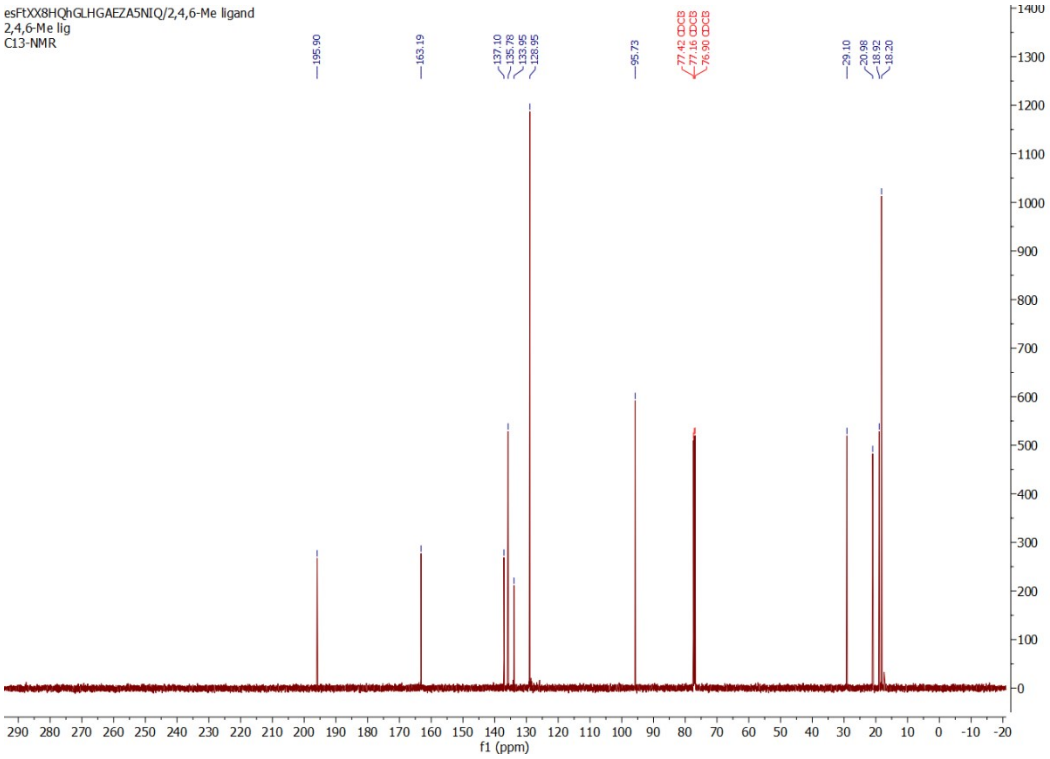

Figure S47. $^{13}C\{^{1}H\}$ NMR spectrum ($CDCl_3$, 25 °C, 125.813 MHz MHz) of **3g**.

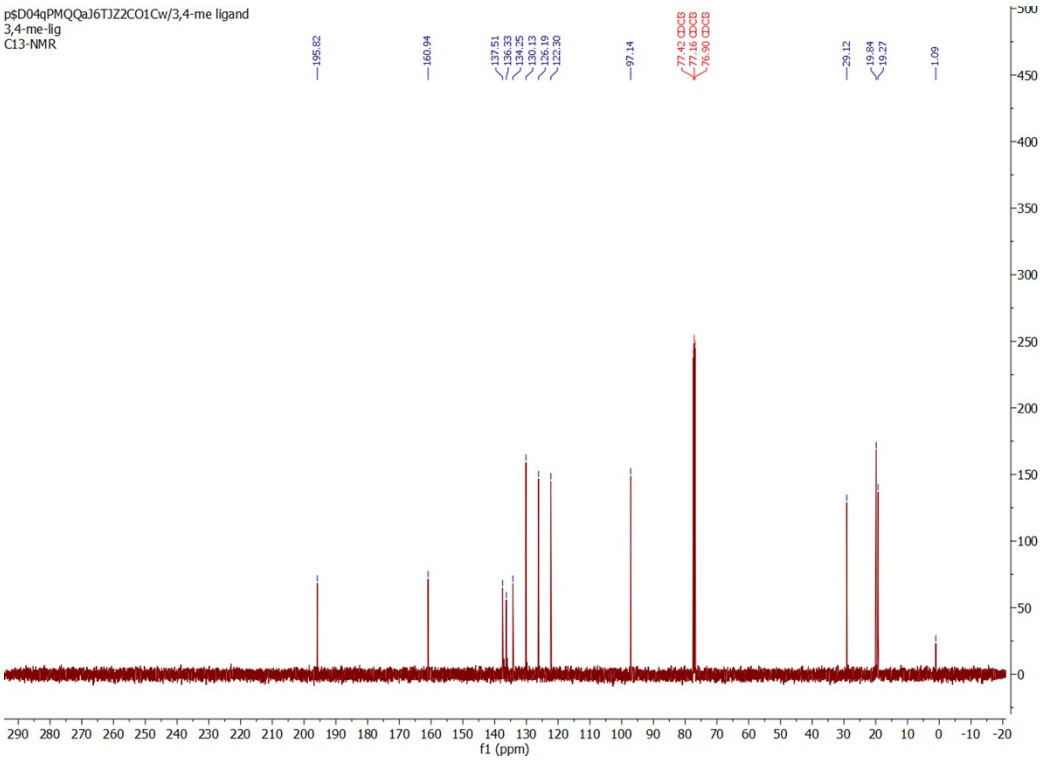

Figure S48. $^{13}C\{^{1}H\}$ NMR spectrum ($CDCl_3$, 25 °C, 125.813 MHz MHz) of **3h**.

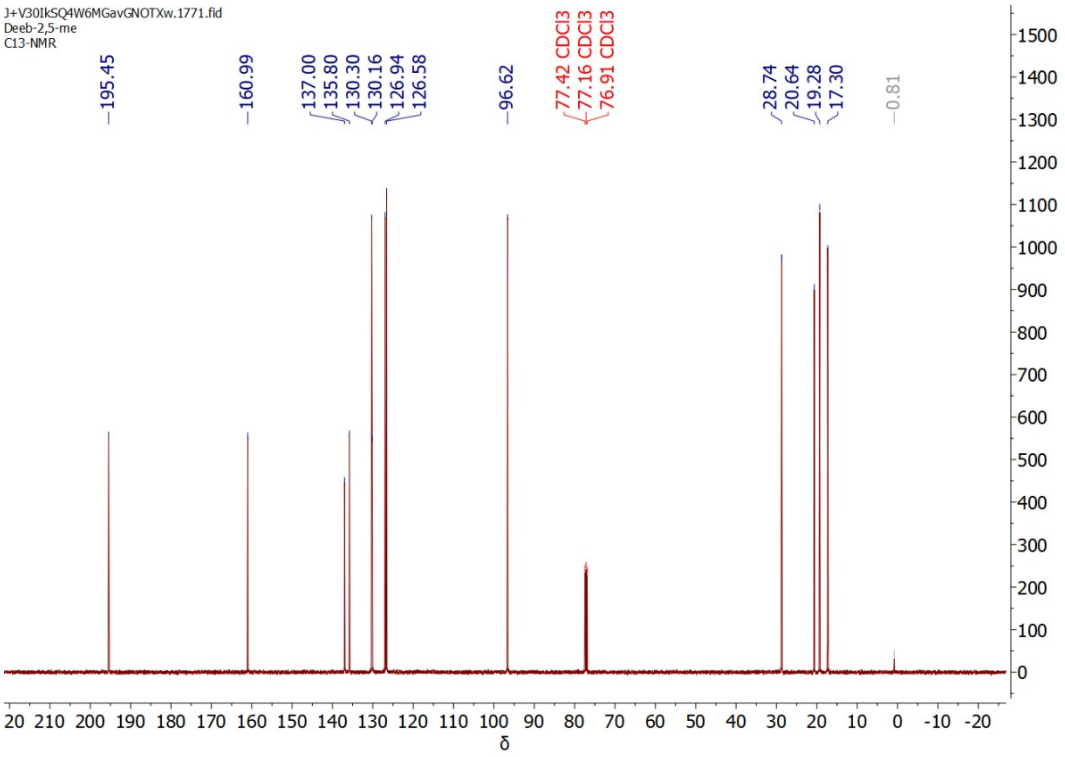

Figure S49. $^{13}C\{^{1}H\}$ NMR spectrum ($CDCl_3$, 25 °C, 125.813 MHz MHz) of **3i**.

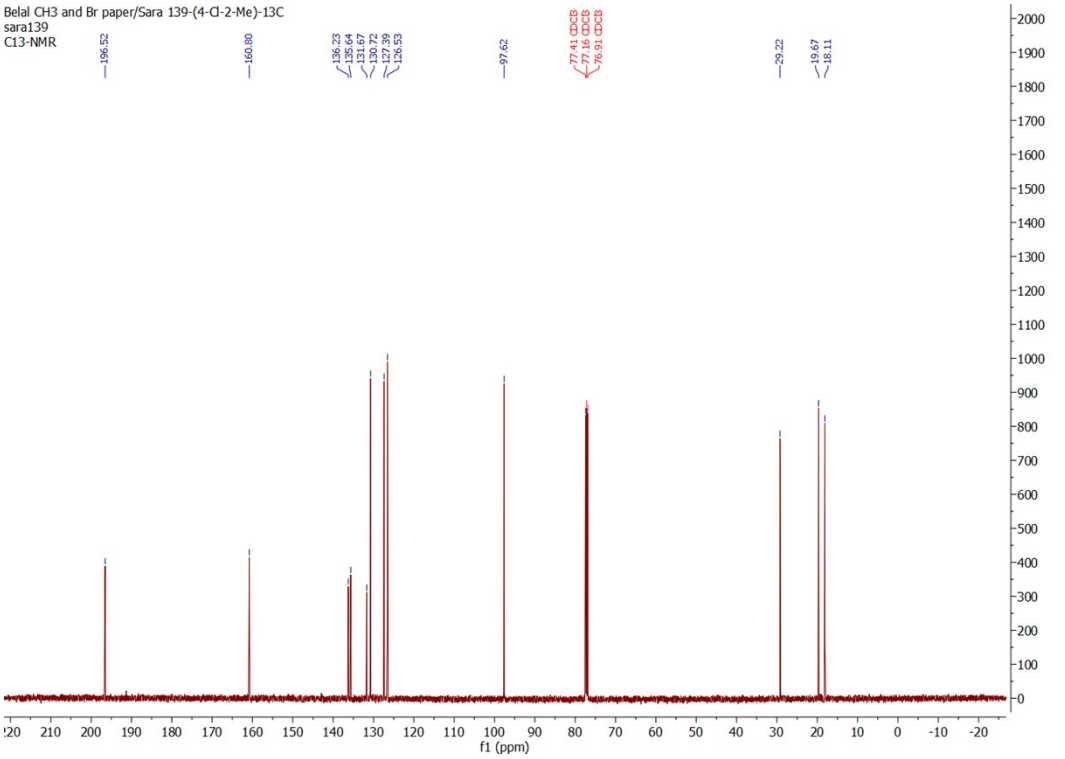

Figure S50. $^{13}C\{^{1}H\}$ NMR spectrum ($CDCl_3$, 25 °C, 125.813 MHz MHz) of **3j**.

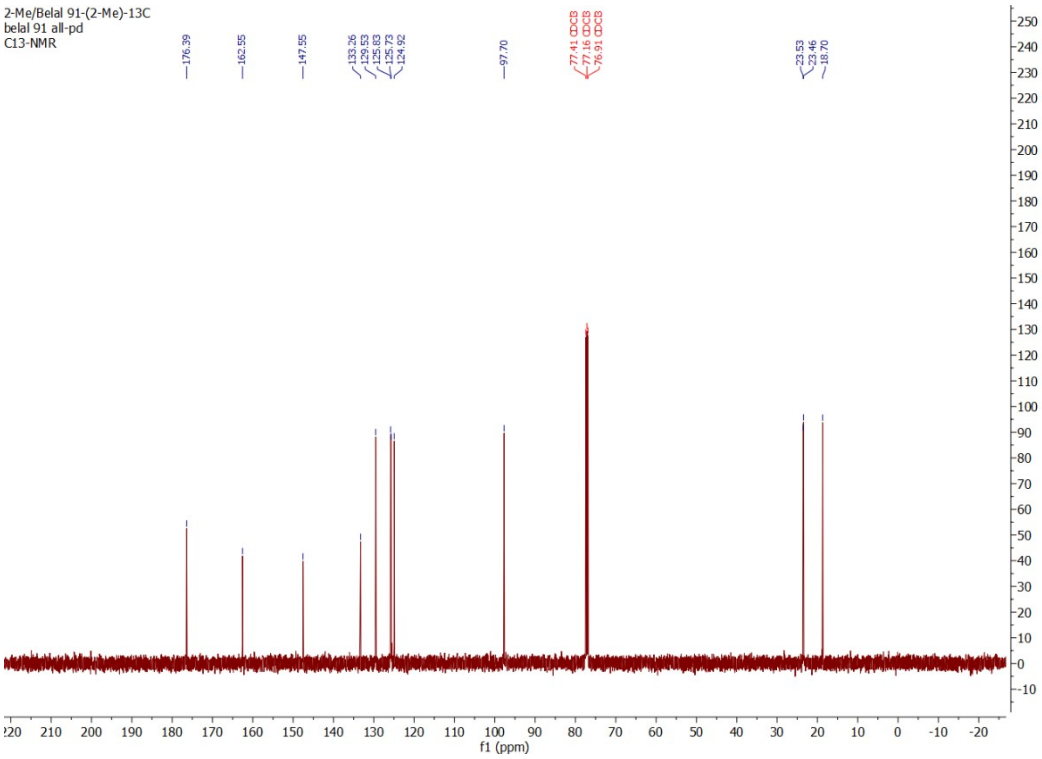

Figure S51. $^{13}C\{^{1}H\}$ NMR spectrum ($CDCl_3$, 25 °C, 125.813 MHz MHz) of **4a**.

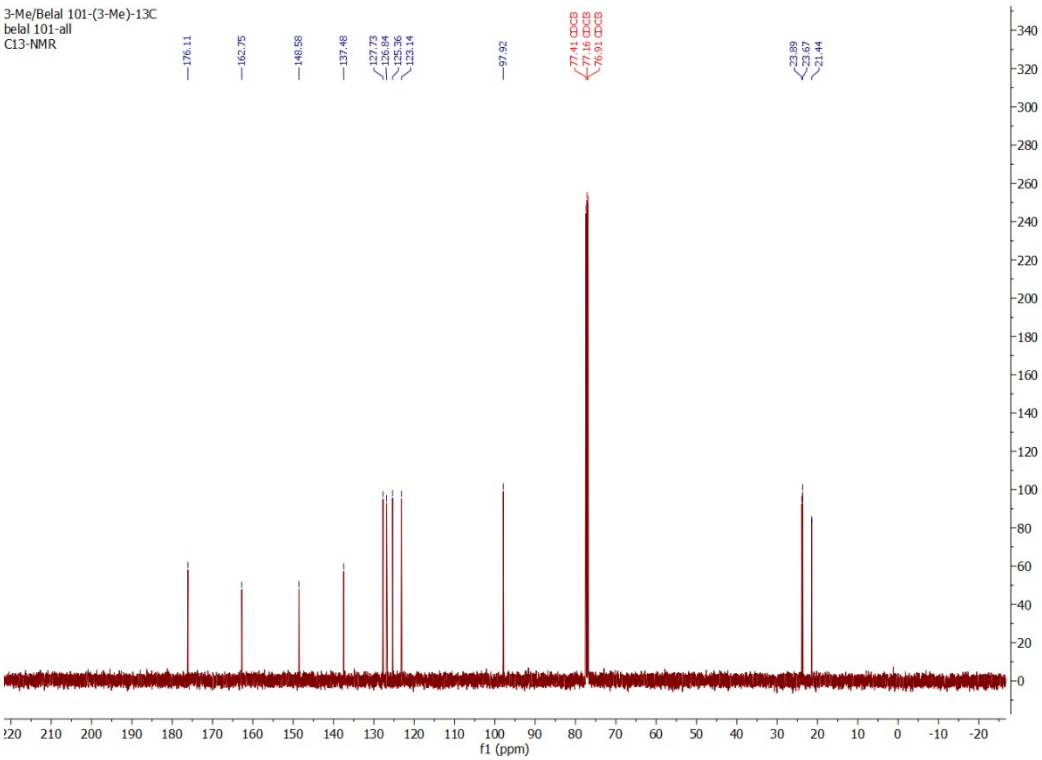

Figure S52. $^{13}C\{^{1}H\}$ NMR spectrum ($CDCl_3$, 25 °C, 125.813 MHz MHz) of **4b**.

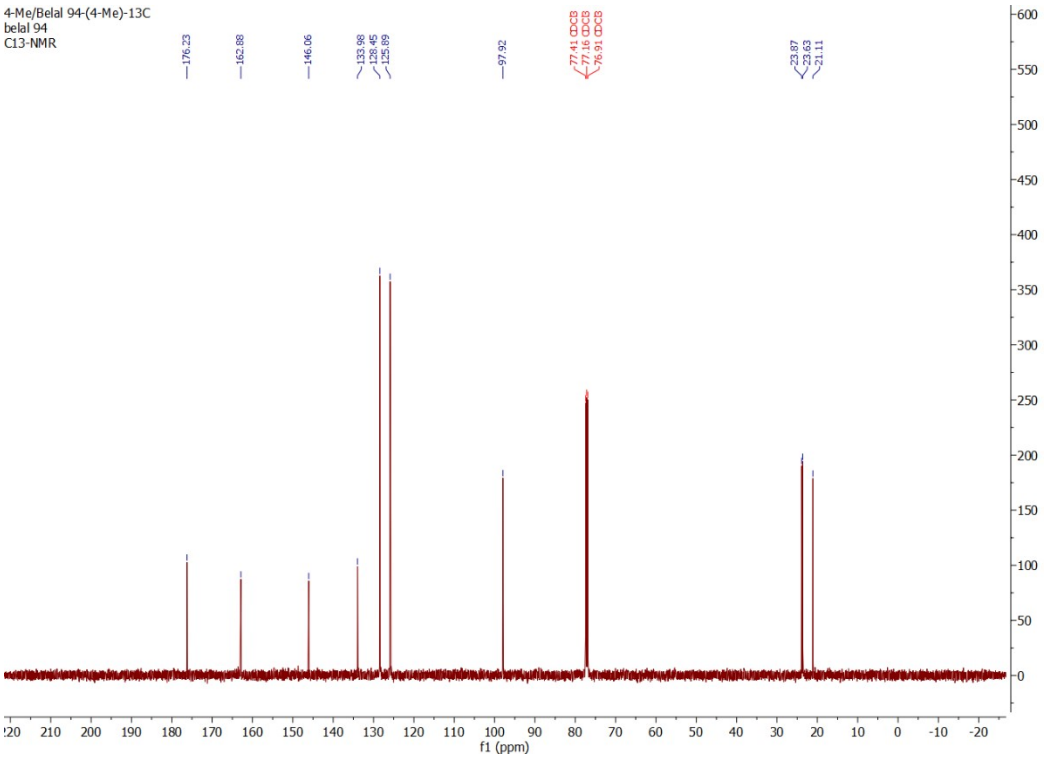

Figure S53. $^{13}C\{^{1}H\}$ NMR spectrum ($CDCl_3$, 25 °C, 125.813 MHz MHz) of **4c**.

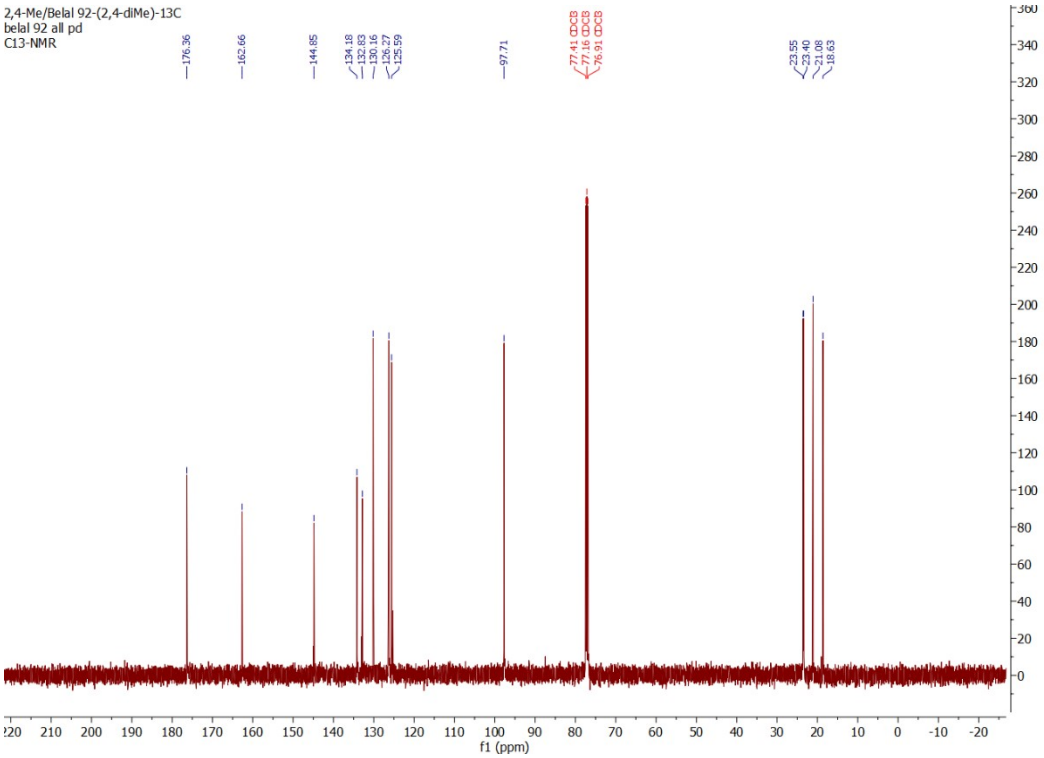

Figure S54. $^{13}C\{^{1}H\}$ NMR spectrum ($CDCl_3$, 25 °C, 125.813 MHz MHz) of **4d**.

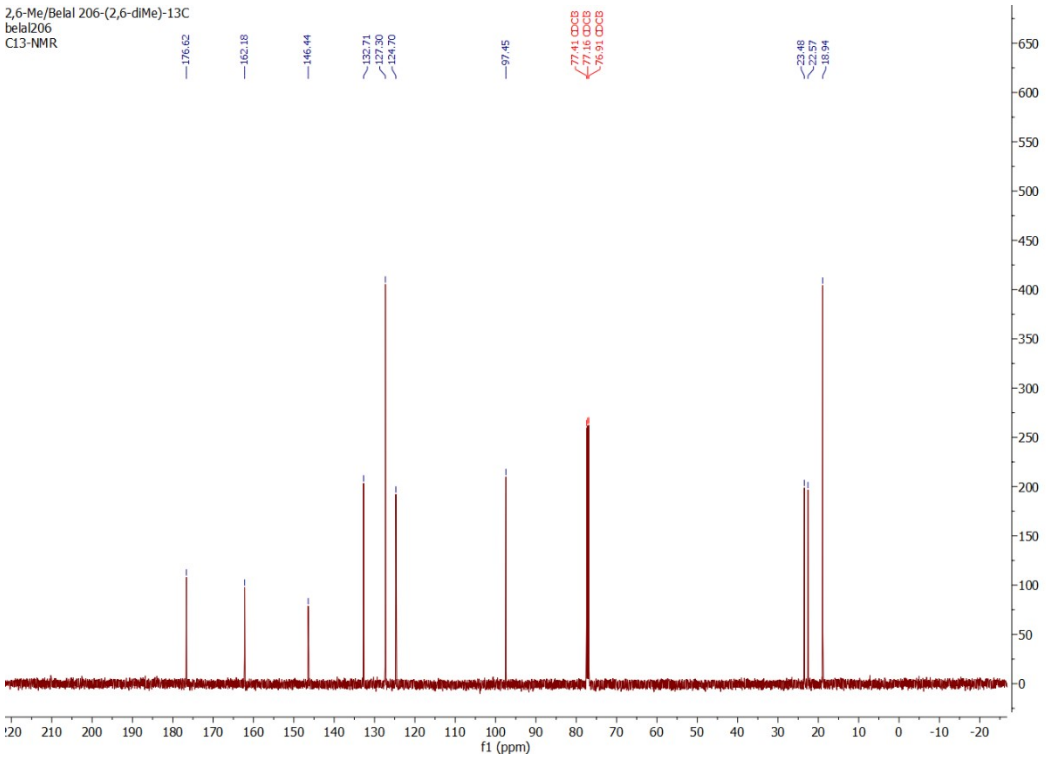

Figure S55. $^{13}C\{^{1}H\}$ NMR spectrum ($CDCl_3$, 25 °C, 125.813 MHz MHz) of **4e**.

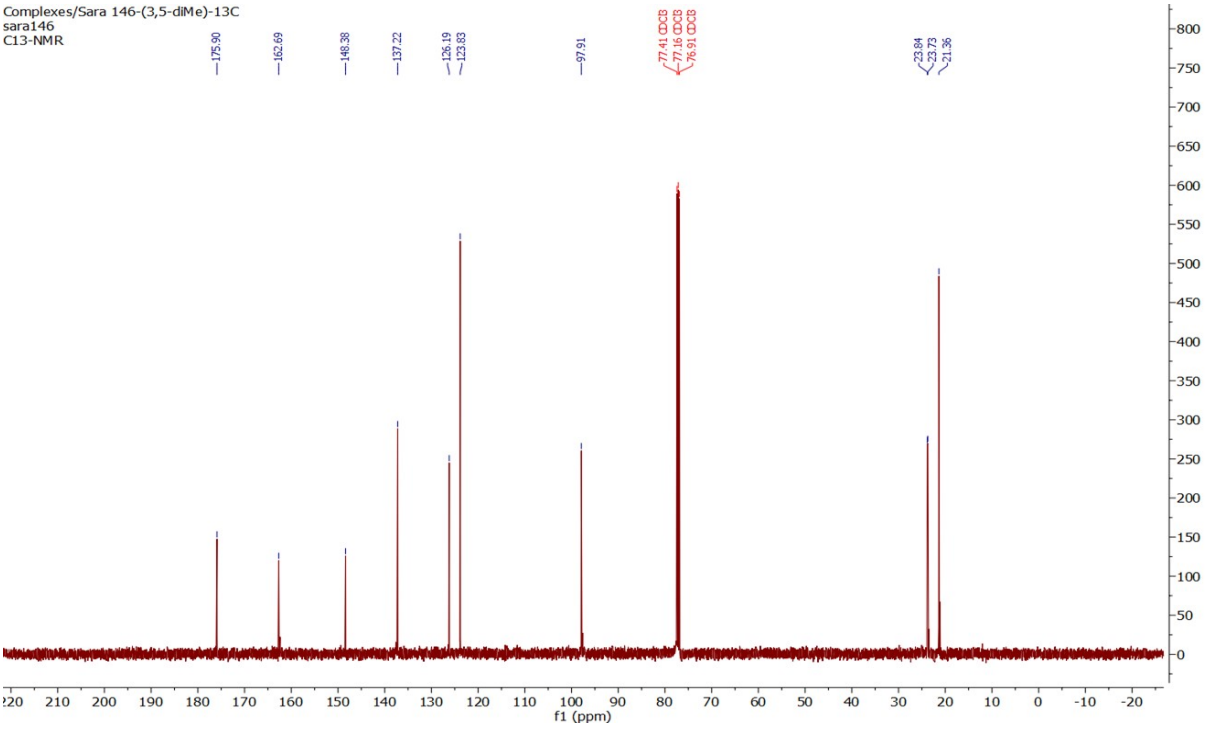

Figure S56. $^{13}C\{^{1}H\}$ NMR spectrum ($CDCl_3$, 25 °C, 125.813 MHz MHz) of **4f**.

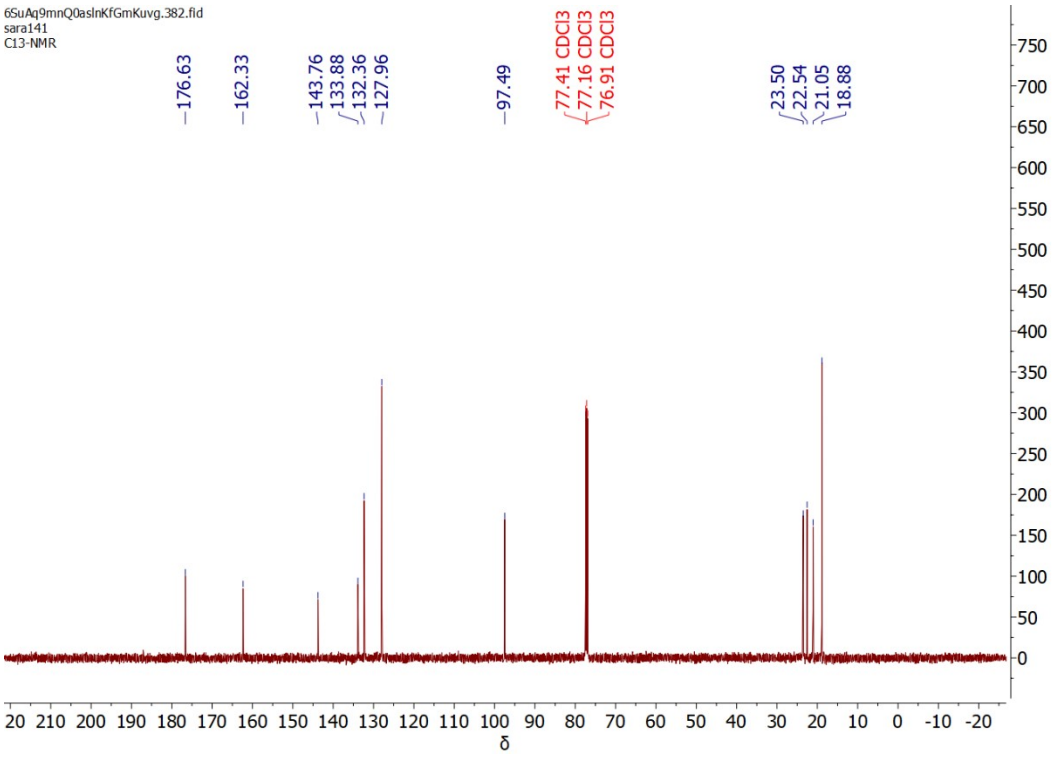

Figure S57. $^{13}C\{^{1}H\}$ NMR spectrum ($CDCl_3$, 25 °C, 125.813 MHz MHz) of **4g**.

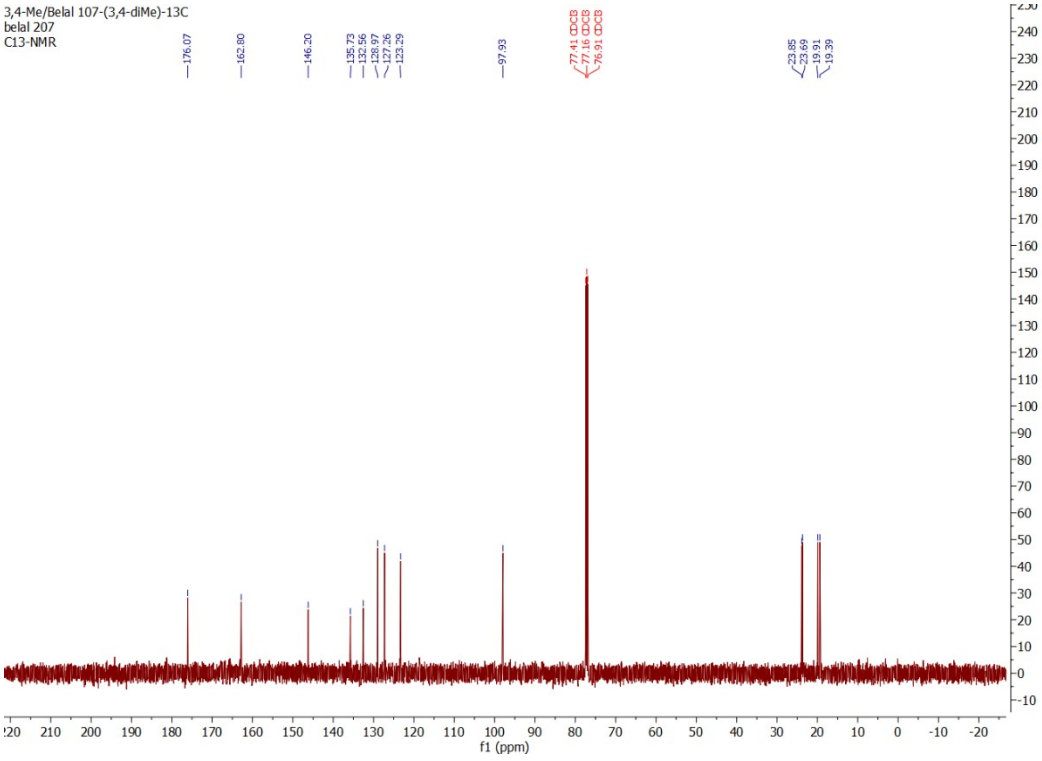

Figure S58. $^{13}C\{^{1}H\}$ NMR spectrum ($CDCl_3$, 25 °C, 125.813 MHz MHz) of **4h**.

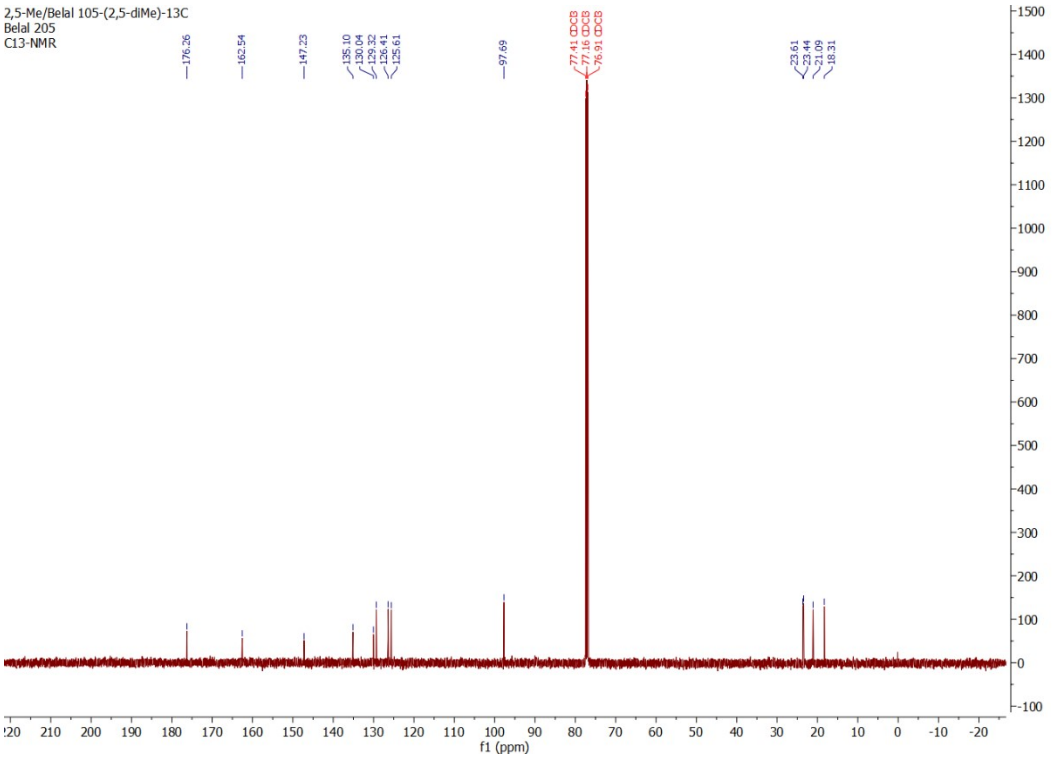

Figure S59. $^{13}C\{^{1}H\}$ NMR spectrum ($CDCl_3$, 25 °C, 125.813 MHz MHz) of **4i**.

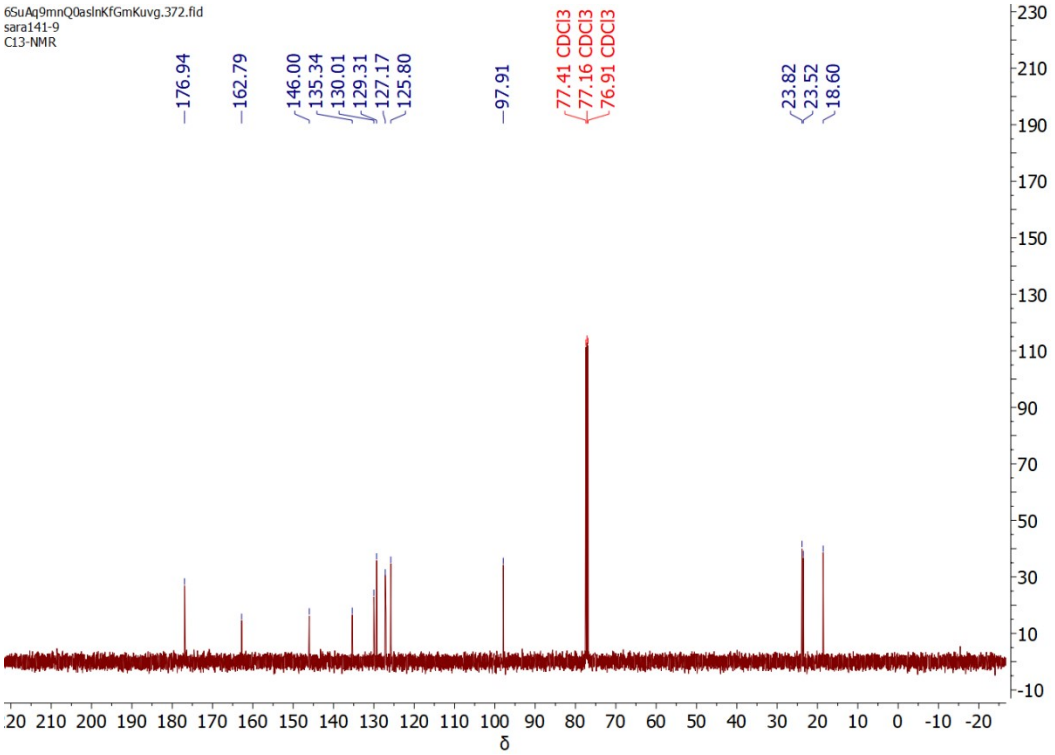

Figure S60. $^{13}C\{^{1}H\}$ NMR spectrum ($CDCl_3$, 25 °C, 125.813 MHz MHz) of **4j**.

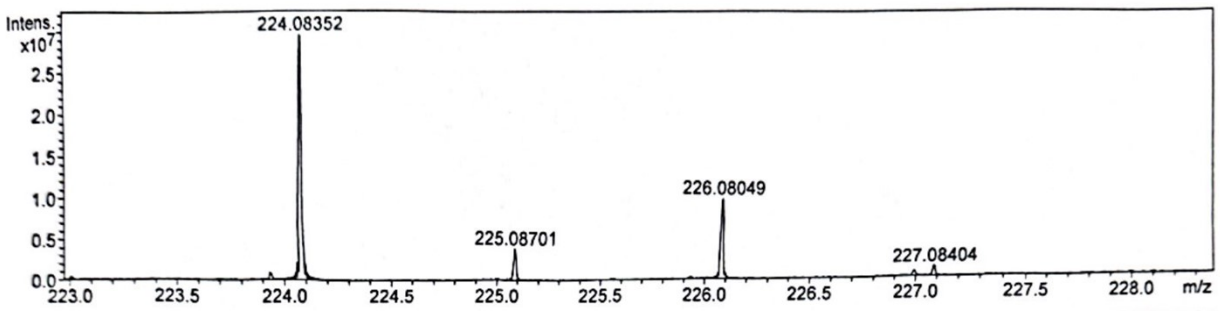

Figure S61. HR-ESI-MS (positive ion mode) spectrum of **3j**. Monoisotopic mass for $C_{12}H_{15}ClNO$ (M+H) Calc. 224.08367 found 224.08352.

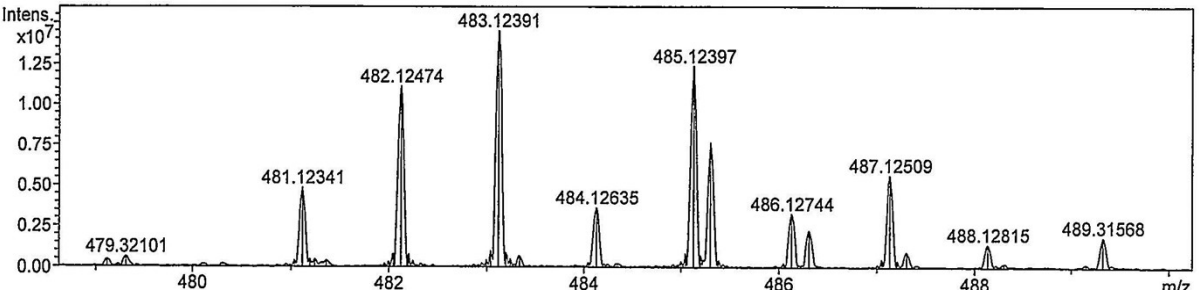

Figure S62. HR-ESI-MS (positive ion mode) spectrum of **4a**. Monoisotopic mass for $C_{24}H_{29}N_2O_2Pd$ (M+H) Calc. 483.12584 found 483.12391.

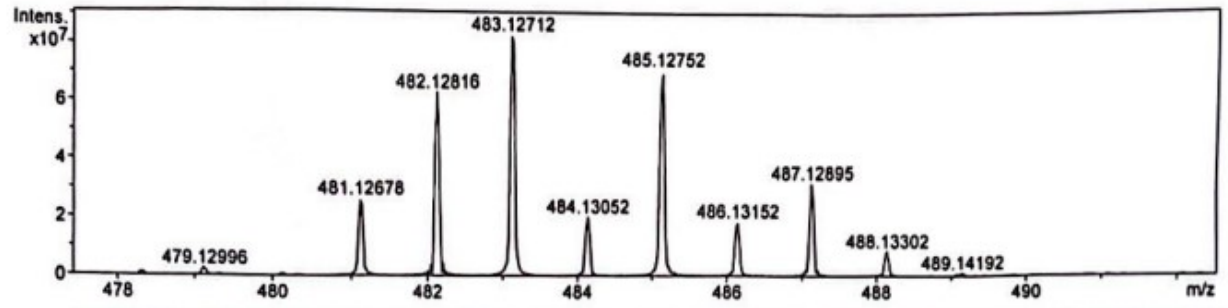

Figure S63. HR-ESI-MS (positive ion mode) spectrum of **4b**. Monoisotopic mass for $C_{24}H_{29}N_2O_2Pd$ (M+H) Calc. 483.12584 found 483.12712.

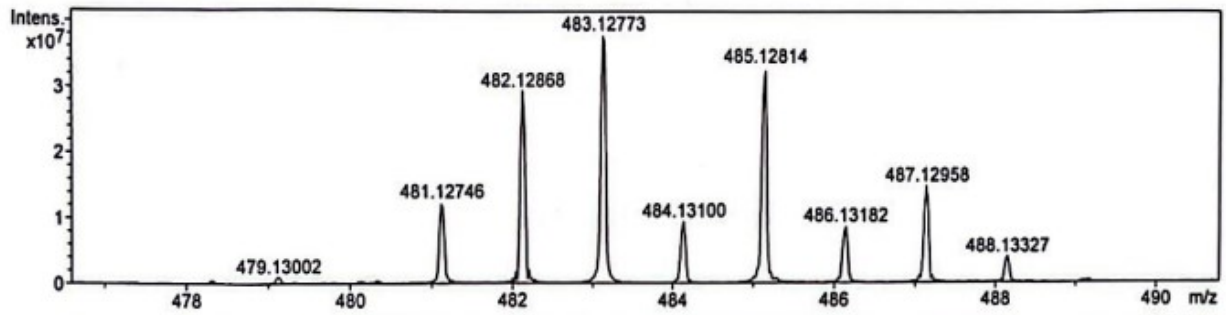

Figure S64. HR-ESI-MS (positive ion mode) spectrum of **4c**. Monoisotopic mass for $C_{24}H_{29}N_2O_2Pd$ (M+H) Calc. 483.12584 found 483.12773.

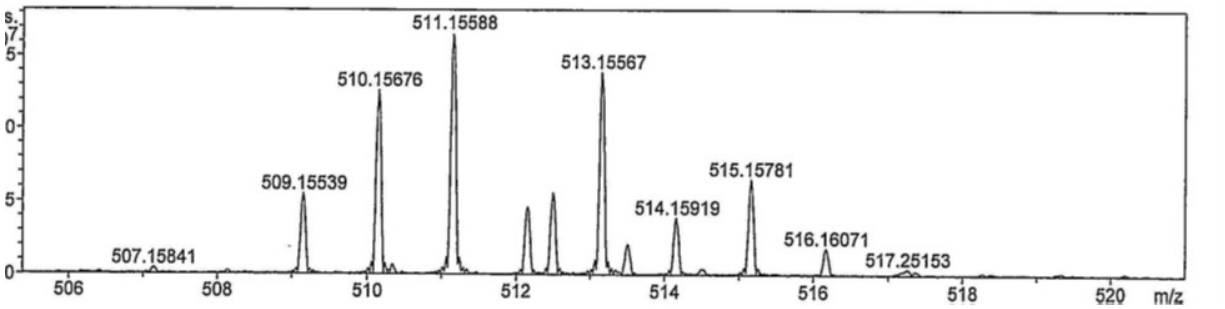

Figure S65. HR-ESI-MS (positive ion mode) spectrum of **4d**. Monoisotopic mass for $C_{26}H_{33}N_2O_2Pd$ (M+H) Calc. 511.15714 found 511.15588.

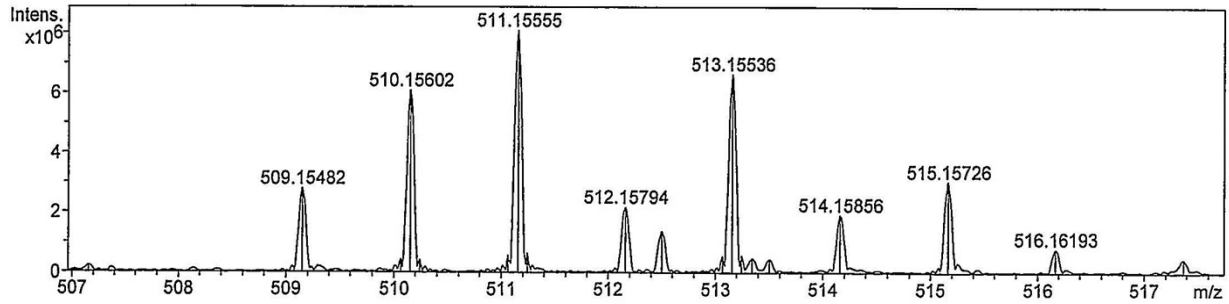

Figure S66. HR-ESI-MS (positive ion mode) spectrum of **4e**. Monoisotopic mass for $C_{26}H_{33}N_2O_2Pd$ (M+H) Calc. 511.15714 found 511.15555.

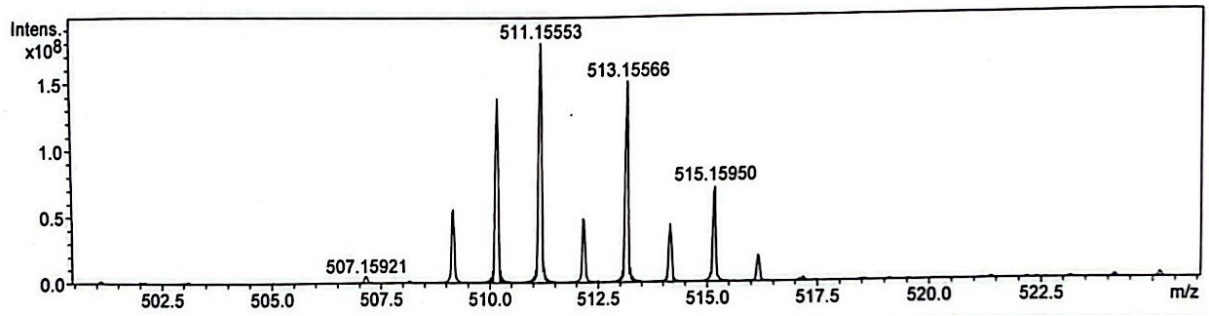

Figure S67. HR-ESI-MS (positive ion mode) spectrum of **4f**. Monoisotopic mass for $C_{26}H_{33}N_2O_2Pd$ (M+H) Calc. 511.15714 found 511.15553.

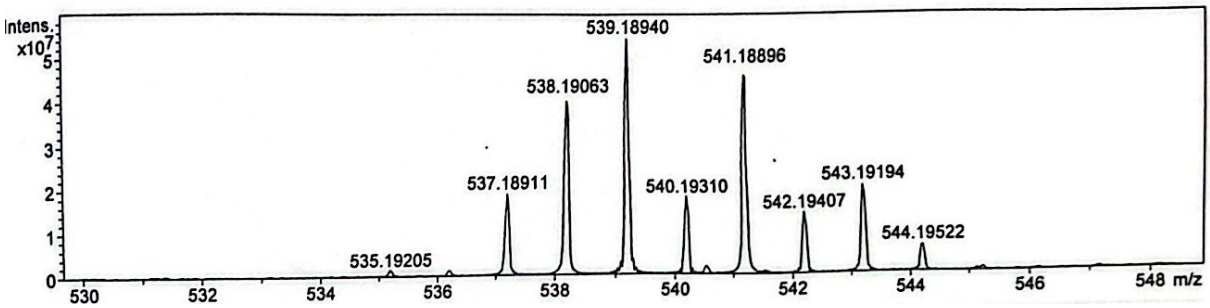

Figure S68. HR-ESI-MS (positive ion mode) spectrum of **4g**. Monoisotopic mass for $C_{28}H_{37}N_2O_2Pd$ (M+H) Calc. 539.18844 found 539.18940.

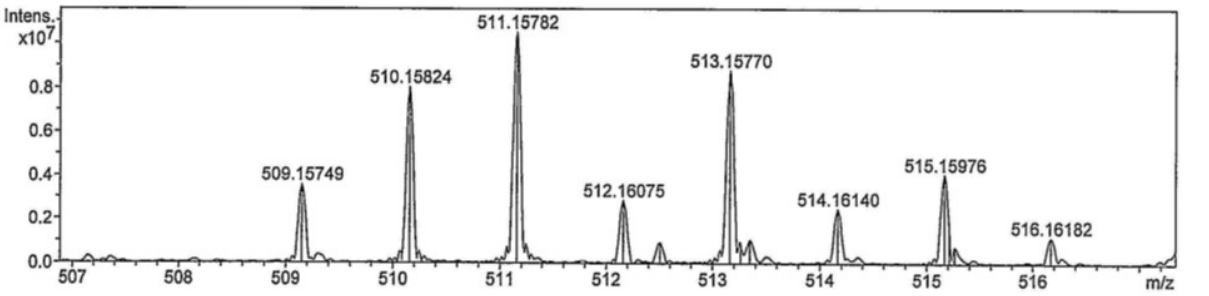

Figure S69. HR-ESI-MS (positive ion mode) spectrum of **4h**. Monoisotopic mass for $C_{26}H_{33}N_2O_2Pd$ (M+H) Calc. 511.15714 found 511.15782.

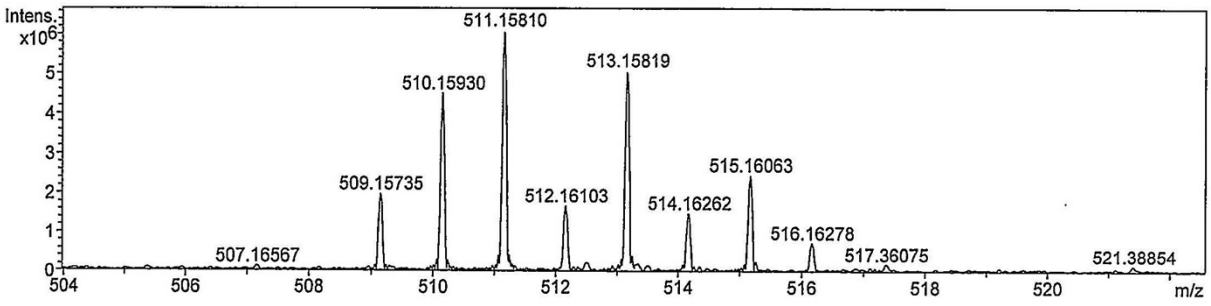

Figure S70. HR-ESI-MS (positive ion mode) spectrum of **4i**. Monoisotopic mass for $C_{26}H_{33}N_2O_2Pd$ (M+H) Calc. 511.15714 found 511.15810.

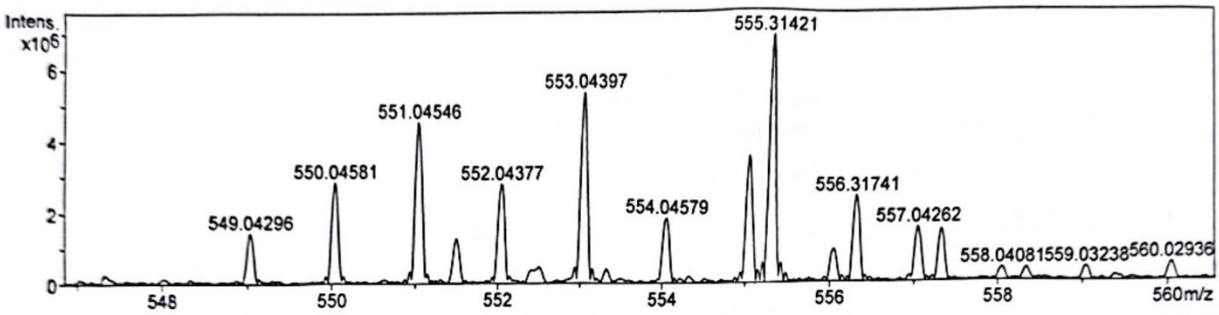

Figure S71. HR-ESI-MS (positive ion mode) spectrum of **4j**. Monoisotopic mass for $C_{24}H_{27}Cl_2N_2O_2Pd$ (M+H) Calc. 552.08032 found 552.04377.

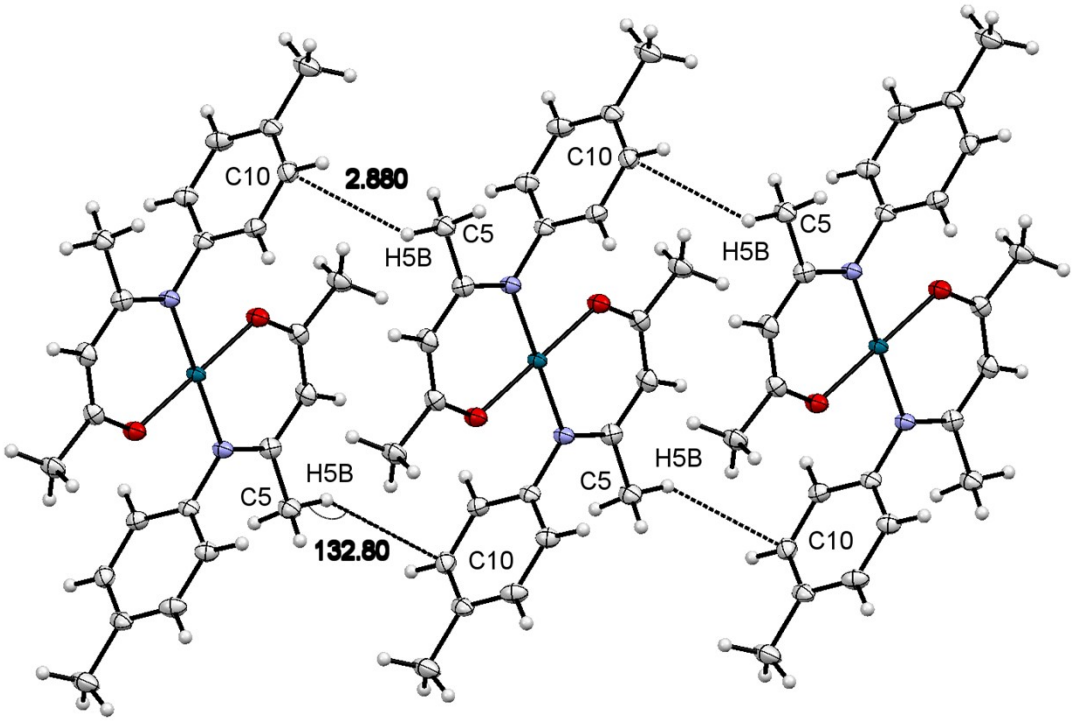

Figure S72. Illustration of C–H···π contacts in **4c**.

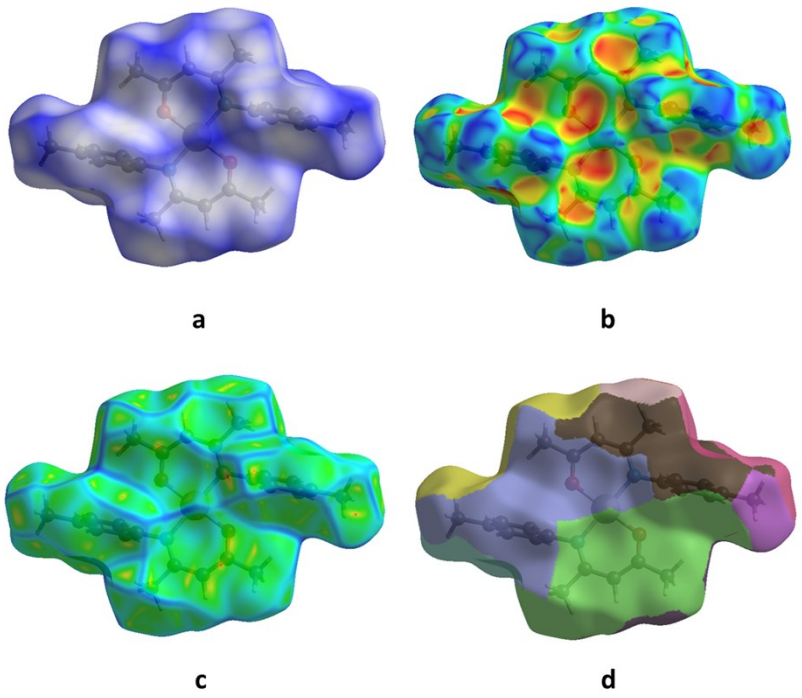

Figure S73. (**a**) Hirshfeld surface of **4c** mapped with d_{norm} in the range 0.0179 to -1.3052 a.u. (**b**) Hirshfeld surface of **4c** mapped with *Shape Index* in the range -1 to 1 a.u. (**c**) Hirshfeld surfaces with curvedness of **4c**. (**d**) Hirshfeld surfaces with Fragment patch of **4c**.

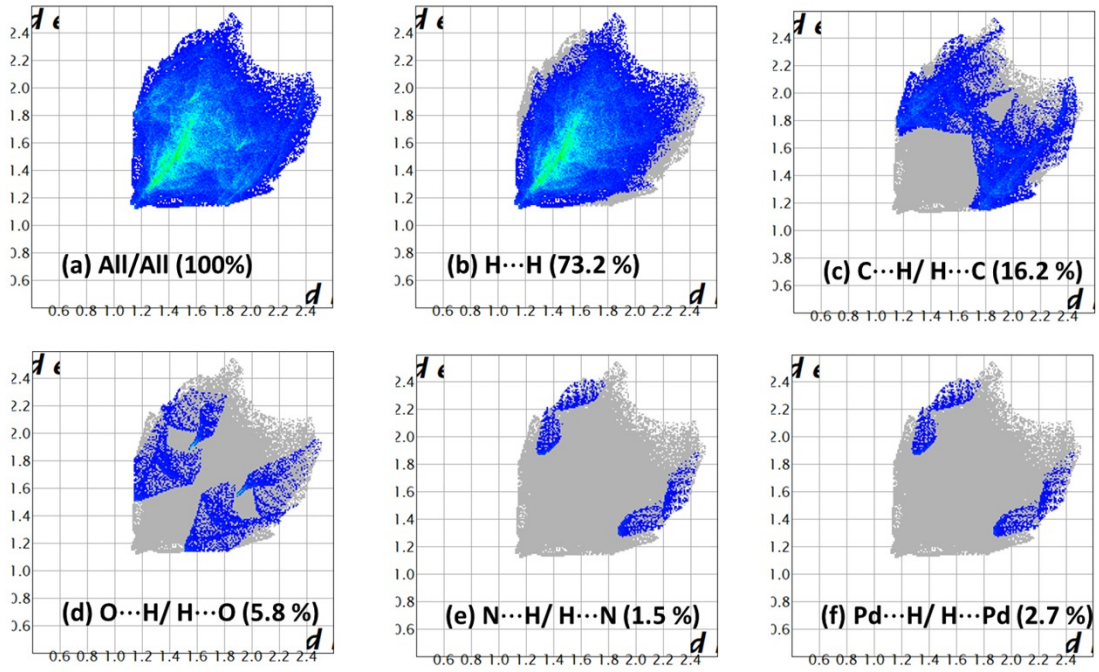

Figure S74. Full 2-D fingerprint plot for **4c** and (**a**) the decomposed contacts representing (**b**) H···H (73.2 %), (c) C···H/H···C (16.2 %), (d) O···H/H···O (5.8 %), (e) N···H/ H···N (1.5 %), and (f) Pd···H/H···Pd (2.7 %) intermolecular interactions.

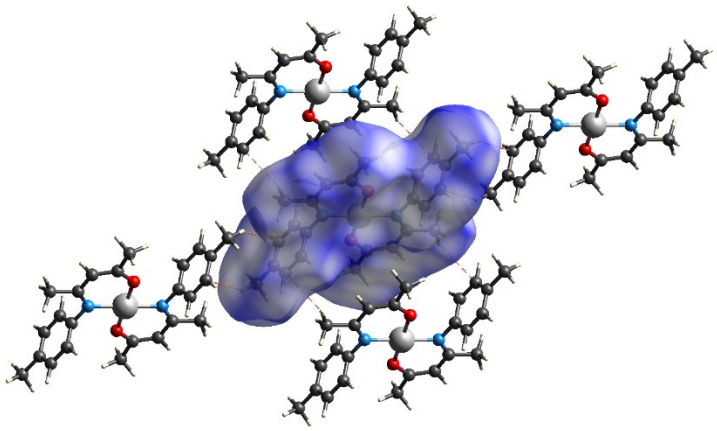

Figure S75. Hirshfeld surface contacts in **4c**.

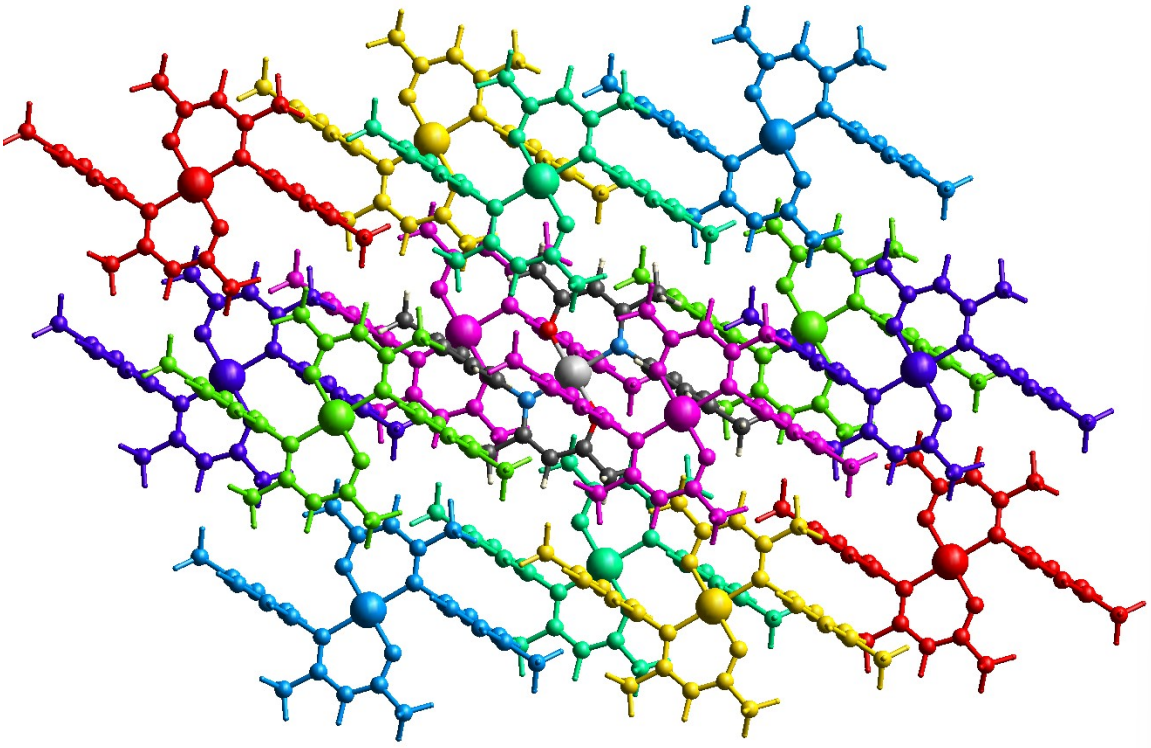

Figure S76. Intermolecular interaction topology network between neighbouring molecules within each molecular crystal structure

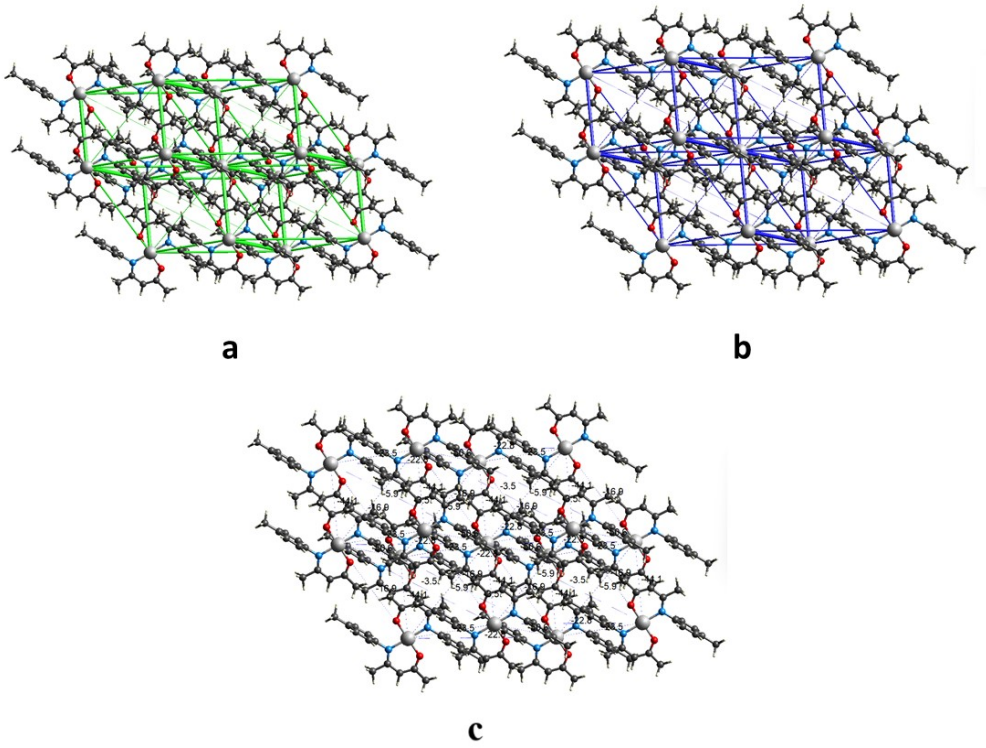

Figure S77. (**a**) Dispersion intermolecular interaction topology energy framework between neighbouring molecules. (**b**) Total intermolecular interaction topology energy framework between neighboring molecules. (**c**) Total intermolecular interaction (annotated) energy framework between neighboring molecules.

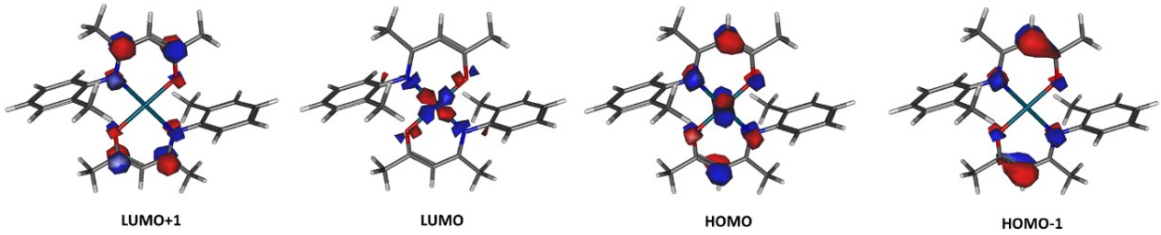

Figure S78. The isosurface densities of the frontier orbitals: LUMO+1, LUMO, HOMO, HOMO-1 of compound **4a** (isosurface value 0.06).

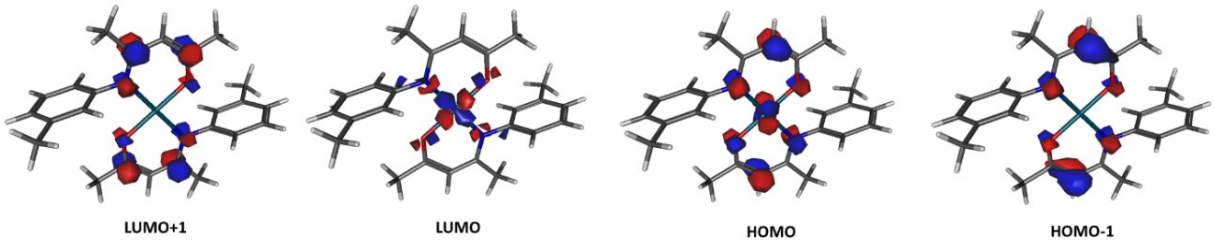

Figure S79. The isosurface densities of the frontier orbitals: LUMO+1, LUMO, HOMO, HOMO-1 of compound **4b** (isosurface value 0.06).

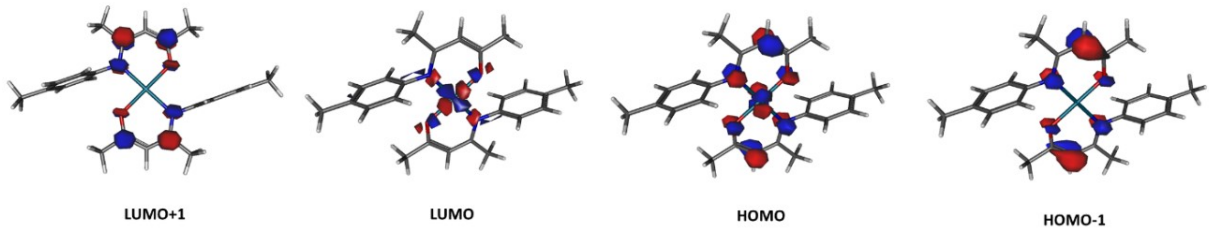

Figure S80. The isosurface densities of the frontier orbitals: LUMO+1, LUMO, HOMO, HOMO-1 of compound **4c** (isosurface value 0.06).

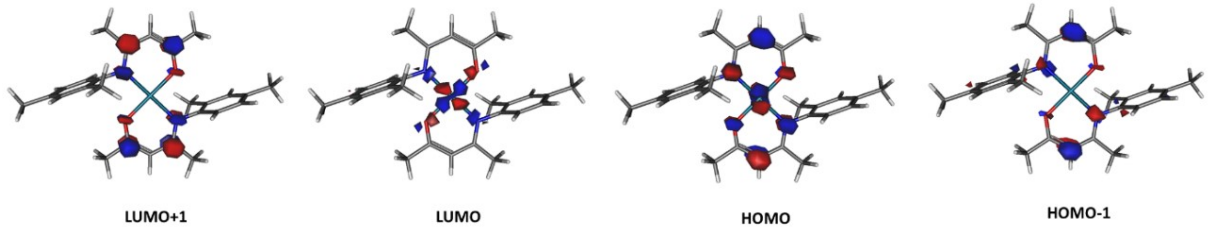

Figure S81. The isosurface densities of the frontier orbitals: LUMO+1, LUMO, HOMO, HOMO-1 of compound **4d** (isosurface value 0.06).

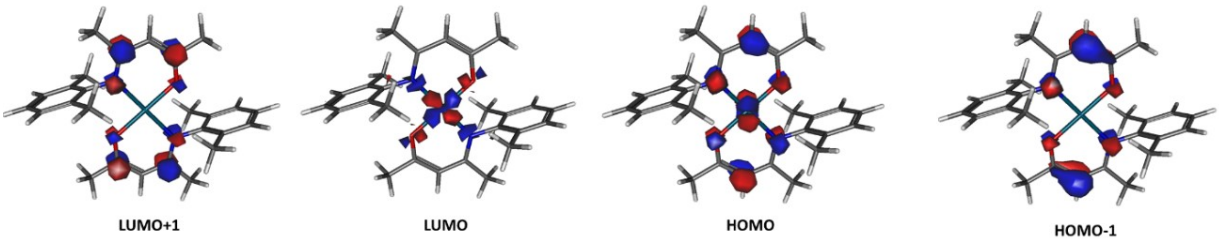

Figure S82. The isosurface densities of the frontier orbitals: LUMO+1, LUMO, HOMO, HOMO-1 of compound **4e** (isosurface value 0.06).

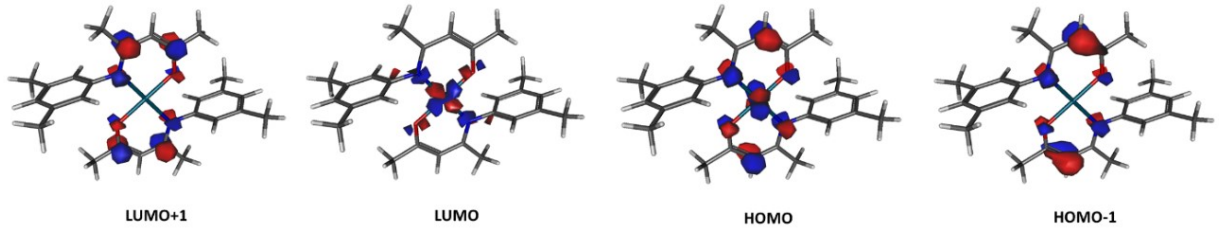

Figure S83. The isosurface densities of the frontier orbitals: LUMO+1, LUMO, HOMO, HOMO-1 of compound **4f** (isosurface value 0.06).

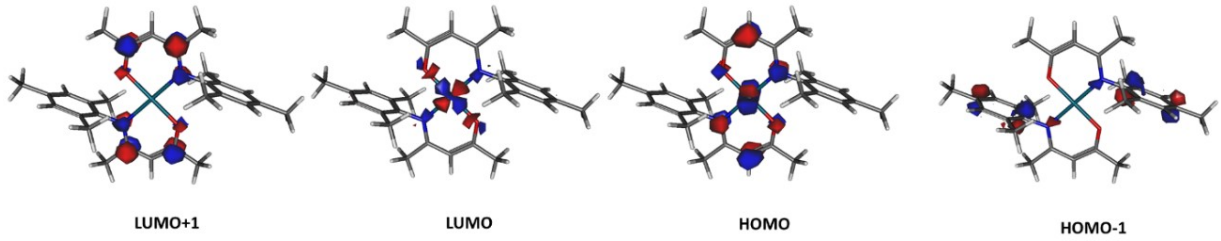

Figure S84. The isosurface densities of the frontier orbitals: LUMO+1, LUMO, HOMO, HOMO-1 of compound **4g** (isosurface value 0.06).

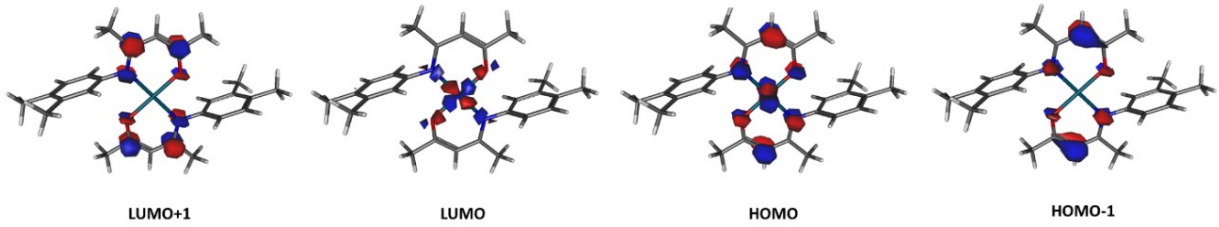

Figure S85. The isosurface densities of the frontier orbitals: LUMO+1, LUMO, HOMO, HOMO-1 of compound **4h** (isosurface value 0.06).

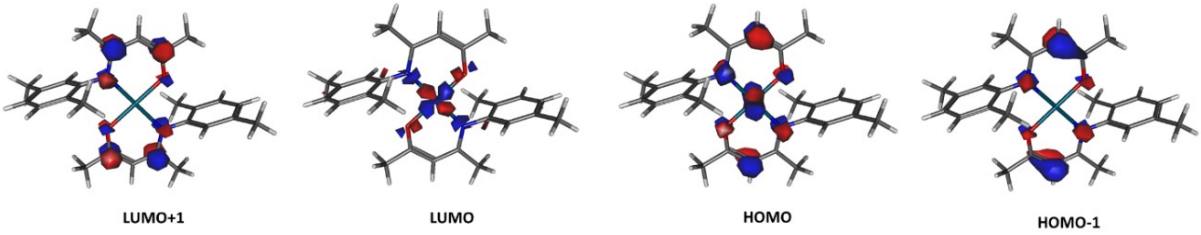

Figure S86. The isosurface densities of the frontier orbitals: LUMO+1, LUMO, HOMO, HOMO-1 of compound **4i** (isosurface value 0.06).

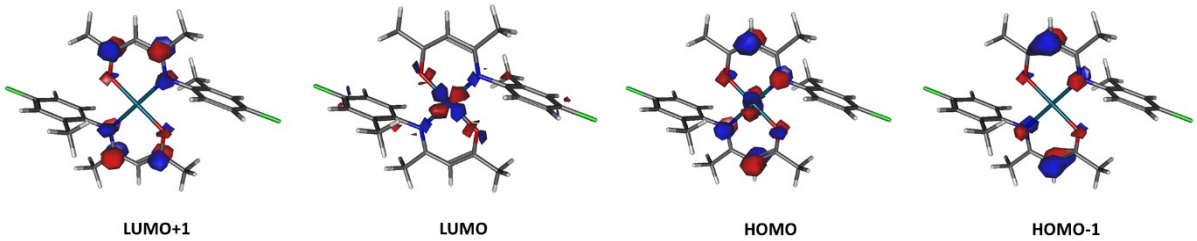

Figure S87. The isosurface densities of the frontier orbitals: LUMO+1, LUMO, HOMO, HOMO-1 of compound **4j** (isosurface value 0.06).

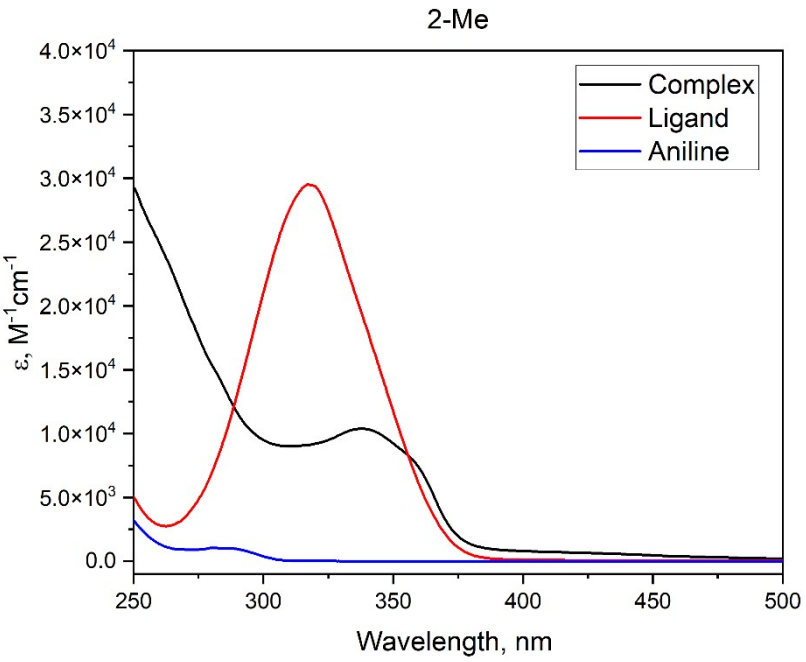

Figure S88. Electronic absorption spectra ($CHCl_3$, ambient temperature) of **2a**, **3a** and **4a**.

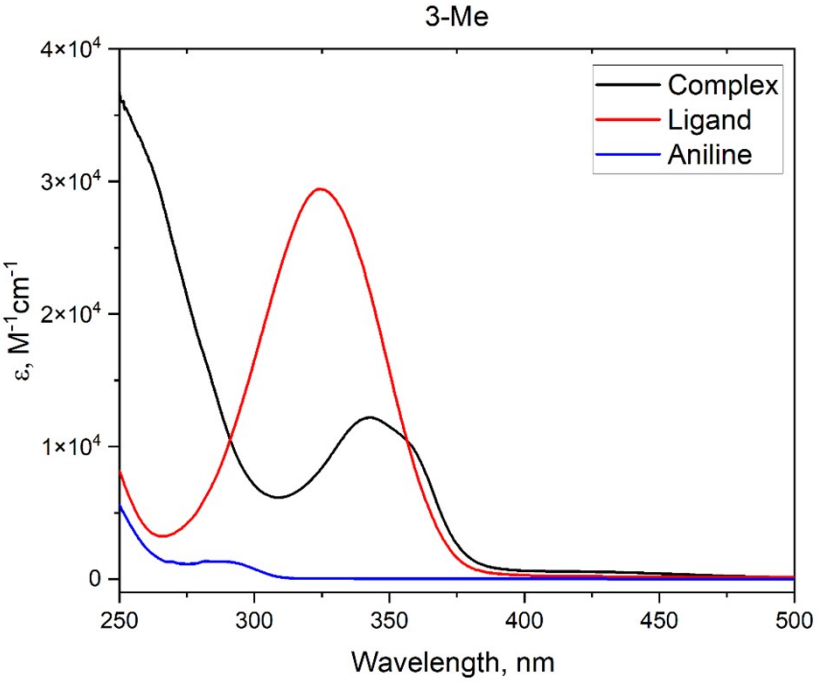

Figure S89. Electronic absorption spectra ($CHCl_3$, ambient temperature) of **2b**, **3b** and **4b**.

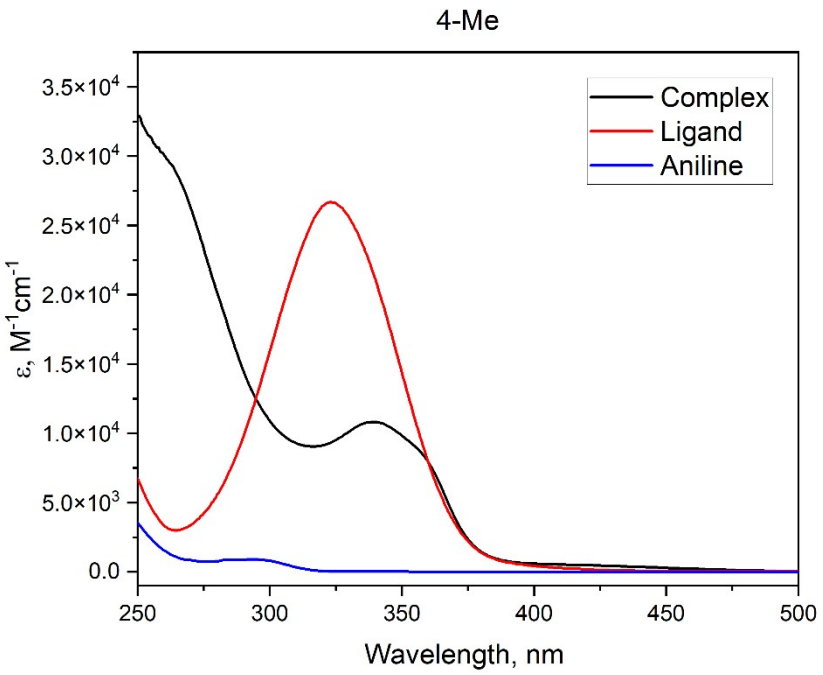

Figure S90. Electronic absorption spectra ($CHCl_3$, ambient temperature) of **2c**, **3c** and **4c**.

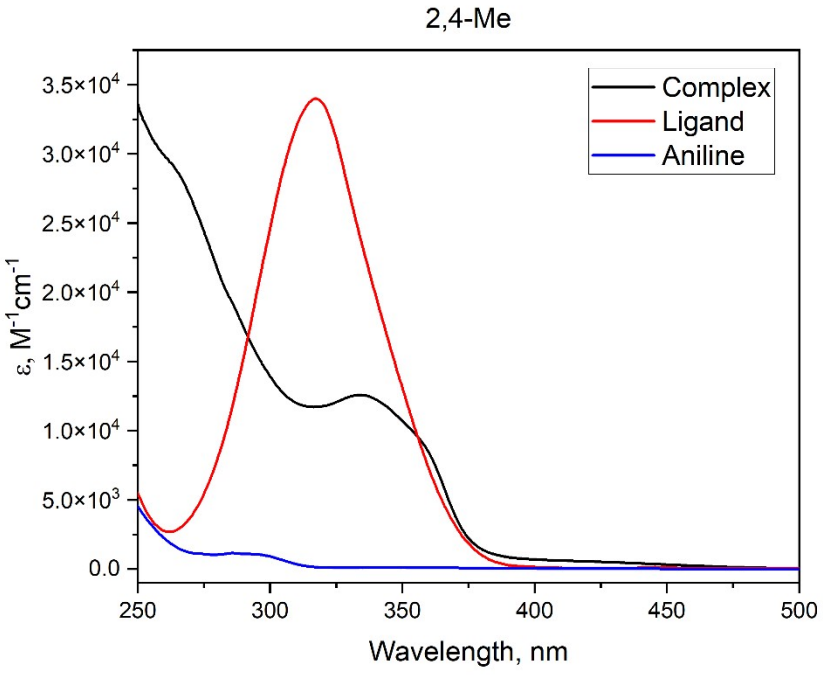

Figure S91. Electronic absorption spectra ($CHCl_3$, ambient temperature) of **2d**, **3d** and **4d**.

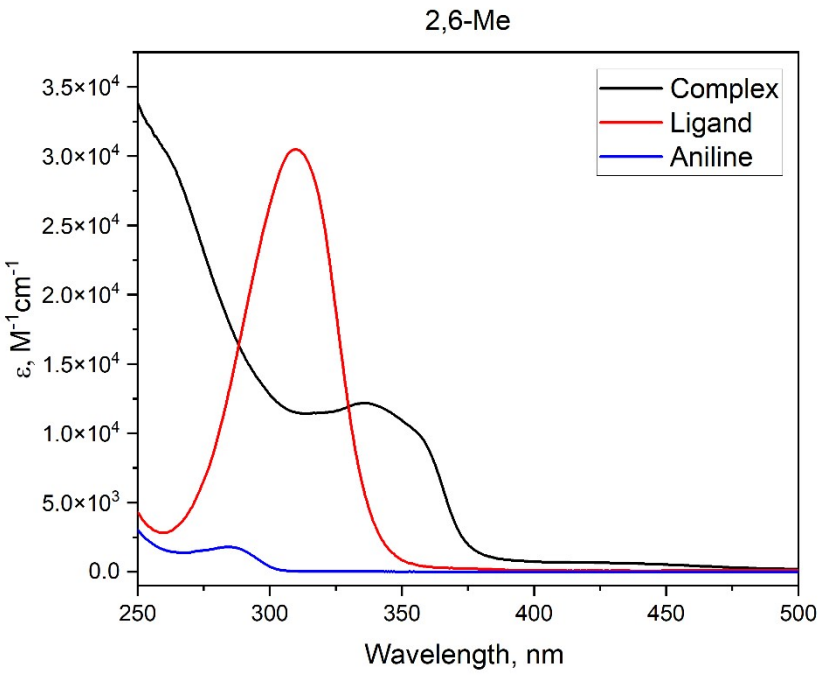

Figure S82. Electronic absorption spectra ($CHCl_3$, ambient temperature) of **2e**, **3e** and **4e**.

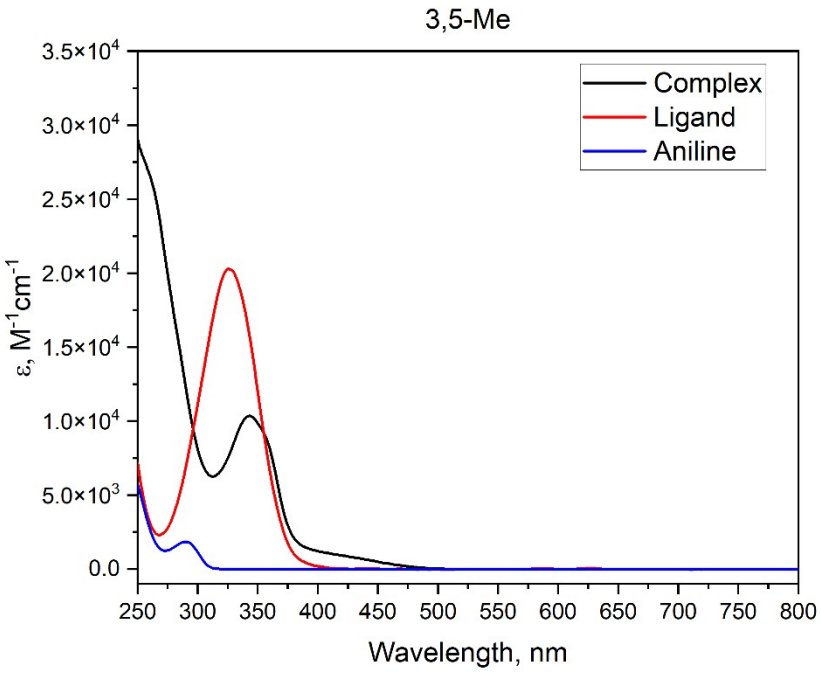

Figure S93. Electronic absorption spectra ($CHCl_3$, ambient temperature) of **2f**, **3f** and **4f**.

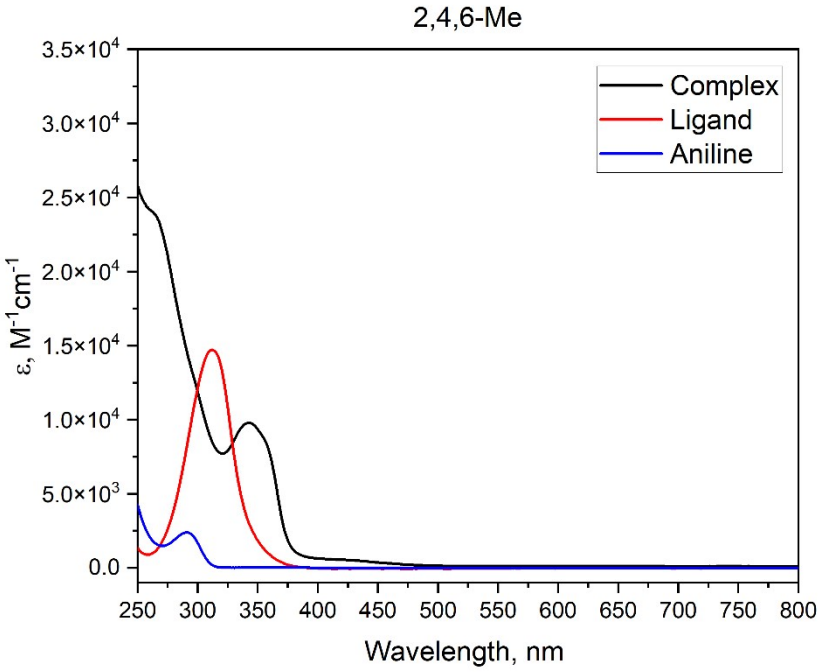

Figure S94. Electronic absorption spectra ($CHCl_3$, ambient temperature) of **2g**, **3g** and **4g**.

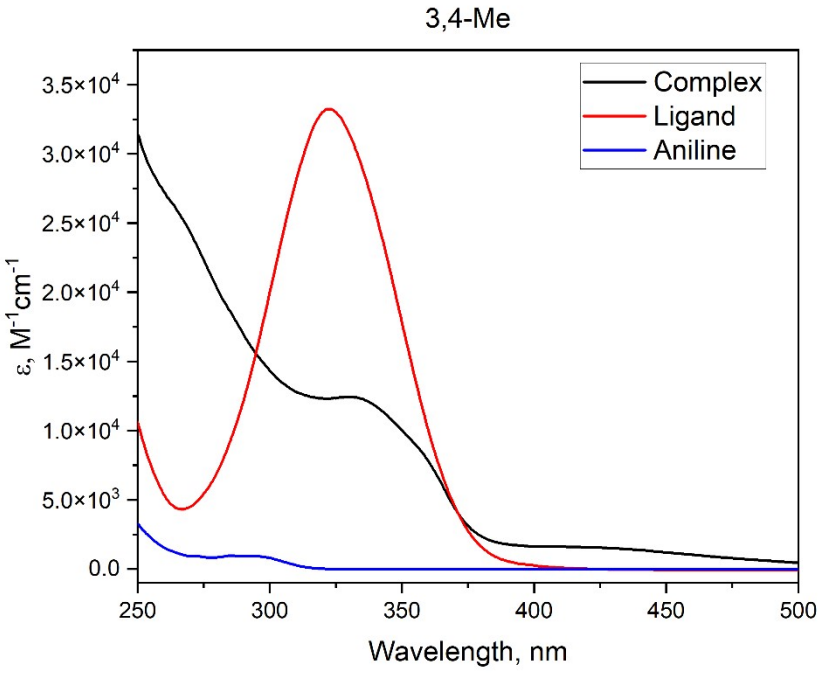

Figure S95. Electronic absorption spectra ($CHCl_3$, ambient temperature) of **2h**, **3h** and **4h**.

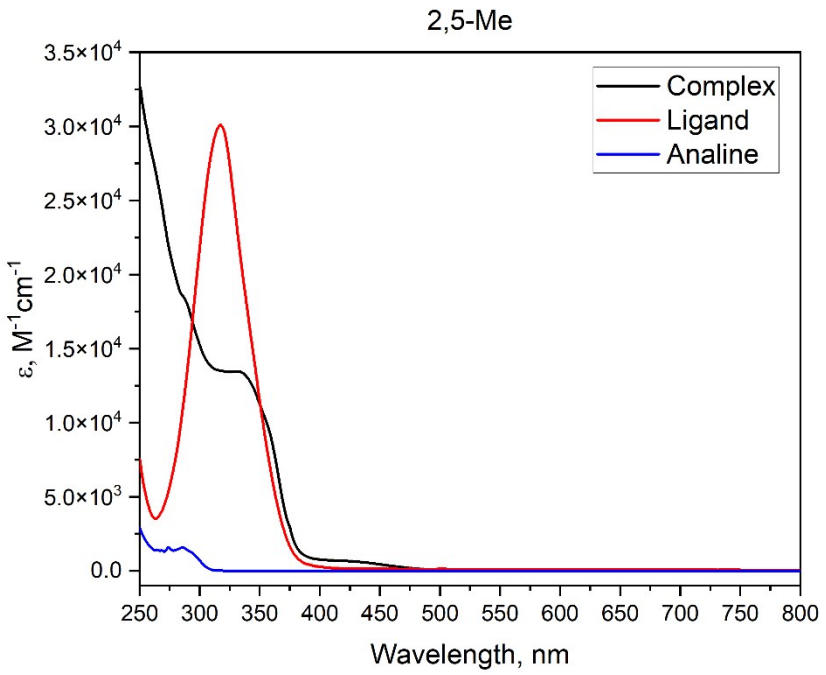

Figure S96. Electronic absorption spectra ($CHCl_3$, ambient temperature) of **2i**, **3i** and **4i**.

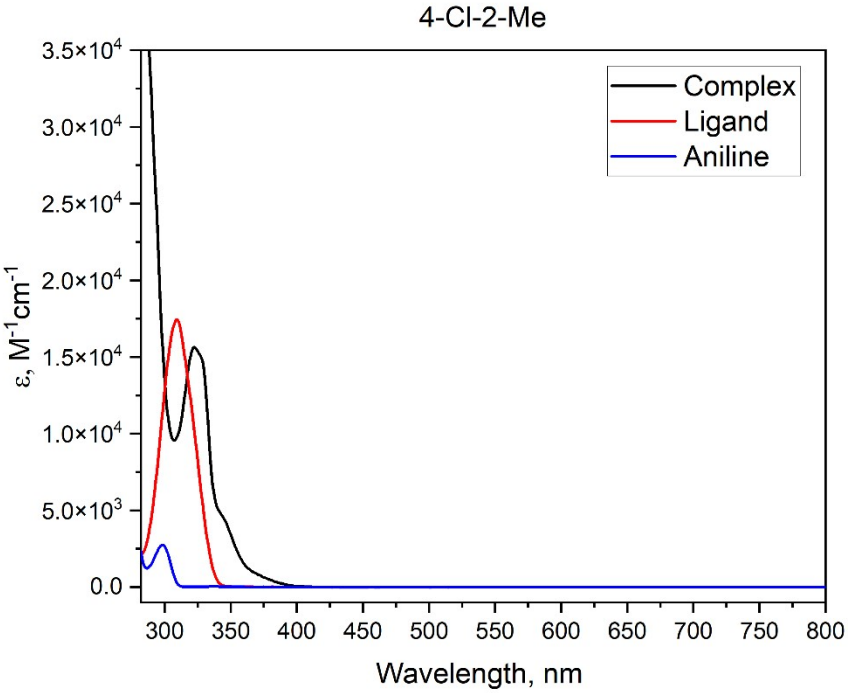

Figure S97. Electronic absorption spectra ($CHCl_3$, ambient temperature) of **2j**, **3j** and **4j**.

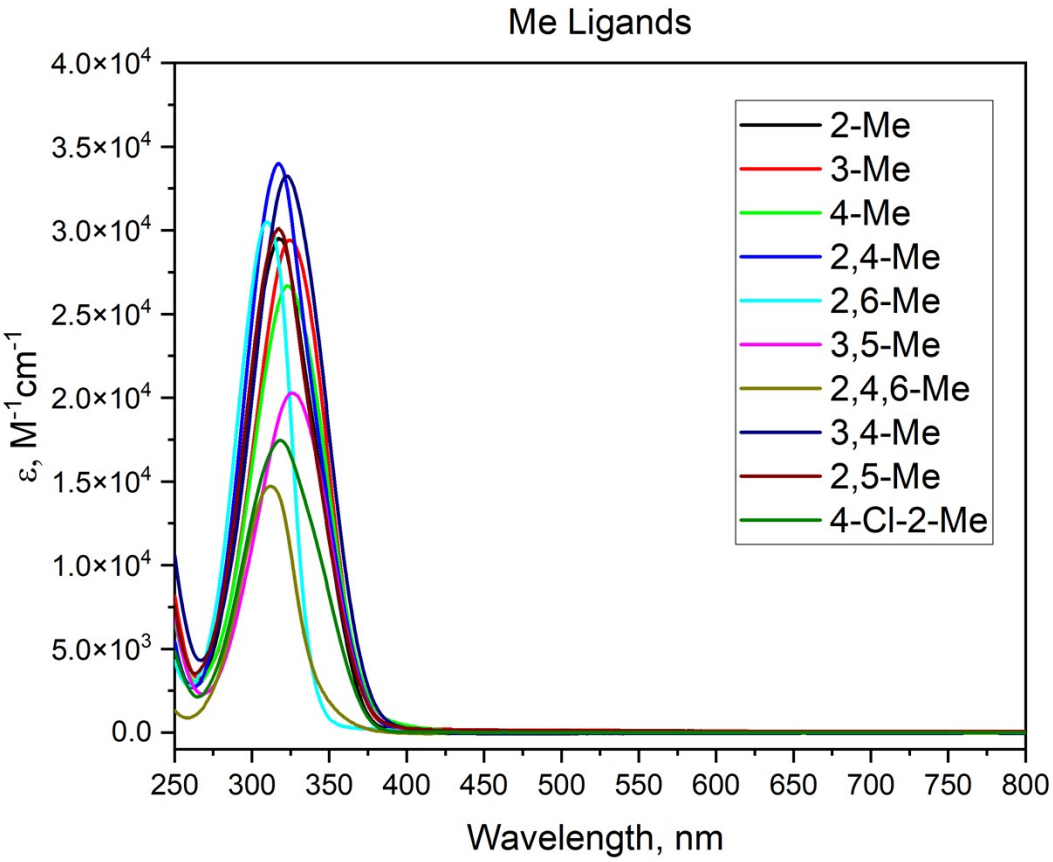

Figure S98. Electronic absorption spectra ($CHCl_3$, ambient temperature) of **3a-j**.

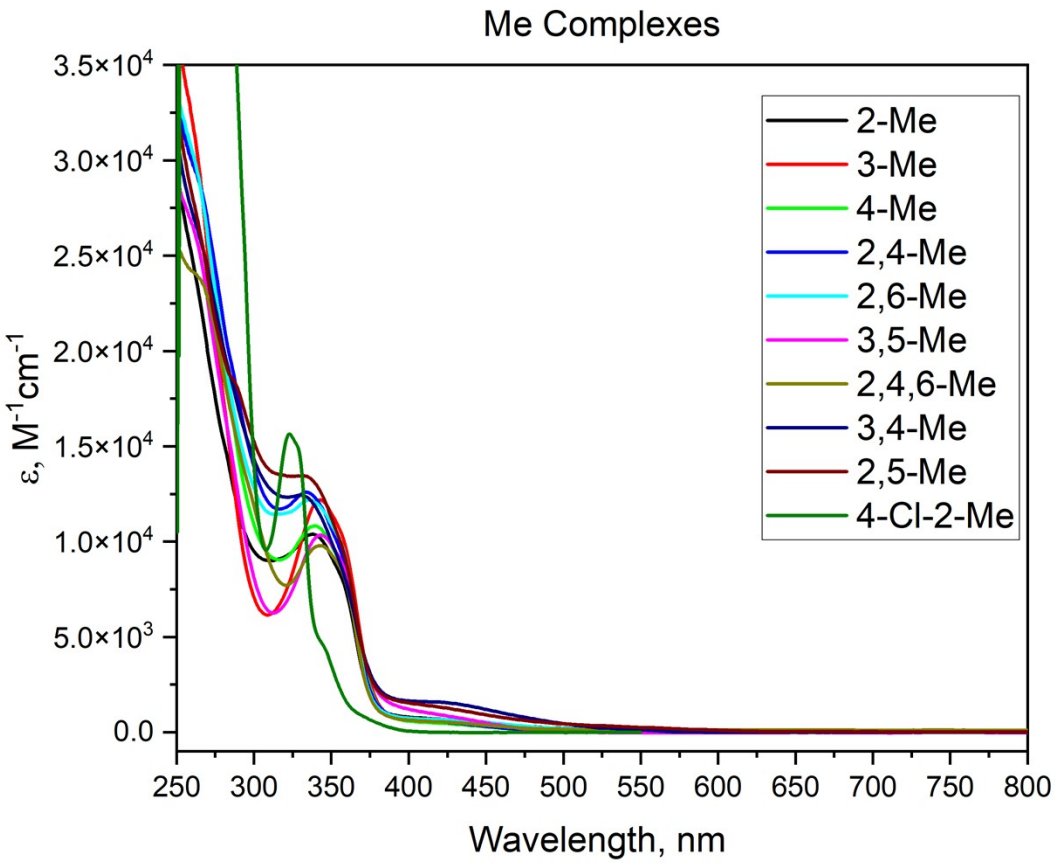

Figure S99. Electronic absorption spectra ($CHCl_3$, ambient temperature) of **4a-j**.

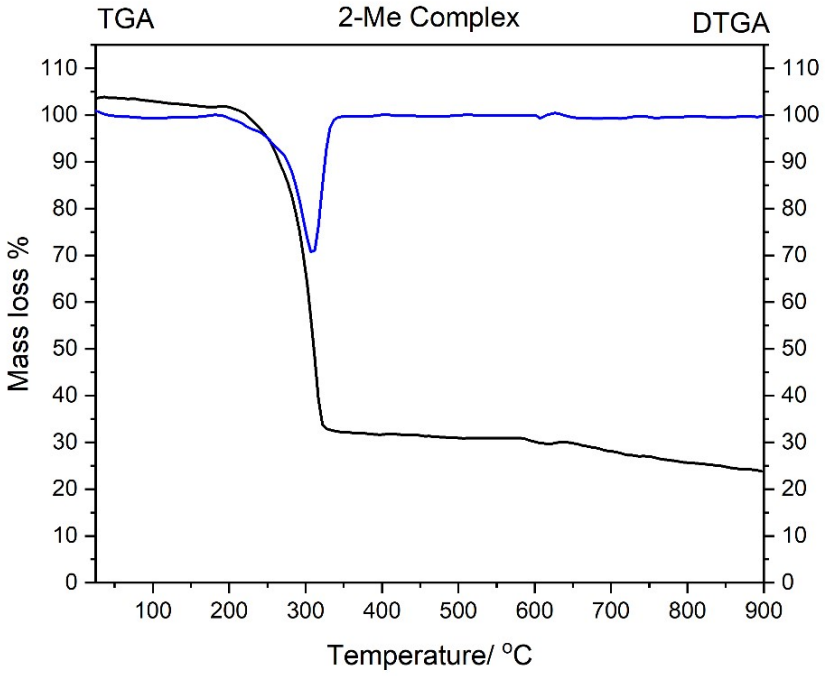

Figure S100. TGA thermogram for compound **4a**.

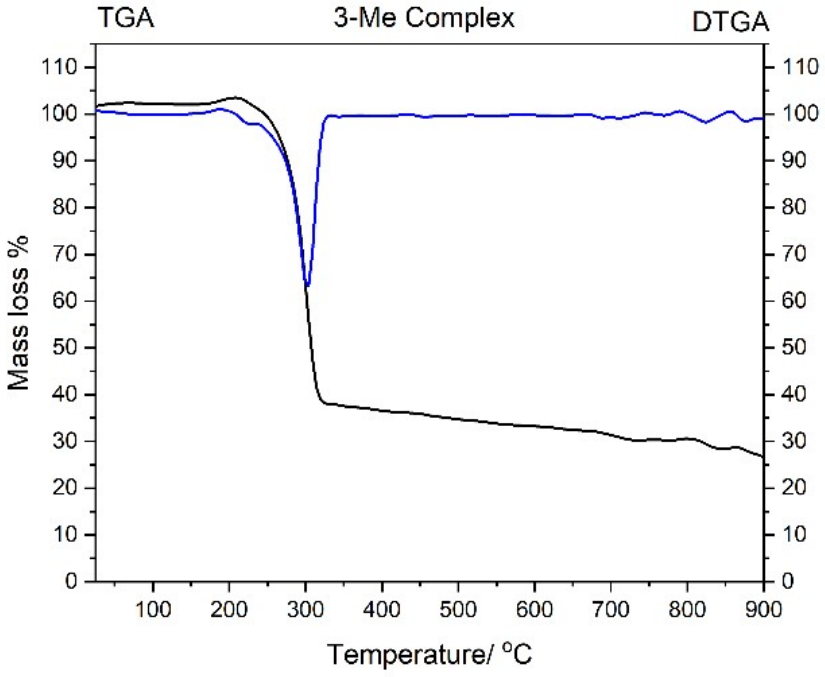

Figure S101. TGA thermogram for compound **4b**.

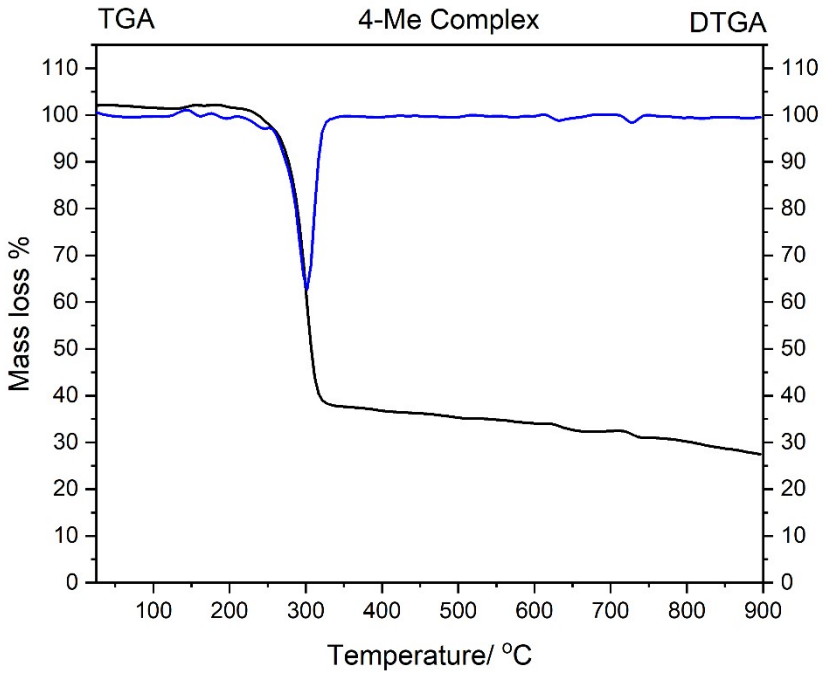

Figure S102. TGA thermogram for compound **4c.**

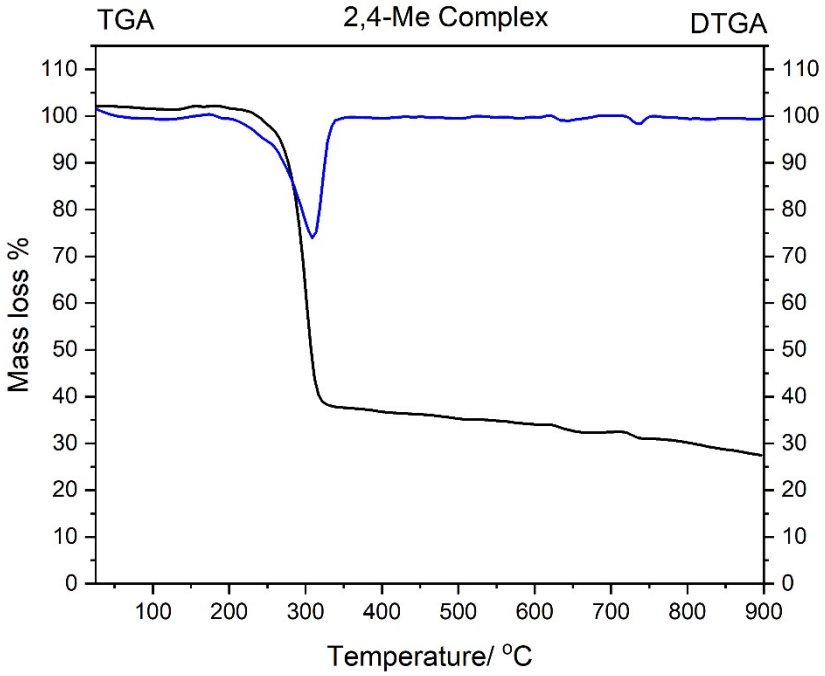

Figure S103. TGA thermogram for compound **4d.**

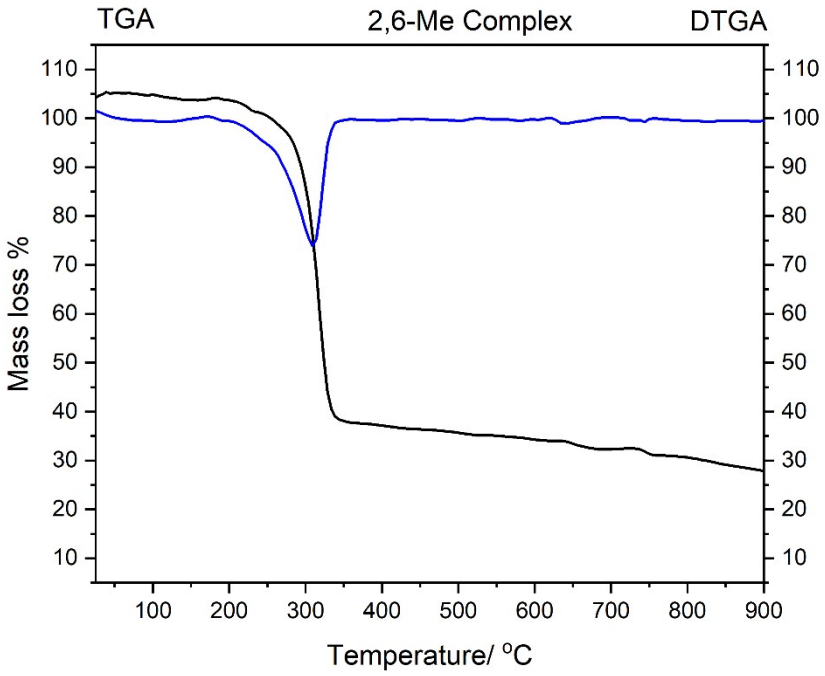

Figure S104. TGA thermograms for compound **4e.**

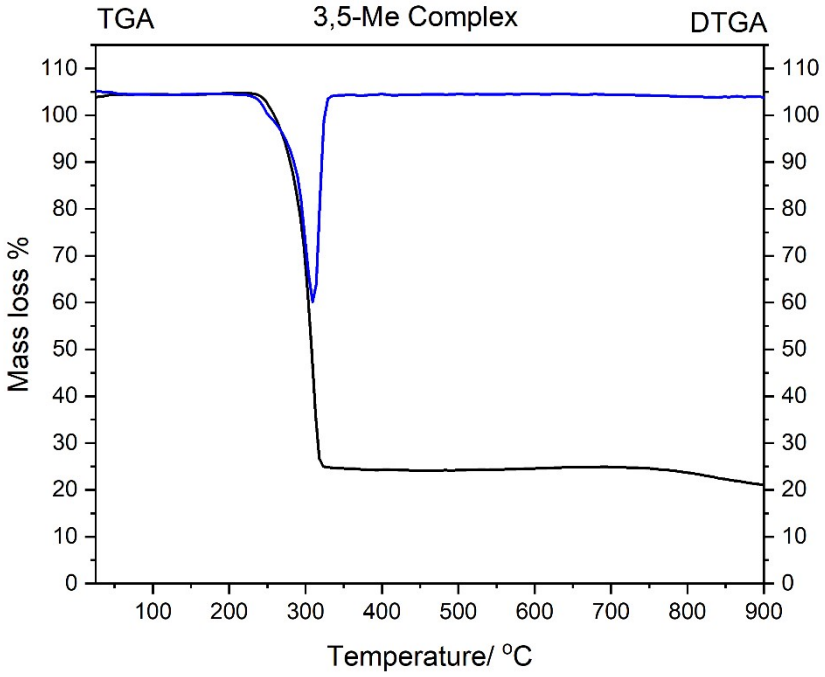

Figure S105. TGA thermograms for compound **4f**.

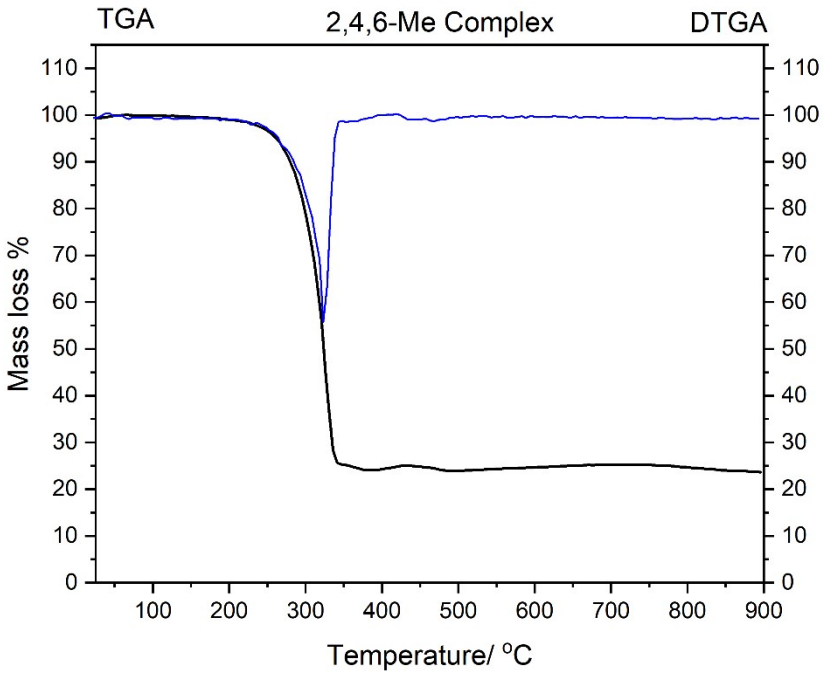

Figure S106. TGA thermograms for compound **4g**.

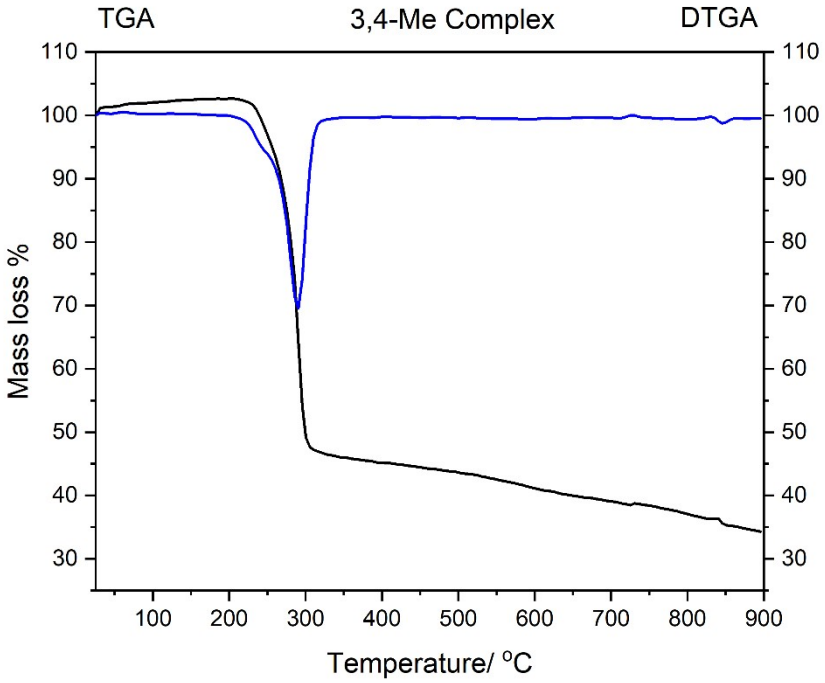

Figure S107. TGA thermograms for compound **4h**.

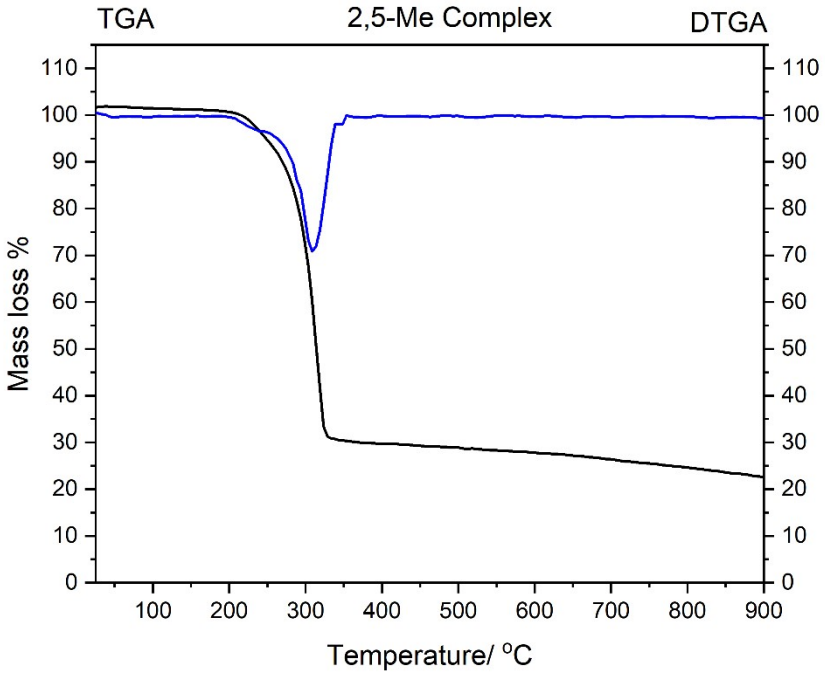

Figure S108. TGA thermograms for compound **4i**.

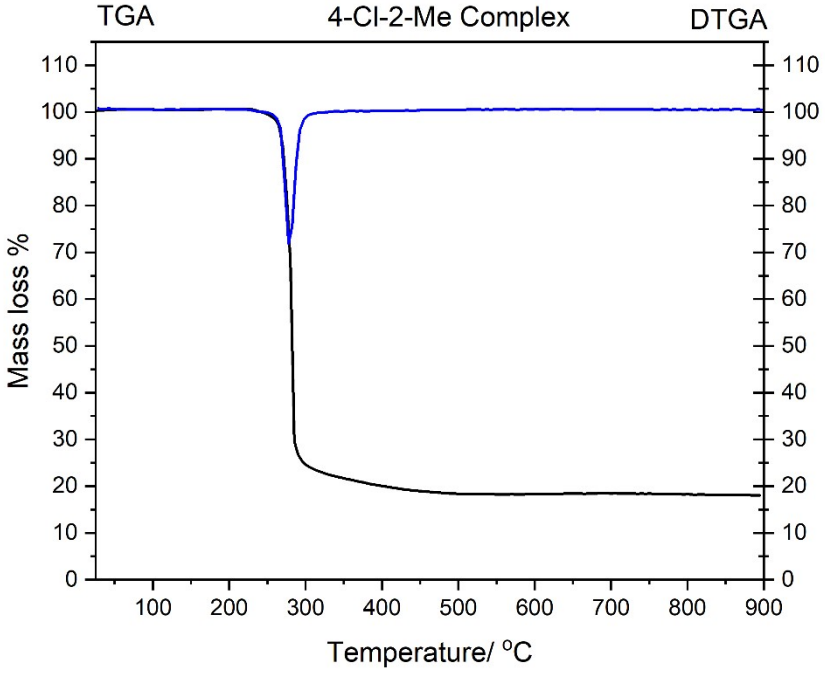

Figure S109. TGA thermograms for compound **4j**.

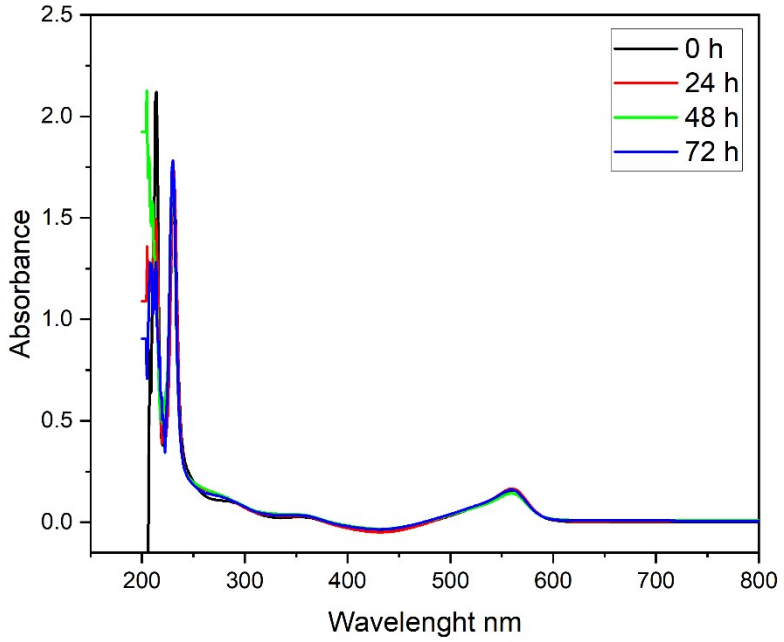

Figure S110. UV–Vis absorption spectra of the most active Pd(II) complex **4i** recorded in media at 25 °C.

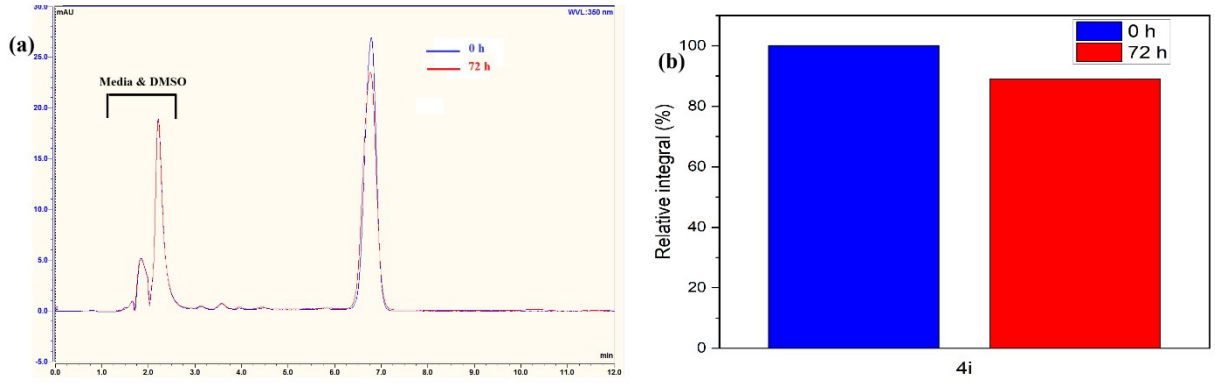

Figure S111. Monitoring the stability of complex **4i** in aqueous solution (3% DMSO) with HPLC. (a) Chromatograms at 350 nm. (b) Relative integral values.

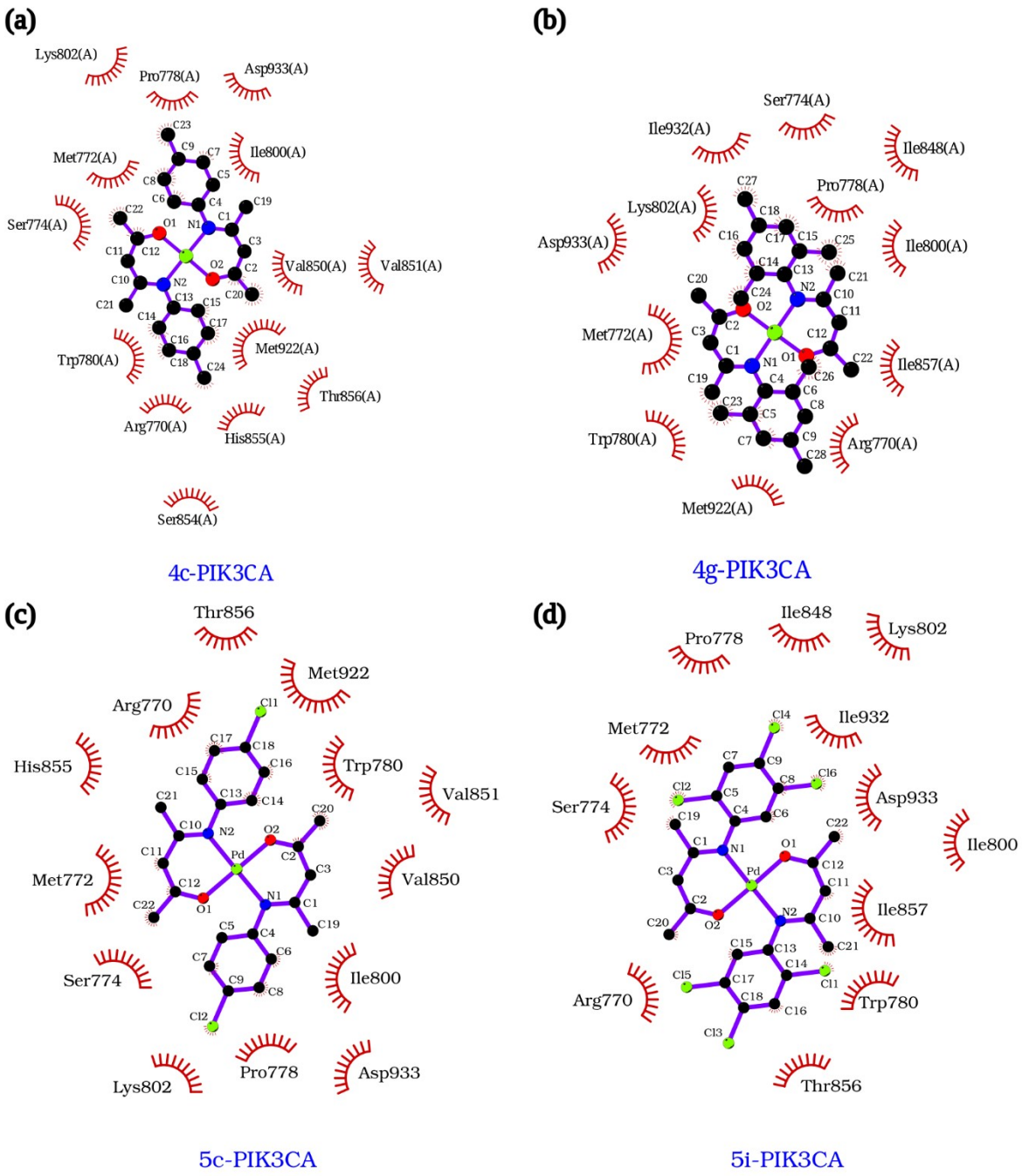

Figure S112. Ligand-protein interaction diagrams for the best- and worst-docked methyl- and chloride-substituted Pd(II) complexes on PIK3CA-E545K protein: (**a**) **4c**-PIK3CA, (**b**) **4g**-PIK3CA, (**c**) **5c**-PIK3CA and (**d**) **5i**-PIK3CA.

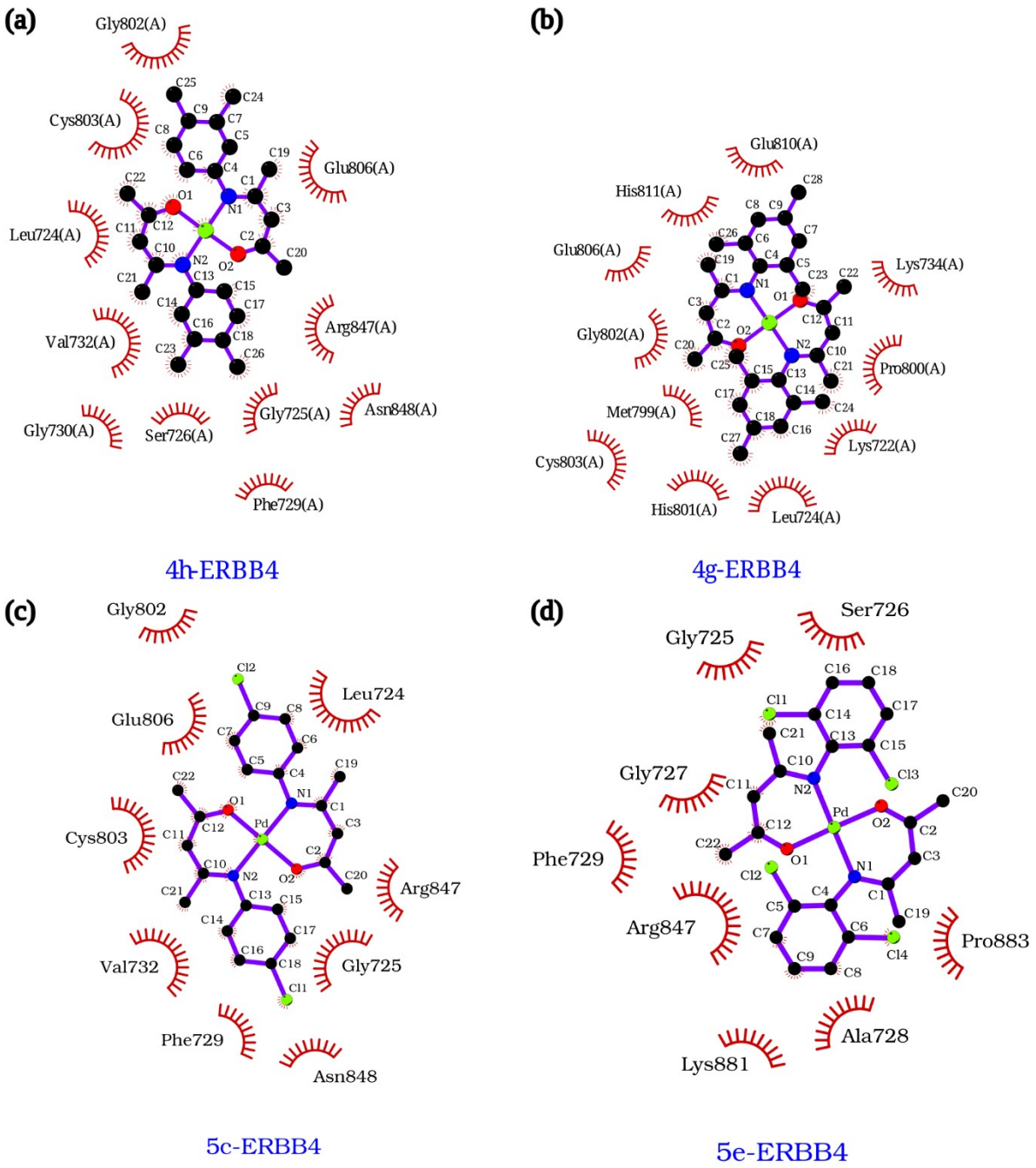

Figure S113. Ligand-protein interaction diagrams for the best- and worst-docked methyl- and chloride-substituted Pd(II) complexes on ERBB4-Y1242C protein: (**a**) **4h**-ERBB4, (**b**) **4g**-ERBB4, (**c**) **5c**-ERBB4 and (**d**) **5e**-ERBB4.

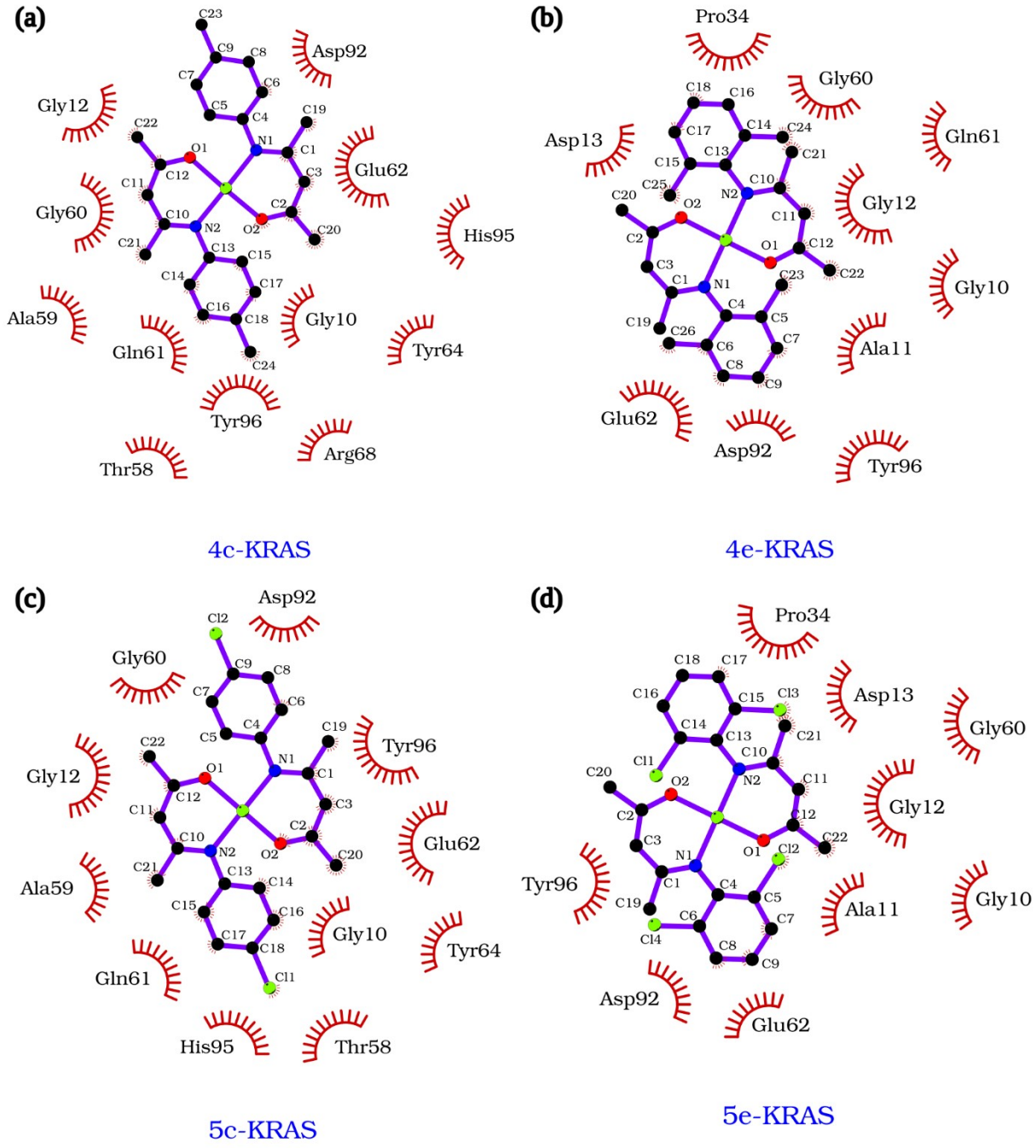

Figure S114. Ligand-protein interaction diagrams for the best- and worst-docked methyl- and chloride-substituted Pd(II) complexes on KRAS-G13D protein: (**a**) **4c**-KRAS, (**b**) **4e**-KRAS, (**c**) **5c**-KRAS and (**d**) **5e**-KRAS.

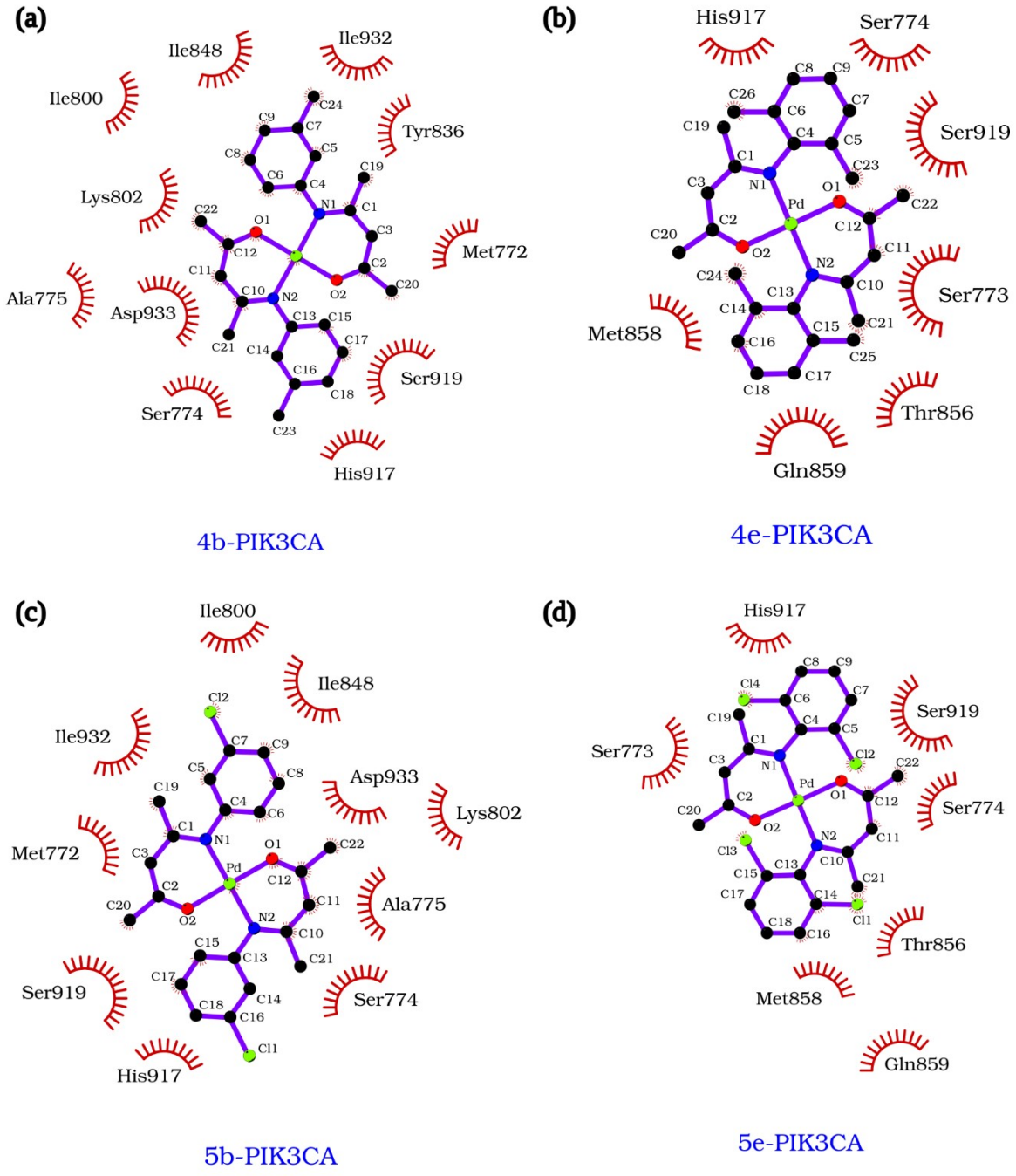

Figure S115. Ligand-protein interaction diagrams for the best- and worst-docked methyl- and chloride-substituted Pd(II) complexes on PIK3CA-H1047R protein: (**a**) **4b**-PIK3CA, (**b**) **4e**-PIK3CA, (**c**) **5b**-PIK3CA, and (**d**) **5e**-PIK3CA.

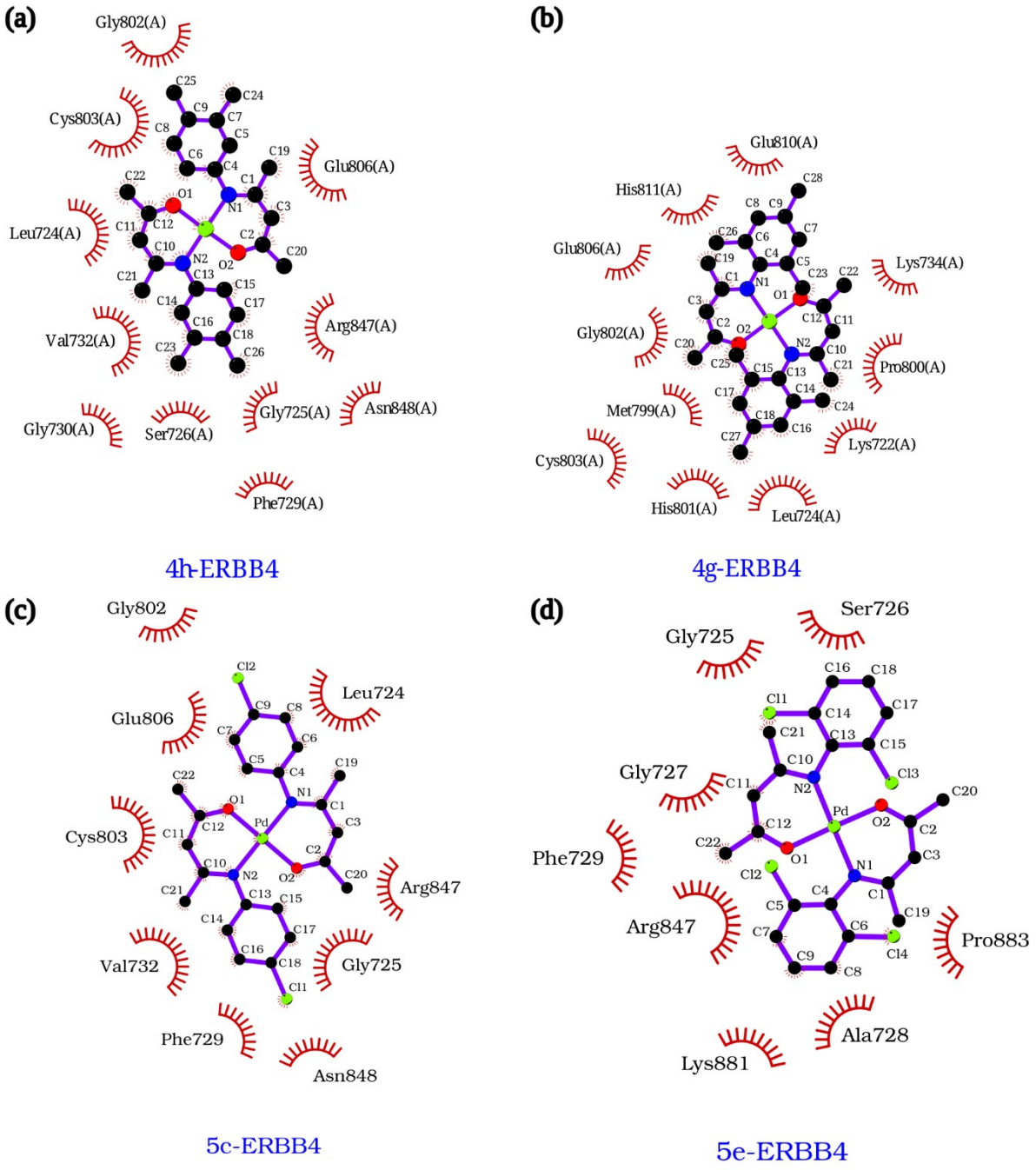

Figure S116. Ligand-protein interaction diagrams for the best- and worst-docked methyl- and chloride-substituted Pd(II) complexes on ATM-A112V protein: (**a**) **4b**-ATM, (**b**) **4g**-ATM, (**c**) **5b**-ATM, and (**d**) **5i**-ATM.

References:

1 G. K. Anderson, M. Lin, A. Sen and E. Gretz, in *Inorganic Syntheses*, ed. R. J. Angelici, John Wiley & Sons, Inc., Hoboken, NJ, USA, 2007, pp. 60–63.

2 D. M. Granum, P. J. Riedel, J. A. Crawford, T. K. Mahle, C. M. Wyss, A. K. Begej, N. Arulsamy, B. S. Pierce and M. P. Mehn, *Dalton Trans.*, 2011, **40**, 5881.

3 I. Hilker, J. F. G. A. Jansen and W. Posthumus, 2014.

4 M. Kidwai, S. Bhardwaj, N. K. Mishra, V. Bansal, A. Kumar and S. Mozumdar, *Catal. Commun.*, 2009, **10**, 1514–1517.

5 O. Marvi and L. Z. Fekri, *Comb. Chem. High Throughput Screen.*, 2018, **21**, 19–25.

6 H. Neelakantan, H.-Y. Wang, V. Vance, J. D. Hommel, S. F. McHardy and S. J. Watowich, *J. Med. Chem.*, 2017, **60**, 5015–5028.

7 G. Xie, Y. Li, J. Sun and C. Qian, *Inorg. Chem. Commun.*, 2009, **12**, 796–799.

8 D. Zheglova, D. Genov, S. Bolvig, P. Hansen, M. Hanfland and E. Dooryhee, *Acta Chem. Scand. - ACTA CHEM SCAND*, 1997, **51**, 1016–1023.

9 E. Yoshida and S. Yamada, *Bull. Chem. Soc. Jpn.*, 1965, **38**, 2179–2182.

10 A. N. Nesmeyanov, O. V. Nogina and V. A. Dubovitskii, *Bull. Acad. Sci. USSR Div. Chem. Sci.*, 1968, **17**, 514–520.

11 F. Neese, *WIREs Comput. Mol. Sci.*, 2012, **2**, 73–78.

12 C. Adamo and V. Barone, *J. Chem. Phys.*, 1999, **110**, 6158–6170.

13 F. Weigend and R. Ahlrichs, *Phys. Chem. Chem. Phys.*, 2005, **7**, 3297.

14 V. Barone and M. Cossi, *J. Phys. Chem. A*, 1998, **102**, 1995–2001.

15 M. Cossi, N. Rega, G. Scalmani and V. Barone, *J. Comput. Chem.*, 2003, **24**, 669–681.

16 R. Bauernschmitt and R. Ahlrichs, *Chem. Phys. Lett.*, 1996, **256**, 454–464.

17 I. K. Petrushenko and K. B. Petrushenko, *Spectrochim. Acta. A. Mol. Biomol. Spectrosc.*, 2018, **190**, 239–245.

18 A.-R. Allouche, *J. Comput. Chem.*, 2011, **32**, 174–182.

19 G. M. Sheldrick, *Acta Crystallogr. A*, 1990, **46**, 467–473.

20 Sheldrick, Gt M., 1997.

21 G. M. Sheldrick, *Acta Crystallogr. Sect. C Struct. Chem.*, 2015, **71**, 3–8.

22 G. M. Sheldrick, *Acta Crystallogr. A*, 2008, **64**, 112–122.

23 P. R. Spackman, M. J. Turner, J. J. McKinnon, S. K. Wolff, D. J. Grimwood, D. Jayatilaka and M. A. Spackman, *J. Appl. Crystallogr.*, 2021, **54**, 1006–1011.

24 M. Turner, J. McKinnon, S. Wolff, D. Grimwood, P. Spackman, D. Jayatilaka and M. Spackman, *Univ. West. Aust.*

25 R. B. Manawar, M. B. Gondaliya, M. K. Shah, M. M. Jotani and E. R. T. Tiekink, *Acta Crystallogr. Sect. E Crystallogr. Commun.*, 2019, **75**, 1423–1428.

26 D. Fabra, J. P. Mészáros, A. I. Matesanz, G. Spengler, F. Aguilar Rico, G. Moreno-Alcántar, A. Casini, É. A. Enyedy and A. G. Quiroga, *Inorg. Chem.*, 2025, **64**, 22852–22865.

27 F. Navas, F. Mendes, I. Santos, C. Navarro-Ranninger, S. Cabrera and A. G. Quiroga, *Inorg. Chem.*, 2017, **56**, 6175–6183.

28 Z. Sondka, N. B. Dhir, D. Carvalho-Silva, S. Jupe, Madhumita, K. McLaren, M. Starkey, S. Ward, J. Wilding, M. Ahmed, J. Argasinska, D. Beare, M. S. Chawla, S. Duke, I. Fasanella, A. G. Neogi, S. Haller, B. Hetenyi, L. Hodges, A. Holmes, R. Lyne, T. Maurel, S. Nair, H. Pedro, A. Sangrador-Vegas, H. Schuilenburg, Z. Sheard, S. Y. Yong and J. Teague, *Nucleic Acids Res.*, 2024, **52**, D1210–D1217.

29 X. Liu, Q. Zhou, J. R. Hart, Y. Xu, S. Yang, D. Yang, P. K. Vogt and M.-W. Wang, *Proc. Natl. Acad. Sci.*, 2022, **119**, e2215621119.

30 E. R. Wood, L. M. Shewchuk, B. Ellis, P. Brignola, R. L. Brashear, T. R. Caferro, S. H. Dickerson, H. D. Dickson, K. H. Donaldson, M. Gaul, R. J. Griffin, A. M. Hassell, B. Keith, R. Mullin, K. G. Petrov, M. J. Reno, D. W. Rusnak, S. M. Tadepalli, J. C. Ulrich, C. D. Wagner, D. E. Vanderwall, A. G. Waterson, J. D. Williams, W. L. White and D. E. Uehling, *Proc. Natl. Acad. Sci.*, 2008, **105**, 2773–2778.

31 C. Nilewski, S. Labadie, B. Wei, S. Malhotra, S. Do, L. Gazzard, L. Liu, C. Shao, J. Murray, Y. Izrayelit, A. Gustafson, N. F. Endres, F. Ma, X. Ye, J. Zou and M. Evangelista, *ACS Med. Chem. Lett.*, 2024, **15**, 21–28.

32 L. Buckbinder, D. J. St. Jean, T. Tieu, B. Ladd, B. Hilbert, W. Wang, J. T. Alltucker, S. Manimala, G. V. Kryukov, N. Brooijmans, G. Dowdell, P. Jonsson, M. Huff, A. Guzman-Perez, E. L. Jackson, M. D. Goncalves and D. D. Stuart, *Cancer Discov.*, 2023, **13**, 2432–2447.

33 K. Stakyte, M. Rotheneder, K. Lammens, J. D. Bartho, U. Grädler, T. Fuchß, U. Pehl, A. Alt, E. Van De Logt and K. P. Hopfner, *Nat. Struct. Mol. Biol.*, 2021, **28**, 789–798.

34 R. Krivák and D. Hoksza, *J. Cheminformatics*, 2015, **7**, 12.

35 R. Krivák and D. Hoksza, *J. Cheminformatics*, 2018, **10**, 39.

36 O. Trott and A. J. Olson, *J. Comput. Chem.*, 2010, **31**, 455–461.

37 J. Eberhardt, D. Santos-Martins, A. F. Tillack and S. Forli, *J. Chem. Inf. Model.*, 2021, **61**, 3891–3898.

38 N. M. O'Boyle, M. Banck, C. A. James, C. Morley, T. Vandermeersch and G. R. Hutchison, *J. Cheminformatics*, 2011, **3**, 33.

39 A. K. Rappe, C. J. Casewit, K. S. Colwell, W. A. Goddard and W. M. Skiff, *J. Am. Chem. Soc.*, 1992, **114**, 10024–10035.

40 A. C. Wallace, R. A. Laskowski and J. M. Thornton, *Protein Eng. Des. Sel.*, 1995, **8**, 127–134.

41 R. A. Laskowski and M. B. Swindells, *J. Chem. Inf. Model.*, 2011, **51**, 2778–2786.

42 T. D. Goddard, C. C. Huang, E. C. Meng, E. F. Pettersen, G. S. Couch, J. H. Morris and T. E. Ferrin, *Protein Sci.*, 2018, **27**, 14–25.

43 E. F. Pettersen, T. D. Goddard, C. C. Huang, E. C. Meng, G. S. Couch, T. I. Croll, J. H. Morris and T. E. Ferrin, *Protein Sci.*, 2021, **30**, 70–82.

44 E. C. Meng, T. D. Goddard, E. F. Pettersen, G. S. Couch, Z. J. Pearson, J. H. Morris and T. E. Ferrin, *Protein Sci.*, 2023, **32**, e4792.

45 D. Taher, Naim. H. Al-Said, M. Albanna, M. Kloda, M. Mustafa, W. Helal, K. I. Assaf, W. Hourani, W.-R. Kotob, S. Saleh, A. Makahleh and M. M. Rabba'a, *Inorganica Chim. Acta*, 2025, **583**, 122711.

46 D. Taher, S. Saleh, A. Y. Habashneh, W. Hourani, M. Mustafa, W. Helal, M. Al-Noaimi, S. M. Obeidat, M. Kloda, T. Alhindi, M. H. Kailani and A. Ghazzy, *J. Mol. Struct.*, 2025, **1340**, 142542.